DEVELOPMENT OF HUMAN BODY VIBRATORY MODELS AND DYNAMIC ANALYSIS OF MOTORCYCLE-RIDER SYSTEM

Ph.D. Thesis

MANOJ GUPTA

ID No. 2012RME9554

DEPARTMENT OF MECHANICAL ENGINEERING

MALAVIYA NATIONAL INSTITUTE OF TECHNOLOGY JAIPUR

AUGUST 2019

Development of Human Body Vibratory Models and Dynamic Analysis of Motorcycle-Rider System

Submitted in

fulfillment of the requirements for the degree of

Doctor of Philosophy

by

Manoj Gupta
ID:2012RME9554

Under the Supervision of

Dr. T. C. Gupta

DEPARTMENT OF MECHANICAL ENGINEERING

MALAVIYA NATIONAL INSTITUTE OF TECHNOLOGY JAIPUR

AUGUST 2019

DECLARATION

I, **Manoj Gupta**, declare that this thesis titled, '**Development of Human Body Vibratory Models and Dynamic Analysis of Motorcycle-Rider System'** and the work presented in it, are my own. I confirm that:

- This work was done wholly or mainly while in candidature for a research degree at this university.
- Where any part of this thesis has previously been submitted for a degree or any other qualification at this university or any other institution, this has been clearly stated.
- Where I have consulted the published work of others, this is always clearly attributed.
- Where I have quoted from the work of others, the source is always given. With the exception of such quotations, this thesis is entirely my own work.
- I have acknowledged all main sources of help.
- Where this thesis is based on work done by myself, jointly with others, I have made clearly exactly what was done by others and what I have contributed myself.

Date: 15th August 2019

Manoj Gupta

(2012RME9554)

CERTIFICATE

This is to certify that the thesis entitled '**Development of Human Body Vibratory Models and Dynamic Analysis of Motorcycle-Rider System**' being submitted by **Mr. Manoj Gupta (2012RME9554)** is a bonafide research work carried out under my supervision and guidance in fulfillment of the requirement for the award of the degree of **Doctor of Philosophy** in the department of **Mechanical Engineering**, Malaviya National Institute of Technology, Jaipur, India. The matter embodied in this thesis is original and has not been submitted to any other University or Institute for the award of any other degree.

Place: Jaipur   **Dr. T. C. Gupta**
Date: Associate Professor
                                                       Department of Mechanical Engineering
                                                       MNIT Jaipur, India

ACKNOWLEDGEMENTS

Abstract

Adverse effects of short term and long term vibration exposure on human body has been documented in numerous studies. Multitudinous experiments on human subjects, to quantify vibration dose value leading to various injuries, are not recommended due to varied nature of external excitations as well as ethical concerns. Estimation of body segments or locations that are prone to vibration injuries is only possible through simulation.

This thesis attempts to investigate the effects of vibrations transmitted to a person due to road undulations while travelling on different transportation system, with emphasis on the rider of a motorcycle. Towards this objective, initially multi degree of freedom vibratory models of human body in different postures are developed and vibratory model of sitting posture is incorporated with motorcycle to analyze dynamic of motorcycle-rider system running in a straight line.

Existing vibratory models of human body are either lumped parameter models that have limited resemblance with actual body structure or continuum models that have large number of elements/degree of freedom, with main focus on the spine. For better correspondence with actual human body, in the present work, vibratory models that resemble anatomical structure and based on anthropometric measurements have been developed.

In the first stage, lumped parameter model of subject in standing posture is developed by representing human body segments as truncated ellipsoids. Using experimental measurements of driving point impedance parameters, an iterative scheme has been developed to identify modal damping ratios of body segments. In second stage, a finite element (FE) vibratory model of standing subject under vertical excitation is formulated. FE model is preferred as these models better represent continuous nature of human body and also enable identification of locations prone to vibration related injuries. For FE formulation also, truncated ellipsoids elements are used to represent different parts of human body. Shape functions of truncated ellipsoidal finite elements have been derived based on exact

solution of deformation of an ellipsoid under uni-axial load. Modeling individual body segments as viscoelastic elements, Hamilton's principle is employed to derive equations of motion. Driving point mechanical impedance values computed from FE model of standing subject matched available experimental measurements; therefore, FE model of seated person was formulated following similar procedure. Driving posture of a motorcycle rider was imitated by inclusion of a lumped parameter model of human arm in FE model of seated person. After validation, seated model of human body is combined with multi-body dynamic model of motorcycle in the final stage; motorcycle-rider moving along a straight line. Comparison of results between two motorcycle models, first one assuming the rider as rigid body attached to the vehicle and second one modeling the rider using FE vibratory model developed in this study; clearly establishes the effect of flexibility of human body on dynamic response of combined motorcycle-rider system.

The methodology developed in this thesis enables formulation of human body vibratory models that are simple to formulate, have low degrees of freedom and resemble the anatomical structure. Employing anthropometric measurements and mass of the person, subject specific vibratory models in different postures can be developed to estimate locations in human body susceptible to vibration prone injuries due to vertical excitation and undulations coming from the road through vehicle suspension and seat.

Contents

List of figures

List of Tables

List of Abbreviations

A = Cross sectional area

AM = Apparent Mass

a, b, c = Semi axis of ellipsoidal segment

$[\mathbf{B}]$ = Element strain-displacement matrix

$DPMI$ = Driving Point Mechanical Impedance

d = Truncated vertical axis for ellipsoidal segment

E = Elastic modulus of body segment

F_{fp} = Equivalent force at feet-platform interface

g = Gravitational acceleration

$[\mathbf{H}]$ = Viscous damping matrix of individual finite element

$[\underline{\mathbf{H}}]$ = Viscous damping matrix of complete finite element model

$[\mathbf{K}]$ = Stiffness matrix of individual finite element

$[\underline{\mathbf{K}}]$ = Stiffness matrix of complete finite element model

ΔL = Extension of ellipsoidal segment

$[\mathbf{M}]$ = Mass matrix of individual finite element

$[\underline{\mathbf{M}}]$ = Mass matrix of complete finite element model

M_{total} = Mass of the subject

m = Mass

N = Shape function

$NAMS$ = Normalized apparent mass of the subject

P = Number of discrete value of frequencies in 0-20 Hz

$\{\mathbf{Q}\}$ = Nodal displacement amplitude vector

$\{\mathbf{q}\}$ = Nodal displacement vector

R = Value of objective function

STHT	=	Seat to Heat Transmissibility
T	=	Kinetic energy
TR	=	Transmissibility
t	=	Time
U	=	Strain energy
u	=	Internal displacement field of finite element
v	=	Volume
W	=	Work done
Y	=	Amplitude of motion applied to the platform
y	=	Motion applied to the platform

Greek Letters

δ	=	first variation of quantity
σ	=	stress
ε	=	strain
ρ	=	density of human body
η	=	average dynamic viscosity of body segment
ϕ	=	phase difference
ω	=	frequency

Subscripts and Superscripts

G	=	due to gravity
H	=	for hand segment
LA	=	for lower arm segment
NMS	=	for normalized apparent mass
UA	=	for upper arm segment
SA	=	for swinging arm
i	=	index for ellipsoidal finite elements

r	=	index for un-prescribed/unknown nodes
s	=	index for specified/prescribed nodes
ext	=	due to external forces
max	=	for maximum value of parameter
n	=	for natural frequency
ex	=	experimental
th	=	theoretical
vis	=	due to viscous forces
$\{\dot{\ }\}$	=	differentiate w.r.t. time
$\{\ddot{\ }\}$	=	double differentiate w.r.t. time
$[\_]$	=	matrix/vector for assembled finite element model
T	=	Transpose of a vector/matrix

Chapter 1

Introduction

The human body is subjected to external excitations while driving, travelling, operating different machineries and performing other day to day activities. Many researchers have pursued studies related to Whole Body Vibration (WBV) of human subjects to estimate adverse effects due to vibration amongst industrial (i.e., machine, hand-tool) operators, motorist, passengers etc. Short term exposure to WBV leads to discomfort, headaches, reduced concentration, back pain; whereas long term exposure can result in lower back injuries, spinal dislocation, white finger syndrome, and other muscular disorders. Since a human body is continuous, flexible and energy absorbing system from vibrations point of view; the literature survey showed the clear need and possibility of improving human body vibratory model. It was also felt that considering driver's body as a flexible structure to study the vibration effects is still not explored systematically, so it aroused interest in human body vibration as potential research area. Also, the area relates to the safety and comfort of a person. My research supervisor, based on previous experience in experimental and theoretical studies of vibration effects on human body, also endorsed choosing human body vibration as the field of research.

In the present thesis, the aim was to develop a subject-specific dynamic model of combined motorcycle-rider system, capable of predicting human body segments/locations more susceptible to vibration related injuries. Compared to a person travelling in a four-wheeler, the mass of average motorcycle rider (and passenger if applicable) is significant vis-à-vis the mass of motorcycle itself. Also, the

human body behaves essentially as a multi degree of freedom vibratory system. Therefore, dynamic properties of human body can have a significant effect on the response of motorcycle-rider system. The inclusion of human body characteristics into dynamic model of motorcycle becomes necessary in order to have a true assessment of the road induced motorcycle oscillations on the human being (rider).

During literature survey it was found that the mathematical models of the human body, available in the literature, are not appropriate and sufficient to couple with motorcycle models. So, the development of human body vibratory became a requirement and substantial part the present research work. Considering the availability of experimental studies in the literature, first the vibratory models for the standing and sitting posture were developed, with the proposed modelling procedure and then were established. Once the proposed idea of modelling human body as truncated ellipsoidal segments using anthropometric data got established; it was extended to motorcycle-rider system while including few additional modifications for the hands and upper legs. Thus the motorcycle rider model consists of 1) truncated viscoelastic ellipsoidal finite elements, 2) rigid rods for upper legs and 3) spring-mass-damper system for arms holding the motorcycle handle. It is to note that the motorcycle model does not mix different methods; instead, in this modelling established models for different parts of human body have been used.

The research work has broadly been divided into two steps; first step was the establishment of a validated human body vibratory model for motorcycle rider system and second step was to combine the human body model with a detailed motorcycle model; so that effects of human body on response of complete system can be estimated. It was hypothesized that a procedure should be established to develop human body models that represent its anatomical structure sufficiently (form

2

vibration point of view) and also enables construction of subject specific (or group specific) models. These models should take into account effect of the 'build' (height, dimensions of body segments, mass, active nature of person etc.) of human body upon its dynamic response. Therefore, it was decided to emphasize development of human body models that were simple to construct, having low degrees of freedom while having correspondence with anatomical structure, and which take into account at least some aspects of the 'build' of human body.

1.1 Outline of Research Work

Initially, a lumped parameter vibratory model of standing subject under vertical excitation was developed. The human body was partitioned into fifteen ellipsoidal segments, each ellipsoidal segment representing a distinct section of the human body. Model parameters were computed using anthropometric measurements and total mass of the subject. Damping was included in the vibratory model, first using damping ratio of individual segment and thereafter through modal damping ratios identified from experimental measurements available in the literature. Satisfactory match between experimental data and theoretical computation based on anthropometric lumped parameter model was achieved.

To improve the equivalence between experimental measurements and theoretical predictions calculated from anthropometric human body vibratory model; and also to incorporate continuous nature of actual human body; a finite element (FE) based model of standing subject was developed. Human body segments were approximated as two noded truncated ellipsoidal finite elements, whose dimensions were again determined from anthropometric measurements. Shape functions for ellipsoidal elements were derived from the exact solution of a truncated ellipsoid under uni-axial

load. Using Kelvin-model of viscoelasticity, governing equations for a standing subject under vertical excitation were derived using Hamilton's principle. Better correspondence between experimental measurements and theoretically computed driving point impedance parameters using finite element vibratory model was achieved. Subsequently, using similar methodology, finite element vibratory model of seated person was developed with arms in vertical hanging position. To correspond with the posture of a motorcycle rider (specifically arms at an angel to vertical), the seated FE model was modified slightly by including existing lumped parameter model of bent arm. Finally, the FE model of motorcycle rider in a seated driving posture was combined with a straight line model of motorcycle and effects on dynamic response of the vehicle were studied.

1.2 Contributions of the Present Research Work

Main contributions of the research work can be summarized as follows:

1. Computation of driving point mechanical impedance and acceleration transmissibility for anthropometric human body vibratory model.

2. Development of novel iterative scheme to estimate modal damping ratios using experimental measurements of transmissibility and its application to human body vibratory model.

3. Reference values for elastic moduli of human body segments in standing posture.

4. Development of truncated ellipsoidal finite elements for FE vibratory model of human body in standing and sitting posture using shape functions based on exact solution of uni-axial deformation of ellipsoid.

5. Estimation of elastic moduli and average dynamic viscosity of human body segments for finite element vibratory model with low d.o.f., in standing and sitting posture.

6. Development of seated human body vibratory model in normal driving posture of a motorcycle rider.

7. Study of vibrations transmitted to head of the rider driving a motorcycle, due to road undulations, considering human body as flexible multi degrees of freedom system.

1.3 **Thesis Organization** The thesis is organized into seven different chapters which are briefly described below:

Chapter 1: Introduction

This chapter describes motivation behind the current research work. Scope of the research problem and the steps followed for solving the same are outlined. It also lists major contributions of the research work and describes organization of thesis in brief.

Chapter 2: Literature Survey

Previous studies concerning Whole Body Vibration of humans and motorcycle modeling are reviewed in this chapter. Experimental studies dealing with measurement of different parameters for person subjected to external excitations are discussed. Thereafter theoretical studies dealing with development of human body vibratory models, both lumped parameter and finite element based are described. The limitations and scope for improvement of these studies are pointed out to identify research gaps. Finally, a brief

review of different approaches to motorcycle modeling is provided to identify straight line motorcycle model adopted in the present thesis.

Chapter 3: Lumped Parameter Models of Standing Subject

The chapter details the methodology used to develop lumped parameter human body vibratory models for a standing subject under vertical excitation from feet-platform interface. Scheme to partition human body into ellipsoidal elements; comparable with actual human body segments, and identification of model parameters from anthropometric data is described. Standing human vibratory models based on damping ratio and modal damping ratios are developed and methodology used for identification of model parameters is illustrated.

Chapter 4: Finite Element Model of Standing Subject

Improving upon lumped parameter human body vibratory model, development of finite element model of a standing subject is described in this chapter. Procedure to generate shape functions from exact solutions and derivation of governing differential equation from Hamilton's principle are detailed. Identification of average parameters of ellipsoidal finite elements using optimization is explained and mode shapes for a standing subject under vertical excitation are drawn.

Chapter 5: Finite Element Model of Seated Subject

Building on the FEM model of standing subject, Chapter 5 details the finite element model of seated subject under simultaneous excitation form feet and

pelvis. Development of vibratory model of a seated person in with hands in straight down posture is expounded upon in this chapter.

Chapter 6: Straight Line Model of Motorcycle and Dynamic Analysis of Motorcycle-Rider Model

Vibratory model of motorcycle rider through inclusion of a lumped parameter model of bent arm is developed in this chapter. It also describes the straight line motorcycle model adopted in present study. Lagrangian approach to develop the multi-body model of motorcycle is detailed and numerical scheme to solve for straight line motion is explained. Finally multi-body model of motorcycle is combined with FEM model of seated human body and results are examined to show the effects of human body on dynamic response of motorcycle.

Chapter 7: Conclusions

The final chapter summarizes the findings of human body vibratory models developed in research study. It also research contributions and scope of further improvement.

Appendices

The studies reviewed in Chapter 2 as well as other studies referred to in different chapters are listed. Appendices contain data related to human body vibratory models and motorcycle model.

Chapter 2

Literature Survey

2.1 Introduction

This chapter reviews studies related to WBV of human body and different approaches employed by researchers to construct motorcycle model. Classification of human body vibration studies and basic terminologies related to the same are introduced in section 2.2 and 2.3 respectively. In section 2.4, these studies are reviewed in detail to identify different methods employed by the researchers to quantify adverse effects of external excitations on people. In section 2.5, different motorcycle models available in the literature are reviewed to identify a suitable model for dynamic analysis of motorcycle-rider model. Research Gap based on literature survey of different studies is discussed in section 2.6 and section 2.7 lists primary objective of proposed work.

2.2 Human Body Vibration

Different approaches employed by researchers to investigate adverse effects of vibration exposure on health and well-being of people can be broadly classified into three categories:

a) **Statistical studies or field surveys**: Substantial data has been gathered by conducting field surveys among heavy vehicle operators, construction workers, miners, travelling passengers etc. to understand effects of long term vibration exposure on human health. Attempts have been made to correlate nature, magnitude and duration of exposure with the different types of

vibration injuries reported. These studies have played an important role in issuance of regulatory guidelines about safe vibration dose values for people who are continuously exposed to WBV in their day to day environment.

b) **Experimental studies:** Numerous experimental studies have been conducted on groups of people, under controlled environment, to identify effect of various factors related to vibration exposure on the dynamic response of human body. These factors can be broadly classified as ones related to the input excitation and other related to the human body. Important factors related to input excitation that have been investigated through experimental studies are magnitude, direction and nature of applied excitation. Mass, age, gender, body structure and its posture are the main factors related to human body whose effect on dynamic response has been studied in experimental settings. These experimental studies have identified 'resonant frequencies' i.e., those frequency of applied excitation at which human body response exhibit distinct peaks. Also the effect of aforementioned factors on resonant frequencies and magnitude of dynamic response at resonant frequencies has been measured through experimental studies.

c) **Theoretical modeling:** Primarily, due to ethical concerns and due to the varied nature of external excitations, it is not possible to conduct experimental studies for identifying safe vibration level for persons in different work environments. Theoretical vibratory models of human body or some of its parts, both lumped parameter and continuous, have been developed to overcome this limitation. Parameters of these vibratory models are chosen such that their dynamic response imitates the response measured in experimental studies under similar excitation conditions. After validation,

these models are employed in lieu of actual human being for design and comfort studies related to different environments.

2.3 Biodynamic Response Terminologies:

Different terminologies have been defined by researchers to study vibration effects on human body quantitatively and also to enable comparison between experimental measurements and theoretical predictions computed using human body vibratory models.

a) **Driving point mechanical impedance:** Ratio of the force transmitted at the force platform (seat/floor)-person interface and velocity at the same interface.

b) **Seat to head transmissibility:** Ratio of the acceleration measured at the force platform (seat/floor)-person interface and acceleration measured at person's head.

c) **Apparent mass**: Ratio of the force transmitted at the force platform (seat/floor)-person interface and acceleration at the same interface.

d) **Normalized Apparent mass**: Ratio of the apparent mass and static weight of person in the case of standing subject or Ratio of the apparent mass and apparent mass at very low frequencies (generally taken as 0.5 Hz)

2.4 Human Body Vibration Studies

The effects of vibratory stimulus on human body are assessed by the quantitative analysis of parameters such as Apparent Mass, Driving Point Mechanical Impedance (DPMI), Seat/Platform-to-Head Transmissibility, Absorbed Energy etc. (Griffin, 1990) through theoretical and experimental studies. Experimental measurement of these parameters are conducted by subjecting a person to external excitations under

controlled environment while accounting for factors such as body posture, magnitude and axis of the excitation. Experimental studies are then used to develop lumped parameter multi degree of freedom (d.o.f.) vibratory models of the human body.

Amongst early researchers, Garg and Ross (1976) measured platform-to-head transmissibility of 12 subjects in standing posture. The input harmonic vibrations to the platform were in the frequency range of 1-50 Hz with small amplitude. A 16 mass linear lumped parameter model of the standing subject was developed. Mass and stiffness parameters of the model were estimated from published literature (Hirsch & Nachemson, 1954; Coermann, 1962; Suggs & Abrams, 1973; Dempster 1995) and damping parameters were determined through matching average experimental frequency response with the theoretical response. Muskian and Nash (1976) formulated a three degree of freedom (d.o.f) lumped parameter seated human body model undergoing sinusoidal vibrations. The mass of three bodies in the model representing head, body and pelvis were based on the methodology reported by Hertzberg and Clauser (1964). The stiffness and damping parameters were estimated by fitting the theoretically computed values of seat to head acceleration ratios with experimentally measured values published in the literature (Magid et al 1962). Moreover, damping coefficients were taken as a function of frequency of excitation so as to have a better match with the experimental data. Considering the fact that dynamic behavior of human body depends upon the physical parameters of the human being; Nigam and Malik (1987) developed a 15 d.o.f. undamped vibratory model for standing posture based on anthropometric data of human body (Bartz & Gianotti, 1975).

Author	Posture	Impedance Parameter	Model Description	Dataset Used for Parameter Estimation / Identification	Resonant Frequencies	Figure of Model
Garg and Ross (1976)	Standing, Erect	Feet to Head Transmissibility	Lumped Parameter Spring-Mass-Damper Model with Sixteen Mass Elements	Matching of Theoretical Response Curve with Experimentally Measured Average Feet to Head Transmissibility of Eight Persons (Garg & Ross, 1976)	1.99 Hz, 6.14 Hz, 19.4 Hz	
Muskian and Nash (1976)	Seated, Erect	Head to Seat Acceleration Ratio	Lumped Parameter Spring-Mass-Damper Model with Three Mass Elements	Matching of Theoretical Response Curve with Experimentally Measured Acceleration Ratio and Natural Frequencies (Magid et al, 1976 and Goldman & Gierke, 1961)	6 Hz	

Nigam and Malik (1987)	Standing, Erect	None	Lumped Parameter Spring-Mass Model with Fifteen Mass Elements (Undamped)	None; Only Matching of Resonant Frequency of Body Segments Using Anthropometric Data	13.82 Hz; 23.92 Hz, 28.77 Hz, 29.53 Hz	
Qassem et al. (1994)	Seated, Erect	Seat to Hand Transmissibility and Hand to Elbow Transmissibility	Lumped Parameter Spring-Mass-Damper Model with Eleven Mass Elements (Connected with both horizontal and vertical springs and dampers)	Matching of Theoretical Response Curve with Experimentally Measured Acceleration Ratio and from Available Literature Natural Frequencies (Mizrahi & Susak 1982, Nigam & Malik 1987, Patil et al. 1978)	1.38 Hz, 2.7 Hz, 1.85 Hz, 1.38 Hz (for different body segments, not the whole body)	
Wei and Griffin (1998)	Seated	Mean Normalized Apparent Mass	Lumped Parameter Spring-Mass-Damper Model with Rigid Support	Matching of Theoretical Response Curve with Modulus and Phase of Mean Normalised Apparent Mass of 60 subjects (Fairely & Griffin 1989)	~ 5 Hz	
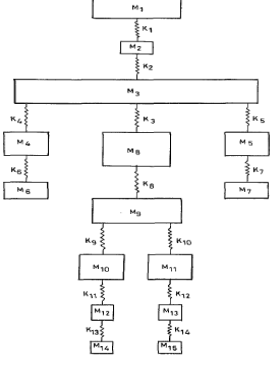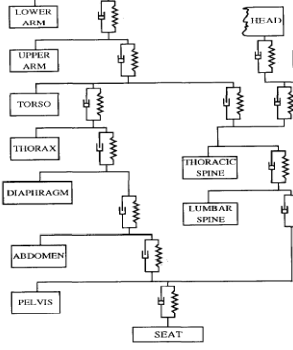
Boileau and Rakheja (1998)	Seated	Both Driving Point Mechanical Impedance and Seat to Head Transmissibility	Lumped Parameter Spring-Mass-Damper Model	Matching of Theoretical Response Curve with Experimental Modulus and Phase of DPMI &STHT in the same study	~ 5 Hz	
Fritz (2000)	Standing, Erect with Hands on Steering Wheel	Transfer Functions Between Ground & Ankle/Hip/Knee Joint	Rigid Body Model with 27 Bodies having 103 d.o.f.	From Published Literature (Markoff 1970, Anderson et al. 1985 etc.) and STHT matching from ISO/CD 5982 data	~5-6 Hz	
Cho & Yoon (2001)	Seated, with Back Support	Hip and Back Transmissibility in Multiple axis	9 d.o.f. Model with Three Rigid Bodies Connected with Spring-Dampers	From Anthropometric Data of Korean males and Transmissibility Measurement from the Same Study	~4-5 Hz	

Matsumoto & Griffin (2001)	Seated	Normalized Apparent Mass, Vertical & Fore-Aft Transmissibility	Four & Five d.o.f. Models connected with Vertical and Rotational Springs and Dampers	From Modal Data of Kitzaki & Griffin, 1997 and Matching of Experimental Data (Matsumoto & Griffin, 1998)	2.53 Hz, 5.66 Hz, 8.62 Hz, 11.5 Hz	
Kitzaki and Griffin (1997)	Seated	Modal Analysis and Normalized Apparent Mass	Two Dimensional Finite Element Model with Beam Elements for Spinal Chord	Matching of Experimental Modal Values from Kitzaki & Griffin (1997) and Inertial Data Available (Liu & Wickstrom, 1973; Williams & Belytschko 1997 etc.)	0.28 Hz, 1.49 Hz, 2.86 Hz, 5.06 Hz	
Kong & Goel (2003)	N.A.	Modal Analysis and Transmissibility at Different Points	Finite Element Model of Human Spine with Beam Elements connected with Joints having Torsional , Lateral, Axial Stiffness	Inertial and Stiffness Data from Computer Topography Scan of Spine and Available Literature (Panjabi et al. 1976, Closkey et al., 1992)	6.82 Hz to 8.91 Hz	
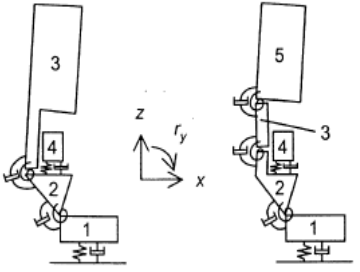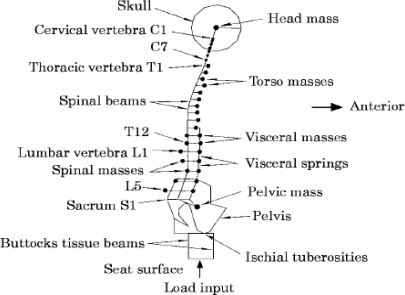
Arnoux et al. (2003)	Seated, with Back Support and hands in Driving Posture	None	Detailed 3-d Finite Element Model of Human Anatomy with 25000 shell/ solid elements	Form Literature (Yamada 1970, Fung 1993, Linde 1994 etc.) and Special Purpose Experimental Studies	N.A.	
Liu et al. (2015)	Seated, Erect	In-Line and Cross-Axis Apparent Mass	Finite Element Model with Five Rigid Bodies Connected with Revolute Joints and Finite Elements for Soft Tissues	From Literature (Dempster 1967, Reynolds 1981) and From Transmissibility Data of Matsumoto & Griffin 2001	1.7 Hz, 6.2 Hz and 13 Hz	
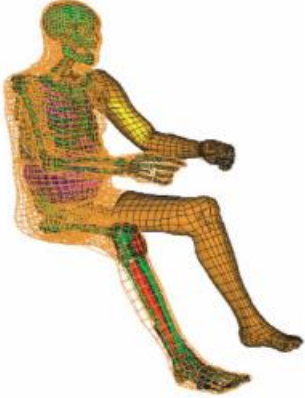
Table 2.1: Summary of Human Body Models Available in the Literature

Bartz & Gianotti (1975) assumed the human body segments to be of ellipsoidal shape to determine the inertial properties of different segments of human body model. Extending this, Nigam and Malik (1987) evaluated the stiffness parameters of the model and then natural frequencies of 50th percentile U. S. male were determined.

To understand the effects of foot-rest, back-rest, posture, muscle tension and vibration magnitude on the dynamic behavior of human body in sitting posture, Fairley and Griffin (1989) conducted experiments upon 60 subjects in seated posture to measure their Apparent Mass while undergoing random excitation in vertical direction. Excitation frequency was from 0-20 Hz and the root mean square (r.m.s) magnitude ranged from 0.25 m-sec^{-2} to 2.0 m-sec^{-2}. Theoretical and experimental studies were conducted by Qassem et al. (1994) to study the effects of vertical and horizontal vibrations coming from seat and hand on the human body. Experiments were performed on 15 seated male students with excitation-frequency 5-500 Hz and transfer functions for arm, torso and head were plotted. For the same, theoretical results were computed using a 12 d.o.f human body model, whose parameter were determined following the scheme available in the literature (Muskian & Nash, 1976; Nigam and Malik, 1987; Bartz & Gianotti, 1975). Modeling the human spine as interconnected finite elements, Kitzaki and Griffin (1997) developed a 2-dimensional human body finite element model to investigate modes of vibration of seated human body. They identified modes of vibration at frequencies ranging from 0.28 Hz to 10 Hz having nodes at C1-C5, T1-T12 and L1-L5 of the spinal column. Model parameters i.e. mass, stiffness and damping were taken from published literature (Liu & Wickstrom, 1973; NASA, 1978; Williams & Belytschko, Kitazaki & Griffin, 1997) and experimental modal analysis.

Simplified 1 d.o.f. and 2 d.o.f lumped parameter human body models for predicting seat transmissibility were proposed by Wei and Griffin (1998). Curve fitting the experimental values of Apparent Mass obtained by Fairley & Griffin (1989) with the theoretical expression, inertial and dynamic parameters of models were determined. In these lumped parameter models, elements were not related to body segments in particular; thus the models only show equivalent mechanical properties of whole human body and are not intended to attribute the contribution of specific body segments. For studying vibration effects on a vehicle driver, Boileau and Rakheja (1998) measured DPMI of seated humans in 0.625-10 Hz range with hands in driving position and a corresponding 4 d.o.f. linear human body model was developed to predict DPMI and STHT. Model parameters were obtained by minimizing the difference between experimental and theoretical results of seated human body for both DPMI and STHT simultaneously. Subsequently the model was modified to a semi-definite 3 d.o.f. model with body mass dependent parameters (Boileau et al, 2002). Experimental results were grouped in three different body mass categories, and constraint optimization was performed to acquire model parameters for different groups.

To understand the effects of vibration on joints of a standing person, Fritz (2000) used a 103 d.o.f. model with 27 rigid bodies whose parameters were identified from published literature (Markoff, 1970; Punjabi et al., 1976; Anderson et al., 1985; Luo & Goldsmith, 1991) and through fitting STHT to the results reported in ISO/CD 5982 (1999) for sitting posture. The model was then used to calculate transfer functions between ground excitation and different body segments for a person in standing posture. Comparison of transfer functions of different segments indicated that ankles and spine withstood higher forces than knees and hips during vibration. For examining

quality of vehicle ride, Cho and Yoon (2001) measured transmissibility between floor & hip surface, floor & back surface and floor & head for 10 subjects under random vibrations ranging from 1-25 Hz in vertical direction. The seated human body was modeled by three rigid masses having total 9 degrees of freedom. The inertial parameters for the 9 d.o.f. model were estimated using the published anthropometric data for Korean adults (Park et al., 1999). Dynamic properties of the model were determined by fitting the experimental data for transmissibility with the theoretical results obtained for the model.

For mathematical modeling of human body in proximity to resonance frequency of about 5 Hz, Matsumoto and Griffin (2001) developed 4 d.o.f and 5 d.o.f lumped parameter human body models including rotational degree of freedom. Geometrical and inertial parameters of the model were obtained from earlier work (Kitazaki & Griffin, 1997) and dynamic parameters were determined by matching experimental results (Matsumoto & Griffin, 1998) with theoretical results for Apparent Mass and transmissibility. Modal analysis identified the principal resonant mode to be the vertical motion of legs and pelvis combined with pitching motion of pelvis. To identify body segments prone to injuries due to ship shock motion, Zong and Kim (2002) used a 4 d.o.f. nonlinear biodynamic model coupled with ship structure. In their model, each lumped mass represented a group of body parts whose parameters were identified from earlier experimental results (Liu et al, 1998). The results showed that body segments in direct contact with ship structure are at increased risk of injury. Matsumoto and Griffin (2003) developed theoretical 1 d.o.f. and 2 d.o.f lumped parameter model for standing posture. Parameters of the model were determined by minimizing the difference between theoretical and experimental values (Matsumoto & Griffin, 1998] of Apparent Mass for standing persons.

To develop biomechanical models for ride quality simulation, Kim et al. (2005) conducted experiments on five seated subjects undergoing random vibration in vertical direction in the range of 1-50 Hz. Results of the experimental study were used to develop a 14 d.o.f human body model with 6 rigid bodies representing human body segments. Inertial properties of the model were determined through data available in the literature (Park et al, 1999; Privitzer & Belytschko, 1980; Adrian & Cooper, 1995). Stiffness and damping properties of the model elements were determined by optimizing transmissibility values of theoretical model with experimental results. To identify the effects of vibration input from seat backrest while driving, Rakheja et al. (2006) conducted experiments on 24 subjects in driving posture. A 4 d.o.f. human body model coupled with inclined seat and pan was developed to study vibration interaction with seat backrest. Theoretical expression for Apparent Mass was derived and model parameters were identified by grouping experimental results in different weight categories and optimizing the difference between theoretical and experimental results.

To estimate effects of magnitude of applied excitation and standing posture on Apparent Mass, Subashi et al. (2006) conducted experiments on 12 standing male subjects. The experimental results indicated that the frequency, at which Apparent Mass and cross-axis Apparent Mass were maximum, varied with the magnitude of the applied excitation and also with the position of bent knees. The authors later used these experimental results to construct 5 d.o.f and 7 d.o.f lumped parameter human body models for simulating response of a standing human body to vertical vibration (Subhashi et al, 2008). In these models, lumped masses represented few segments of the human body. Inertial and geometrical parameters of the model were determined from published literature. Stiffness and damping values for model were estimated by

minimizing difference of NAMS and cross-axis Apparent Mass of theoretical model with the experimental values (Subashi et al., 2006).

Extending the undamped anthropometric model reported by Nigam and Malik (1987), Gupta (2007) estimated damping coefficients of ellipsoidal body segments based on comparison of experimental results for acceleration ratio of head to feet with the values computed from anthropometric vibratory model. Damping parameters were estimated for 50th percentile U. S. male and a group of Indian males. This anthropometric model, based on geometric dimensions of body segments, can provide a better understanding of vibration effect on humans.

To study effects of multi-axis excitation on ride comfort, Kim et al (2011) conducted experiments on a seated person with excitation in the range of 1-20Hz. The person was subjected to translational excitation in two mutually perpendicular axes and rotational excitation about the axis perpendicular to both translational excitation axes. A 5 d.o.f. lumped parameter model was developed whose parameters were obtained through matching experimental and theoretical results for apparent inertia matrix. These parameter values are not representative of physical values related to human body segments. To study effects of backrest on a seated person during multi-axis vibration, Zheng et al (2011) developed 7 d.o.f multi-body human body model. The rigid bodies used in model represented some human body segments whose inertial parameters were obtained from literature (Dempster & Gaughran, 1967; Qiu & Griffin, 2009). Dynamic parameters of the model were obtained by using 'fmincon' optimization in MATLAB to fit experimental data (Qiu & Griffin, 2009) for vertical and cross-axis Apparent Mass of the human body.

To understand resonance behavior of the human body, Kitazaki and Griffin (1999) applied random vibration of constant power spectra on eight male subjects in the seated posture and measured normalized apparent mass vis-à-vis frequency of applied excitation. Experimental data suggested a principle resonant frequency around 4.9 Hz corresponding to an entire body mode. Subsequently, authors used measured experimental data to develop a finite element (FE) model of a seated body (2001) consisting of 134 elements and 87 degrees of freedom (d.o.f.). Inertial and stiffness data of different beam, spring and mass elements were obtained from existing literature and modal damping ratios were estimated by comparing theoretical apparent mass with the experimental measurements.

Subhasi et al (2001) measured NAMS and cross-axis apparent mass (CAMS) of twelve male subjects in different standing postures at multiple root mean square (r.m.s.) values of random excitation and investigated the effect of posture and muscle tension on the dynamic response of human body. Resonant frequencies of both NAMS and CAMS were affected by the r.m.s. value of excitation and posture of the subject. Same authors later developed five and seven d.o.f. lumped parameter models (2003) of standing subjects based on the experimental measurements. Inertial and geometrical parameters of the model were adopted from existing literature and stiffness and damping properties were estimated from comparison of theoretical response curve with experimental data. Modal analysis revealed that the dominant peak of NAMS is associated with the undamped natural frequency of 6.13 Hz.

A finite element model of human body for head-to-sacrum, including the rib cage, thorax and cervical spine, was developed to predict vibration response of spinal column by Kong and Goel (2003). In this model, beam elements were used to model thoracic and cervical segments which are rigidly interconnected. Numerical

simulations showed that the first resonant frequency for vertical vibration decreases as the contribution of self-weight of lower body segments is increased.

A detailed 3-D finite element model of the human body consisting bones, ligaments, muscles, tendons etc. was developed as part of the HUMOS project to replicate injury mechanism of crash victims (Arnoux et al & Behr et al). Body constituents like bones, ligaments, skin were modeled using shell/solid elements whereas soft tissues such as muscles, internal organs, tendons etc. were modeled as elastic/ viscoelastic material. Constituent properties of this exhaustive human body model were obtained either from the existing literature (Yamada, 1970; Shuck and Advani, 1972; Fung, 1993; Linde, 1994) or from some special purpose experimental studies (Arnoux et al., 2001). Comparatively large size of the model (25000 elements) along-with the time step required for simulation (1μsec), limits the usefulness of this model for WBV studies.

Liu et al (2015) developed a 3-D finite element model of the seated person to estimate body-seat interaction i.e., pressure distribution. The model consisted of five rigid bodies joined by revolute joints and surrounded by deformable elements representing soft tissues. Geometrical parameters and mass of the body segments were taken from existing literature (Dempster 1967, Reynolds 1981). Stiffness and damping parameters of the model were adjusted to fit experimentally measured value of vertical in–line and cross-axis apparent mass of a person seated on a rigid seat.

The results of experimental studies have shown that in addition to the frequency of applied excitation, dynamic response of the human body is dependent on magnitude of applied excitation, type of excitation applied (harmonic, random, single-axis, multi-axis), posture of the person and body mass of the person among other factors. Experimental studies on different groups of seated subjects exposed to vertical

excitations have exhibited some consistent patterns during measurement of driving point mechanical impedance (DPMI), normalized apparent mass (NAMS) and seat to head transmissibility (STHT) etc. (Coermann 1962, Fairley and Griffin 1989, Paddan and Griffin 1993). The first and second resonant peaks are found between 4 to 6 Hz and 8 and 12 Hz respectively. Also, the response has been found function of vibration magnitude and sitting posture. The data recorded during these studies has formed the basis of developing models of human body to replicate experimental observations. Model development is desirable to reduce adverse effects of vibration by design modifications of systems generating vibratory environments and also to develop a better mechanism of vibration isolation/reduction based on simulation using the models developed. Lumped parameter models developed in studies discussed above have little to no resemblance to human anatomy for both seated and standing posture. The physical and mechanical properties of body such as mass, stiffness and damping have been estimated either experimentally or by fitting the experimental dynamic response with the theoretical model based response. Although simple to formulate, these models lack in their ability to provide an accurate description of effects of vibration on various segments of the human body. Finite element models that are developed to generate modal information of human body are complex in nature. It is desirable to develop models that can be related readily to human body segments thus being useful in developing a more realistic understanding of effects of vibration on human health.

2.5 Motorcycle Modeling: The preceding section dealt studies related with WBV of human body and modeling of the same. In the present work, dynamic analysis of motorcycle-riser system has been performed utilizing an existing rigid body

motorcycle model. Therefore, a short overview of various approaches used to model a two-wheeler is provided.

An experimental study was conducted by Chen et al (2009) on twelve two-wheelers at different speeds to measure vibration dose value (VDV) to motorcycle riders due to road undulations. The experiments were conducted with different types of scooters and motorcycles on roads with different profiles. The tri-axial acceleration of riders was recorded at pelvis location to determine VDV. The study indicated that compared to riders of four wheelers, two-wheeler riders are exposed to much higher VDV keeping same road profile and speed and this value was found depending significantly on type of road and speed of the two- wheeler. Moreno et al (2011) conducted an experimental study to understand effects of WBV on motorcycle riders and effects of rider's age, mass, size of motorcycle engine and type of road. Using neural networks and ANOVA, vibration exposure time for safe riding was determined based on threshold exposure according to European standards. Results indicated that old motorcycles with small engines travelling on city roads (with high traffic and bumps) resulted in greater vibration exposure for motorcycle riders.

Verma et al. (1980) investigated dynamics of an uncontrolled motorcycle on a level, straight road. Twp lumped masses representing rear frame (with rider) and the front frame were connected by springs with rear wheel and front wheel respectively, to model the motorcycle and include frame compliance. By solving a set of thirty two linear first order differential equations, eigenvalues and eigenvectors of weave, wobble and capsize mode were calculated for a commercial motorcycle.

Author	Methodology Used	Model Description	Rider Description	Results Calculated	Figure of the Model
Verma et al. (1980)	Eight d.o.f. multibody model using Lagrangian dynamics and natural coordinates approach	Modeled motorcycle as four rigid bodies having eight natural coordinates; EOM derived using energy and virtual work approach.	Rider rigidly connected to motorcycle frame and its mass was added to rear frame.	Lateral Dynamics of motorcycle and Eigen values associated with different modes. Also effect of frame compliance on eigenvalues.	
Sharp & Limebeer (2001)	Multi Body Model using AutoSim ®	Using Koenen (1983) tyre model, steering behavior of motorcycle in straight and steady turning motion.	Rider upper body was included as a point mass in model.	Root Locus Plots for Straight and steady turning. Quasi equilibrium state for the same.	
Sharp et al. (2004)	Multi Body Model	Inclusion of Frame compliance, mono-shock suspension and Magic tyre formula in Sharp & Limebeer (2001) model	Lower body was taken as part of main frame and upper body was modelled as having roll d.o.f.	Results for Steady turning and Straight line motion. Parametric study of motorcycle behaviour	
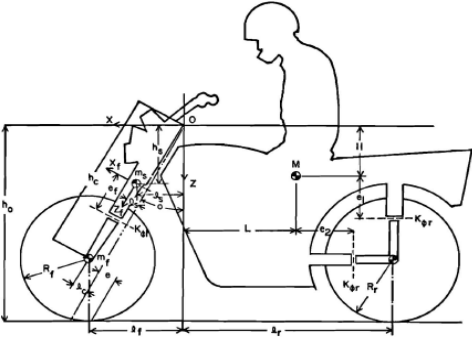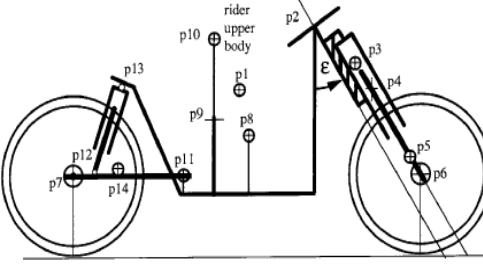
Cossalter et al. (1995)	Three d.o.f linear model treating vehicle as two separate functional blocks.	Maneuverability and handling of motorcycle determined for straight running using tyre force computation	Rider was not included in the model; except as a source of steering torque.	Transfer functions between tyre forces and lateral displacement as a function of frequency	
Cossalter et al. (2000)	Seven d.o.f. multibody model using Constrained Lagrangian dynamics and natural coordinates approach	Modeled motorcycle as four rigid bodies having ten natural coordinates; EOM derived using energy and virtual work approach.	Rider rigidly connected to motorcycle frame and its mass was added to C.G. of frame.	Suspension Parameters and Braking Torque that minimize the stopping distance.	
Cossalter et al. (2002)	Eleven d.o.f. multibody model using Constrained Lagrangian dynamics and natural coordinates approach	Fortran code Fastbike ®. Motorcycle composed of six bodies with forty five natural coordinates; A new tyre model.	Rider rigidly connected to motorcycle frame and its mass was added to C.G. of frame.	Steering angle, steering torque and roll angle for lane change and Slalom maneuvers were calculated.	
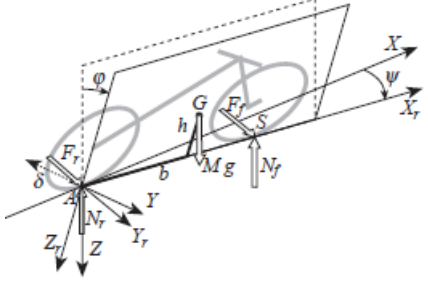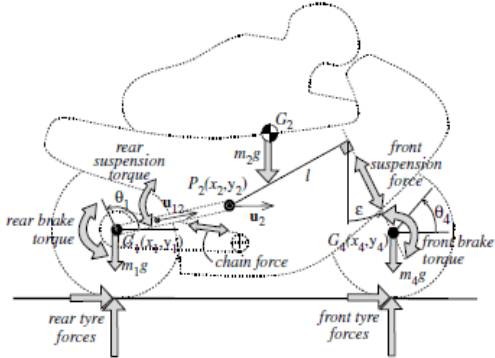
Lai et al. (2003)	Multibody Model of Motorcycle with six d.o.f. using Newton mechanics	Electric Motorcycle composed of three rigid bodies with linearized equation and tyre forces.	The upper body of rider is included having only lean angle of rotation.	Root locus and Bode plots of different transfer functions for straight line motion and cornering.	
Zhu et al. (2012)	Non-linear state space model with ten degree of freedom.	Motorcycle model with four rigid bodies connected with rider upper body and non-linear tyre model.	Lower torso with rear frame and upper torso mass connected with rotational spring and dampers	Effect of rider lean on steady turning and stability of motorcycle on road surfaces with different friction coefficients	
Sequenzia et al. (2015)	Multibody ADAMS ® model of motorcycle and virtual rider.	Motorcycle model with 11 rigid and one flexible body(chassis) and rider model with fifteen rigid bodies having 28 d.o.f.	Kinematic model of rider. 15 rigid bodies connected by fixed, spherical, revolute and planar joints.	Simulation of motorcycle maneuvers/controls on an entire lap effect of rider movement of bike's roll moment.	
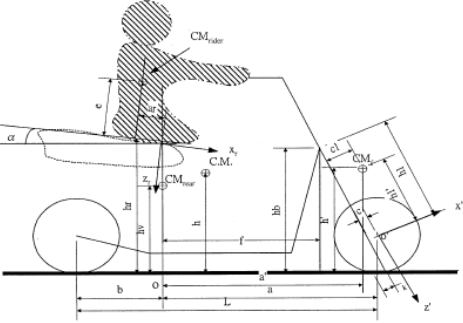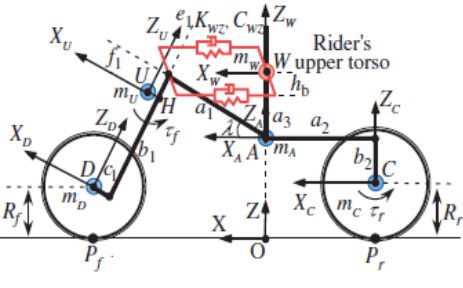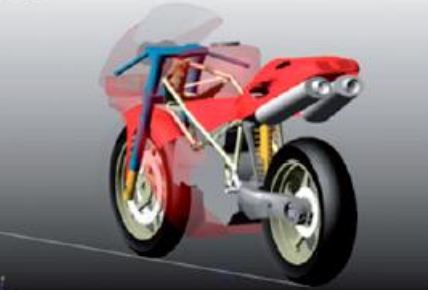
Table 2.2: Summary of Motorcycle Models Available in the Literature

Sharp & Limebeer (2001) developed a mathematical model of motorcycle with rider as a part of rear frame and the wheels were modelled as rigid discs. Using parameter values from Koenen (1983) model, three out of plane modes of vibration of a motorcycle; weave, wobble and capsize, were identified which were dependent on the speed of motorcycle.

The effect of sideslip of tire on the stability of these modes was also studied. In a significant advancement, Pacejka and Bakker (1989) provided magic formula tire model based on extensive measurements and study of tire deformations under different load conditions. The magic formula, modified later on (Pacejka & Bakker, 1992), provides an empirical relationship from which the forces and moments acting from road to tire can be calculated for pure lateral slip, pure longitudinal slip and combined lateral and longitudinal slip. Sharp et al. (2004) made improvements to the earlier model by increasing degree of freedom for main frame, a rigid body for upper body of rider and dynamic tires. Analysis of the model using AUTOSIM, a multibody modelling package, showed that different modes of steering oscillations can be caused depending upon particular wavelength of road undulations.

Zhou et al (2009) developed a 5 degree of freedom (d.o.f.) motorcycle model and simulated response for road undulations. Modelling the motorcycle as lumped parameter system with rider modelled as rigid mass connected by springs and dampers and using Lagrange's formulation; state space equations of the motorcycle-rider system were derived. The response of the system was simulated for vertical excitations of the road which was in agreement with experimental measurements by the same authors.

Cossalter et al (1995) developed a three d.o.f. mathematical model for motorcycle handling and maneuverability which treated the vehicle as two separate functional blocks. Steering system and vehicle system were treated as two separate functional blocks which were connected through tire forces; mass of the rigid rider was included in total mass of the motorcycle. The model accounted for basic inertial properties of the vehicle and estimated forces required to perform a given maneuver. Later on, a seven d.o.f. mathematical model for in-plane dynamic analysis was developed (Cossalter et al, 2000). Using a natural co-ordinates approach, motorcycle was modelled as consisting of four rigid bodies; and the rider was attached rigidly to the rear frame. Equations of motion were derived using Lagrange's multiplier approach and tire forces were taken as function of tire deformation. Using this model, suspension parameters were optimized to minimize the stopping distance during braking.

Based on the same modeling hypothesis, Cossalter & Lot (2002) developed a detailed eleven d.o.f. multibody motorcycle model which simulated both in-plane and out of plane dynamics of the motorcycle. Dividing the motorcycle into a system of six bodies, and by developing an original model for tire forces; a state space formulation of motorcycle dynamics, having 130 variables, was implemented in a Fortran code called FastBike. Theoretical predictions for roll angle, steering angle and steering torque during lane change and Slalom maneuver matched experimental measurements for the same. This model was further improved by inclusion of flexible bodies, various types of suspension linkages and compliance of transmission mechanism (Cossalter et al, 2009)

Using the multibody model developed in Cossalter & Lot (2002), frequency response functions (FRF's) for saddle to road excitations were constructed for frequency range

of 1-20 Hz. Treating the human body as a rigid attachment, and accounting for wheelbase filtering (Cossalter et al., 2006) ; comfort for straight travel of a motorcycle on asphalt roads was also computed. Bevilacqua et al. (2013) and Doria et al. (2013) developed one, three and five d.o.f. biomechanical models of mock-motorcycle with rider to study the effects of roll and yaw oscillations of the motorcycle. Using the measurements collected from specialized tests on mock-setup for roll and yaw oscillations, response to sine sweep oscillation was measured and biomechanical models were developed whose parameters were identified using optimization.

Lai et al. (2003) studied the differences in design and control of electric motorcycles vis-à-vis a conventional motorcycle due to difference in mechanical characteristics of an electric motorcycle. Dividing the electric motorcycle in three different rigid bodies, constant velocity motion of motorcycle was studied, ignoring aerodynamic drag forces. Equations of motion were derived using Newton's law with rider upper body assumed to having roll degree of freedom. Root locus and Bode plots for three modes of motorcycles were plotted and effect of various design parameters, including lower weight of electric motorcycles on perceived rider comfort was analyzed. A nonlinear state space model of motorcycle was developed by Zhu et al. (2012) to study effect of rider motion (lean of upper torso) on motorcycle. Dividing the motorcycle into five rigid bodies with ten d.o.f. and including a nonlinear tyre model, equations of motion were solved to analyze motorcycle motion during steady turning. Stability analysis using a linearized model showed that rider's upper body motion changes the stability of weave modes.

Sequenzia et al (2015) constructed a motorcycle model with flexible frame and rigid mutli-bodies using MDI/ADAMS to simulate the effects of frame flexibility on response of different components during turning and travelling over speed bumps. The

frame was modelled with approx. 12000 shell elements, suspensions were modelled as spring-dampers elements connected by revolute joints, wheels were modelled as discs with gyroscopic effects and rider was composed of 13 rigid parts linked by bushings etc. The model predicted that flexural and torsional deformation of the frame and acceleration of suspension and steering column was lower for model with flexible frame compared to one with rigid frame.

2.6 Research Gap: From the literature survey regarding human body vibration and motorcycle modeling, following research gaps can be listed:

1. Existing Human body vibratory models are either too complicated or they do not resemble with anatomical structure of human body.

2. Anthropometric vibratory models need to be developed and fine-tuned according to the required application i.e. standing; sitting on a car seat; driving a motorcycle.

3. Existing continuums models of human body have large no. of d.o.f. which is not desirable.

4. Motorcycle models have not considered dynamic properties of rider body on overall response of the system.

2.7 Research Objectives:

1. Development and validation of lumped parameter anthropometric vibratory models of human body.

2. Development and validation of finite element based continuum model of human body in standing and sitting posture based on anthropometric data.

3. Development of a finite element based model of motorcycle rider with hands in driving posture.

<center>**Chapter 3**</center>

<center>**Lumped Parameter Models of Standing Subject**</center>

In chapter 2, review of existing literature related to WBV studies of human body indicated a need for vibratory models that not only have some correspondence with the physical structure of human body but are simple to formulate having limited number of degrees of freedom. Existing models of human body can be improved such that individual or group specific vibratory models can be easily formulated. In the present chapter, as a first attempt, lumped parameter models of a standing person subjected to vertical vibration to feet-platform interface, are formulated based on anthropometric data and average properties of human body.

3.1 Human Body Segmentation: Anthropomorphic model of Bartz and Gionatti (1975), which consists of fifteen ellipsoidal segments connected with fourteen joints, shown in Fig.3.1, is adopted to categorize physically distinct segments of a human body. This model assumes that human body segments can be approximated as ellipsoids in shape whose dimensions can be calculated from anthropometric measurements. Bartz and Gionatti (1975) used this model to develop a computer program to calculate average dimensional and inertial parameters of group of males and females.

<center>33</center>
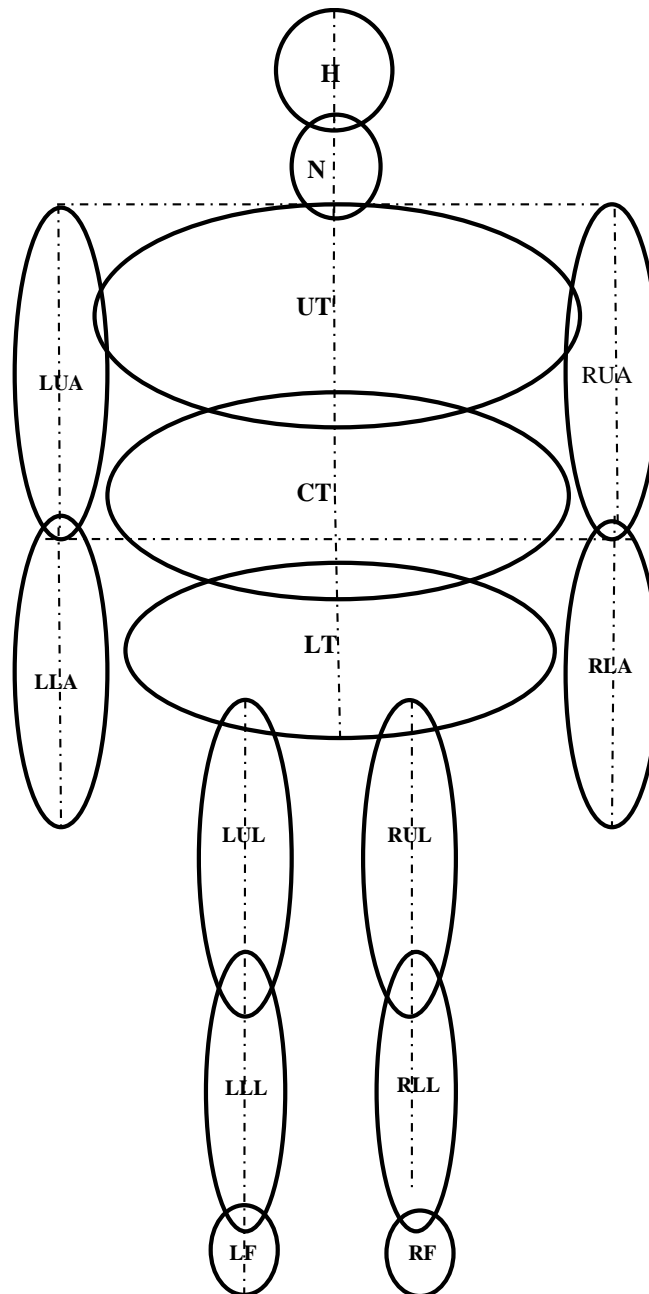
Fig. 3.1: Anthropometric human body model - ellipsoidal elements
(**H**: Head, **N**: Neck, **UT**: Upper Torso, **CT**: Central Torso, **LT**: Lower Torso, **LUA**: Left Upper Arm, **RUA**: Right Upper Arm, **LLA**: Left Lower Arm, **RLA**: Right Lower Arm, **LUL**: Left Upper Leg, **RUL**: Right Upper Leg, **LLL**: Left Lower Leg, **RLL**: Right Lower Leg, **LF**: Left Foot, **RF**: Right Foot)

3.1.1 Ellipsoidal Segments: Dimensions of ellipsoidal body segments are determined employing minimum number of anthropometric measurements, necessary to completely define the model; generally available in anthropometric surveys also. For

i^{th} ellipsoidal body segment; a_i, b_i, c_i are the semi-axes of the ellipsoid as depicted in Fig. 3.2.
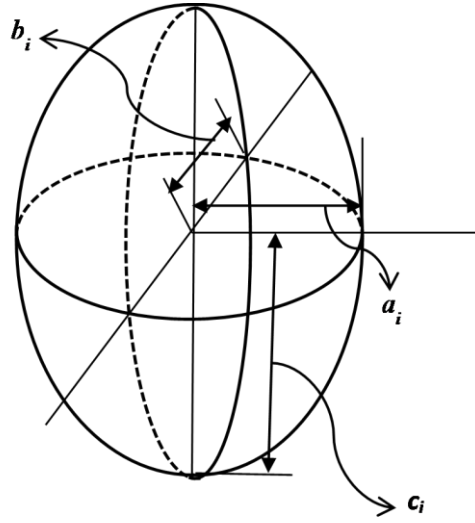
Fig. 3.2: Ellipsoidal segment of human body showing semi axes

Formulae to determine semi-axes (a_i, b_i, c_i) of ellipsoidal segments using anthropometric measurements of a subject are given in Table A of Appendix. In Table A, L_k (k = 1, 2, …, 30) refers to anthropometric dimensions of human body. Table B of the Appendix lists meaning of each L_k and the corresponding values for 50th percentile U.S. male and average Indian male, used for computation of ellipsoidal dimensions in this chapter as well as subsequent chapter of the thesis. As the mass densities of different body parts are almost same (Bartz and Gionatti, 1975); therefore all the ellipsoidal segments can be taken as of equal density. Volume of ith ellipsoidal body segment is $V_i = \dfrac{4}{3}\pi a_i b_i c_i$; mass of the segment (M_i) is obtained by multiplying its volume fraction with static mass (M_{total}) of the subject

$$M_i = \left(\frac{V_i}{\sum\limits_{i=1}^{15} V_i} \right) * M_{total} \qquad i = 1, 2...15 \qquad\qquad (3.1)$$

For lumped parameter vibratory models of human body, ellipsoidal body segments are considered as homogenous, isotropic, and linearly elastic bodies. Since the platform is restricted to move in vertical direction only, the vibrations along vertical axis of ellipsoids are considered to be dominant. Experimental measurements of transmissibility along different axis for standing persons undergoing vertical floor vibration (Paddan & Griffin, 1993) also confirm that the motion of head occurs primarily in the vertical axis. For this, the stiffness of ellipsoids along vertical axis plays major role. Neglecting deformation due to self-weight, the extension of ith ellipsoidal segment (ΔL_i) due to tensile force (F) applied along vertical axis (z axis) is

$$\Delta L_i = \int_{-c_i}^{+c_i} \frac{F}{E_i A_i} dz \qquad (3.2)$$

where, E_i is the Elastic modulus and A_i is the cross-sectional area of ith body segment. Thus the axial stiffness (S_i) of ellipsoidal body segment in vertical direction can be written as (Gupta, 2007)

$$S_i = \frac{F}{\Delta L_i} = \frac{\pi E_i a_i b_i}{c_i \ln\left((c_i + d_i) \middle/ (c_i - d_i) \right)} \qquad i = 1, 2...15 \qquad (3.3)$$

In Eq. (3.3), $d_i = 0.95\, c_i$ represents 5 % truncation of the ellipsoidal segments to account for overlapping contact area of adjacent human body parts. Area contact of truncated ellipsoids represents the actual physical reality of human body segments than point contact due to un-truncated ellipsoidal segments. Damping of ellipsoidal body segments is calculated as:

$$B_i = 2\xi_i \sqrt{(S_i m_i)} \qquad\qquad i = 1, 2 \ldots 15 \qquad\qquad (3.4)$$

where, ξ_i is the corresponding damping ratio for individual ellipsoidal segment.

3.2 Anthropometric Human body vibratory model: The lumped parameter vibratory model for standing subjects, as shown in Fig. 3.3, is constructed by replacing ellipsoidal body segments by rigid masses which are inter-connected through linear springs and dampers. Elemental mass for the model is equal to the mass of corresponding ellipsoidal body segments, determined from Eq. (3.1). Stiffness and damping parameters of connecting springs and dampers in Fig. 3.3 are determined by series combination of stiffness of adjacent segments. The formulae for the stiffness and damping of various elements are given in Table 3.1(Nigam &Malik, 1987).

Table 3.1: Scheme to Combine Ellipsoidal Segments for Lumped Parameter Vibratory Model

j	Ellipsoidal Segments combined (Body Segment No. i)	K_j	C_j
1	Head (1)	S_1	B_1
2	Neck (2) & Upper Torso (3)	$S_2 S_3/(S_2+S_3)$	$B_2 B_3/(B_2+B_3)$
3	Upper Torso (3)& Central Torso (8)	$S_3 S_8/(S_3+S_8)$	$B_3 B_8/(B_3+B_8)$
4	Upper Torso (3) & Right Upper Arm (4)	$S_3 S_4/(S_3+S_4)$	$B_3 B_4/(B_3+B_4)$
5	Upper Torso (3) & Left Upper Arm (5)	$S_3 S_5/(S_3+S_5)$	$B_3 B_5/(B_3+B_5)$
6	Right Lower Arm (6)	S_6	B_6
7	Left Lower Arm (7)	S_7	B_7
8	Central Torso (8) & Lower Torso (9)	$S_8 S_9/(S_8+S_9)$	$B_8 B_9/(B_8+B_9)$
9	Lower Torso (9) & Right Upper Leg (10)	$S_9 S_{10}/(S_9+S_{10})$	$B_9 B_{10}/(B_9+B_{10})$
10	Lower Torso (9) & Left Upper Leg (11)	$S_9 S_{11}/(S_9+S_{11})$	$B_9 B_{11}/(B_9+B_{11})$
11	Right Upper Leg (10) & Right Lower Leg (12)	$S_{10} S_{12}/(S_{10}+S_{12})$	$B_{10} B_{12}/(B_{10}+B_{12})$
12	Left Upper Leg (11) & Left Lower Leg (13)	$S_{11} S_{13}/(S_{11}+S_{13})$	$B_{11} B_{13}/(B_{11}+B_{13})$
13	Right Foot (14)	S_{14}	B_{14}
14	Left Foot (15)	S_{15}	B_{15}

It is to be noted that in Table 3.1, the counter 'j' stands for spring and damper element shown in Fig. 3.3 whereas the counter 'i' stands for ellipsoidal segment shown in Fig. 3.1.
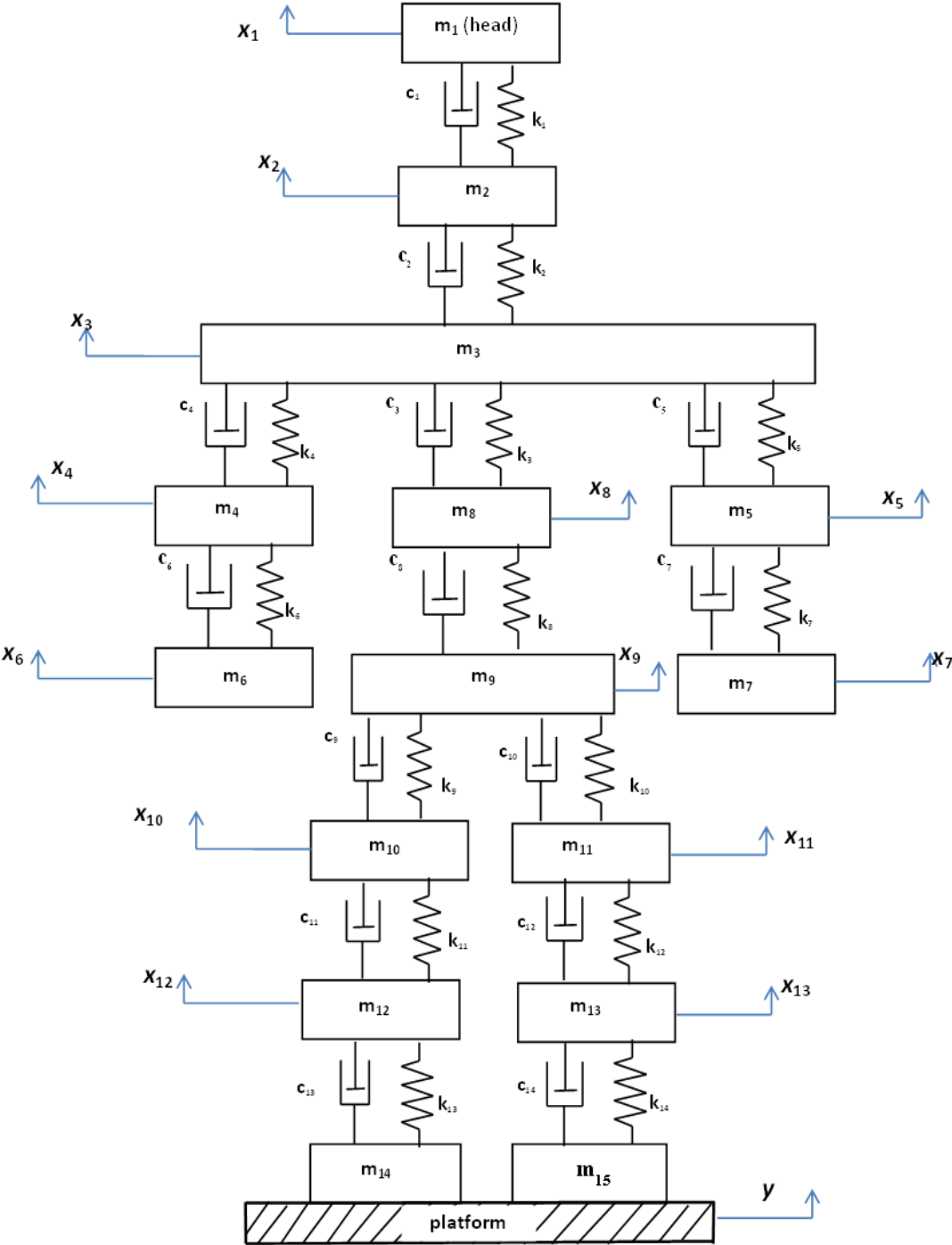
Fig. 3.3: Anthropometric vibratory model of standing human subjected to base excitation

Thus inertial and stiffness properties of the human body vibratory model are determined using anthropometric data, mass of the person and elastic moduli & damping coefficient of ellipsoidal body segments. Rigid masses of vibratory model (Fig. 3.3) represent actual human body segments and their responses in vibratory environment are representative of the response of actual body segments. Determination of E_i and ξ_i (Eqs. 3.3 and 3.4 respectively) enables us to completely determine parameters of anthropometric human body vibratory model.

3.3 Dynamic Response of a standing subject under vertical excitation: For a person in standing posture undergoing vertical vibration from supporting platform, as shown in Fig. 3.3, it is contended that there is no relative motion between the rigid platform and the feet of subject. This assertion is further supported by the description of experimental procedure for measurement of *TR* by Garg & Ross (1976) ('… subject was comfortable but restrained from changing the position of his feet during the experiment…') and by Gupta (2007) ('…subject stands on table with feet strapped to table…'). Thus feet motion in the vibratory model is equivalent to the motion of rigid platform itself and thus the fifteen d.o.f anthropometric human body model under vertical excitation at feet is reduced to a thirteen d.o.f. positive definite system with support motion as shown in Fig. 3.3.

For the system shown in Fig. 3.3, equations of motion under support excitation are

$$[\mathbf{M}]_{13\times13}\left\{\ddot{x}\right\}_{13\times1}+[\mathbf{C}]_{13\times13}\left\{\dot{x}\right\}_{13\times1}+[\mathbf{K}]_{13\times13}\left\{x\right\}_{13\times1}=\left\{F\right\}_{13\times1} \qquad (3.4)$$

where, $[\mathbf{M}]_{13\times13}, [\mathbf{K}]_{13\times13}, [\mathbf{C}]_{13\times13}$ are the mass, stiffness and damping matrix respectively of thirteen d.o.f. vibratory model shown in Fig. 3.3. $\left\{F\right\}_{13\times1}$ and $\left\{x\right\}_{13\times1}$

are the column vectors corresponding to the force generated due to platform motion (y) and the absolute displacement of vibratory model elements respectively.

$$\{\boldsymbol{F}\}_{13\text{x}1} = \left\{0\ 0\ 0\ 0\ 0\ 0\ 0\ 0\ 0\ 0\ 0\ \left(k_{13}y + c_{13}\dot{y}\right)\ \left(k_{14}y + c_{14}\dot{y}\right)\right\}^{\text{T}}$$
$$\{\boldsymbol{x}\}_{13\text{x}1} = \left\{x_1\ x_2\ x_3\ x_4\ x_5\ x_6\ x_7\ x_8\ x_9\ x_{10}\ x_{11}\ x_{12}\ x_{13}\right\}^{\text{T}} \tag{3.5}$$

Similar to the case of support motion of single d.o.f. system, here y and $\dot{y}$ represent displacement and velocity of the platform. Due to the symmetry of anthropometric model, $k_{13} = k_{14}$ and $c_{13} = c_{14}$. For harmonic excitation of the platform;

$$y = Y\ e^{\text{j}\omega t} \tag{3.6}$$

the apparent mass (*AM*) for vibratory model is given as:

$$AM = \frac{F_{interface}}{\ddot{y}}\ \ = \ \frac{\sum\limits_{j=1}^{13} m_j\ \ddot{x}_j + \sum\limits_{j=14}^{15} m_j\ \ddot{y}}{\ddot{y}} \tag{3.7}$$

By dividing apparent mass by the static weight of person; normalized apparent mass (M_{NMS}) is determined.

$$M_{NMS} = \frac{AM}{M_{total}} \tag{3.8}$$

Transmissibility of a human body related to vibrational studies is defined as '… the non-dimensional ratio of response amplitude of a system in steady-state forced vibration to the excitation amplitude expressed as a function of the vibration frequency…' (Griffin,1990). For a person standing in upright posture subjected to vertical excitation from the rigid platform, an important parameter is platform-to-head transmissibility ratio (*TR*) and defined as the ratio of steady state acceleration of head

and acceleration of vibrating platform. For harmonic excitation of platform (Eq. 3.6); platform to head transmissibility (*TR*) of a standing subject is defined as:

$$TR = \frac{\ddot{x}_1}{\ddot{y}} = \frac{\omega^2 X_1}{\omega^2 Y}$$

(3.9)

X_1 and Y are in general complex quantitates representing displacement amplitudes of head and platform respectively and therefore computed value of *TR* in Eq. (3.9) is also a complex quantity having both modulus and phase.

3.4 Anthropometric vibratory model with constant *E*: As detailed in previous sections, driving point impedance parameters for anthropometric human body vibratory model of a standing subject (Fig 3.3) can be computed , for given *E* and *ξ* values of individual ellipsoidal segments. Nigam & Malik (1987), Singh et al. (2015) and Gupta (2007) used constant value of elastic moduli, i.e. the geometric mean of elastic modulus of bones (E_b) and tissues (E_t) of human body, for all ellipsoids. With E_b = 22.6 GN/m^2 and E_t = 7.5 kN/m^2 (Goldman & Gierke, 1961), geometric mean is $E_G = \sqrt{E_b E_t}$ = 13.02 MN/m^2. The elastic moduli of bone (E_b) is in GPa whereas that of tissue (E_t) is in kPa; geometric mean gives a meaningful way of accounting for contribution of both moduli as compared to arithmetic or harmonic mean. Using $E_i = E_G$ for all ellipsoidal segments in Eq. (3.3) and following the scheme given in Table 3.1, stiffness of spring elements of vibratory model are calculated; and listed in of Table 3.3. Anthropometric parameters of 50th percentile U.S. male (listed in Table B of Appendix) were used for computation of the semi-axis of ellipsoidal segments. To calculate B_i values for ellipsoidal segments (Eq. 3.4), corresponding values of damping ratios (ξ_i) are required. As an initial estimate, damping ratio values of

ellipsoidal segments listed in Table 3.2 are used. These values were determined by Gupta (2007) based on the sensitivity of resonant peaks relative to damping ratios of the ellipsoidal segment at different natural frequencies.

Table 3.2 Damping ratios for ellipsoidal segments 50th percentile US male (Gupta, 2007)

Body Segment	H	N	UT	RUA, RLA, LUA, LLA	CT	LT	RUL, RLL, LUL, LLL	LF, RF
Damping Ratio (ξ)	ξ_1	ξ_2	ξ_3	$\xi_4, \xi_5, \xi_6, \xi_7$	ξ_8	ξ_9	$\xi_{10}, \xi_{11}, \xi_{12}, \xi_{13}$	ξ_{14}, ξ_{15}
Value	0.004	0.015	0.002	0.001	0.05	1.0	1.5	1.5

Table 3.3 lists the computed values of different parameters for vibratory model of standing subject for anthropometric data of 50th percentile U.S. male.

Table 3.3: Anthropometric Vibratory Model Parameters of 50th percentile U. S. male with $E_i = E_G$

Mass (M_i)	M_1	M_2	M_3	$M_4=M_5$	$M_6=M_7$	M_8	M_9	$M_{10}=M_{11}$	$M_{12}=M_{13}$	$M_{14}=M_{15}$
Value (kg)	2.86	0.21	17.11	2.45	2.48	15.55	11.88	4.65	3.09	0.97

Stiffness K_i	K_1	K_2	K_3	$K_4=K_5$	$K_6=K_7$	K_8	$K_9=K_{10}$	$K_{11}=K_{12}$	$K_{13}=K_{14}$
Value (kN/m)	681.38	846.54	465.27	142.83	98.23	554.55	131.13	69.17	1918.5
Damping C_i	C_1	C_2	C_3	$C_4=C_5$	$C_6=C_7$	C_8	$C_9=C_{10}$	$C_{11}=C_{12}$	$C_{13}=C_{14}$
Value (N-m/sec)	11.17	10.39	16.82	1.18	0.99	337.14	1932.1	1079.4	4103.2

Employing the values listed in Table 3.3, M_{NMS} for 50th percentile U.S. male in normal standing posture undergoing vertical vibration is calculated for frequency range of 0-20 Hz with a step of 0.05 Hz. Figs. 3.4(a) & 3.4(b) show the comparison between the computed modulus and phase of M_{NMS} value and experimentally measured mean value of M_{NMS} (Matsumoto & Griffin, 1998) for a group of subjects. Experiments were

conducted on twelve male subjects standing in comfortable upright posture over a rigid platform undergoing random vibration of 1.0 ms^{-2} r.m.s. in the vertical direction.

(a)
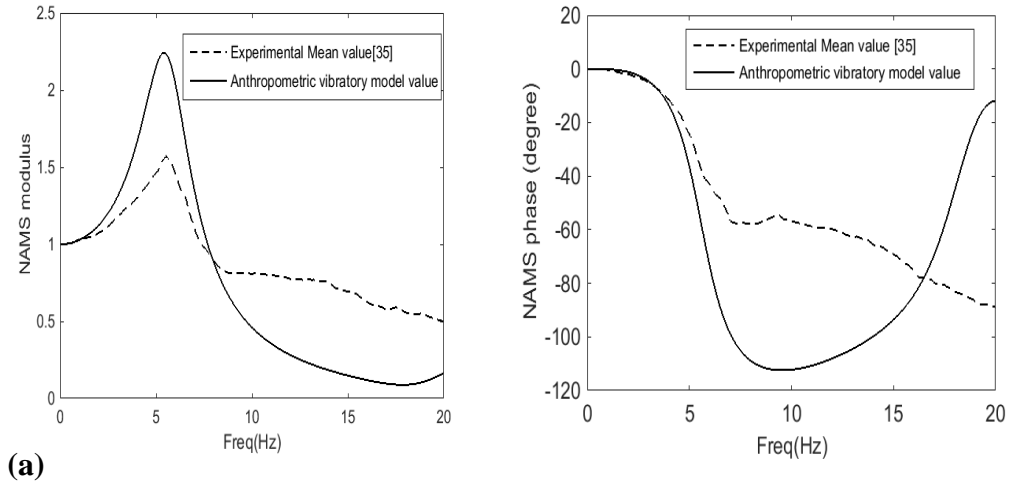
Fig. 3.4: M_{NMS} **computed from anthropometric vibratory model (for ξ values of Table 3.2) and mean experimental data (Matsumoto & Griffin, 1998) (a) modulus of** $_{MNMS}$ **(b) phase of** $_{MNMS}$

Fig. 3.4(a) exhibits good agreement, for the resonant frequency of $_{MNMS}$ modulus, between the experimental values reported in the literature and the values calculated from the anthropometric vibratory model. The difference between magnitudes of experimentally measured and theoretically computed values of M_{NMS} modulus requires further investigation. Fig. 3.4(b) also exhibits good match, for the magnitude of M_{NMS} phase, between the two curves in the frequency range of 0-5 Hz but variation is observed for the frequency range of 5-20 Hz. In the vibratory model, all parameters are based on anthropometric data of 50th percentile US male except for the damping ratios of ellipsoidal body segments. These results indicate that the value of damping ratio of ellipsoidal body segments, i.e. 'ξ_i' should be modified to achieve better correspondence with experimental results for M_{NMS}.

3.4.1 Optimization of damping ratio for ellipsoidal segments: Assigning ξ_i for different body segments as design variables, optimization was performed to improve

agreement between the M_{NMS} values determined from experimental measurements and anthropometric vibratory model respectively. Objective function (Q) was defined as the sum of difference in magnitude and phase of $_{MNMS}$ between the experimental results and the values obtained from vibratory model:

$$\text{Minimize} \quad Q = Q_m + Q_p \tag{3.10}$$

where, Q_m and Q_p is the difference between experimental and theoretical values, of modulus and phase of M_{NMS} respectively.

$$Q_m = \sum_{i=1}^{N}\left[\left(\left|M_{NMS}\left(\omega_i\right)_{ex}\right| - \left|M_{NMS}\left(\omega_i\right)\right|\right)^2\right]$$
$$Q_p = \sum_{i=1}^{N}\left[\left\{\phi\left(M_{NMS}\left(\omega_i\right)_{ex}\right) - \phi\left(M_{NMS}\left(\omega_i\right)\right)\right\}^2\right] \tag{3.11}$$

where, $\left|M_{NMS}\left(\omega_i\right)_{ex}\right|$, $\phi\left(M_{NMS}\left(\omega_i\right)_{ex}\right)$ is mean experimental values of the modulus and phase respectively, for vibration magnitude of 1.0 ms^{-2} r.m.s. (Matsumoto & Griffin, 1998) and $\left|M_{NMS}\left(\omega_i\right)\right|$, $\phi\left(M_{NMS}\left(\omega_i\right)\right)$ is the modulus and phase respectively, determined from Eq. (3.8) for the anthropometric vibratory model. 'N' is the number of discrete values of frequency in the range of 0-20 Hz. Constraints upon ξ during optimization are:

$$0 \leq \xi_i \qquad i = 1, 2...15$$
$$\xi_4 = \xi_5 \; ; \; \xi_6 = \xi_7 \; ; \xi_{10} = \xi_{11} \; ; \xi_{12} = \xi_{13} \; ; \xi_{14} = \xi_{15} \tag{3.12}$$

The lower bound of ξ_i is based on fact that for human body segments, damping ratios are nonnegative. Equality constraints for ξ_i between different ellipsoidal segments are due to the symmetry of human body about mid-sagittal plane. Optimized values of damping ratio were determined through Genetic Algorithm (GA)

technique, which is a global search technique and is provided within MATLAB (Mathworks Inc.). The values of ξ_i corresponding to the minimum value of objective function are listed in Table 3.4

Table 3.4: Optimized damping ratios for ellipsoidal body segments (50th percentile US male)

Damping Ratio (ξ)	ξ_1	ξ_2	ξ_3	$\xi_4, \xi_5,$	ξ_6, ξ_7	ξ_8	ξ_9	$\xi_{10}, \xi_{11},$	ξ_{12}, ξ_{13}	ξ_{14}, ξ_{15}
Value	0.024	0.037	2.492	0.007	0.002	2.954	2.994	1.997	1.598	0.425

.

Figure 3.5 shows the comparison between theoretical and experimental values of M_{NMS} for both modulus and phase.
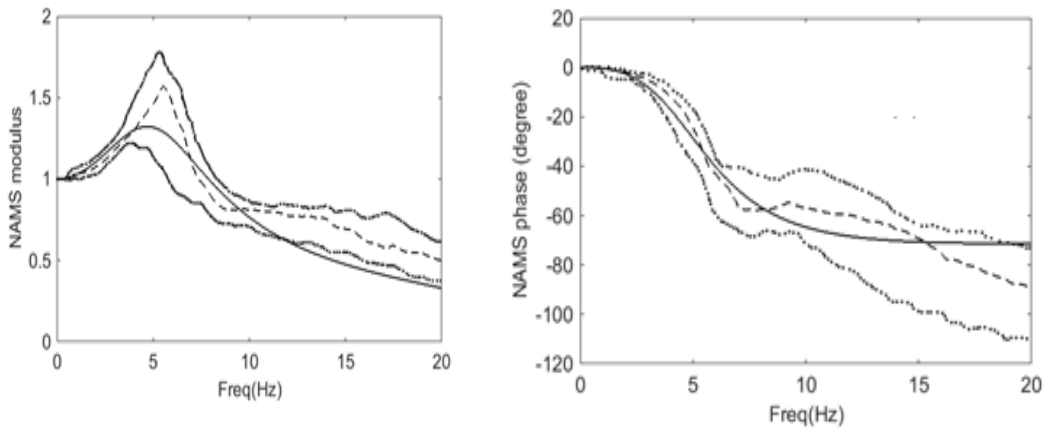
Fig. 3.5: M$_{NMS}$ modulus and phase for standing person subjected to base excitation (-- -- -- experimental mean value; ———— vibratory model value; ◻◻◻◻◻ experimental upper and lower limit)

As observed from Fig. 3.5, the correspondence between the theoretically predicted M_{NMS} and median experimental M_{NMS} still needs to be improved. Therefore, keeping the basic scheme of human body segmentation same as detailed in section 3.1 and 3.2; an improved anthropometric vibratory model of standing subject is formulated.

3.5 Anthropometric vibratory model with optimized E_i and modal damping:
Modal analysis technique was used for computing results from anthropometric

vibratory model of a standing person under base excitation for the improved model. Using modal analysis, system response is written as

$$\{x\} = \sum_{r=1}^{13} \{u\}^r \, \eta_r(t) = [U]\{\eta\} \tag{3.13}$$

where, $\{u\}^r$ is the normalized modal vector and $\eta_r(t)$ represents solution of decoupled single d.o.f. equation corresponding to r^{th} mode. Substituting from Eq. (3.13) in Eq. (3.4) and pre-multiplying by $[U]^{\mathrm{T}}$ yields

$$[\mathbf{I}]\{\ddot{\boldsymbol{\eta}}\} + [\bar{\mathbf{C}}]\{\dot{\boldsymbol{\eta}}\} + \begin{bmatrix} \ddots & & \\ & \lambda_r^2 & \\ & & \ddots \end{bmatrix}\{\boldsymbol{\eta}\} = \{\boldsymbol{P}\} \tag{3.14}$$

where, $\{P\} = [U]^T \{F\}$, is the generalized force vector and λ_r is the modal frequency of rth mode for undamped system. Assuming Rayleigh model of proportional damping, equations of motion for the system are decoupled; resulting in thirteen linearly independent equations:

$$\ddot{\eta}_r + 2\xi_r \lambda_r \dot{\eta}_r + \lambda_r^2 \eta_r = P_r \qquad r = 1, 2, \ldots, 13 \tag{3.15}$$

where, ξ_r is the modal damping ratio associated with r^{th} mode. For harmonic excitation of support;

$$y = Y.\cos(\omega t) \tag{3.16}$$

where, Y is the amplitude of support motion and ω is the frequency of applied excitation. Solution of Eq. (3.15) for r^{th} mode can be written as

$$\eta_r = C_r.\cos(\omega t - \phi_r) \tag{3.17}$$

where $\quad C_r = \dfrac{P_r}{\lambda_r^2} \dfrac{1}{\sqrt{\left\{1-\left(\omega/\lambda_r\right)^2\right\}^2 + \left\{2\xi_r \omega/\lambda_r\right\}^2}}$ $\quad$ and $\quad \phi_r = \tan^{-1}\left[\dfrac{2\xi_r \left(\omega/\lambda_r\right)}{1-\left(\omega/\lambda_r\right)^2}\right]$

Using the solution η_r from Eq. (3.17), the dynamic response can now be determined from Eq. (3.13), which is

$$\{x\} = \sum_{r=1}^{13}\{u\}^r \eta_r(t) = \sum_{r=1}^{13}\{u\}^r C_r \cos\left(\omega t - \phi_r\right) \qquad (3.18)$$

In the present case, under vertical harmonic excitation, platform-to-head transmissibility ratio (*TR*) for the vibratory model is expressed by Eq. (3.9) which is reproduced here as

$$TR = \frac{\ddot{x}_1}{\ddot{y}} = \frac{\omega^2 X_1}{\omega^2 Y} \qquad (3.19)$$

where, $\ddot{x}$ is the acceleration of head (m_1) determined from Eq. (3.18) and $\ddot{y}$ is the acceleration of supporting platform derived from Eq. (3.16). As stated before, X_1 and *Y* are complex quantitates representing displacement amplitudes of head and platform respectively and therefore computed value of *TR* in Eq. (3.19) is also a complex quantity. The modulus of *TR* is used for comparison with experimental data vis-à-vis frequency of applied excitation. The phase difference between support excitation and motion of head varies with the frequency of excitation; but comparison is based on the amplitude for ratio of excitation and response solely.

Numerical simulation of platform-to-head transmissibility ratio (*TR*) using modal analysis revealed that the mode whose frequency is closest to the frequency of

peak in *TR*-frequency curve has dominant participation in dynamic-response i.e. *TR* value and the contribution of other modes is negligible. Keeping this in view, the modal damping ratios were determined from experimentally measured *TR*-frequency plots available in the literature.

3.5.1 Modal damping ratios: As discussed in the preceding section, only one mode is dominant at/near different peaks of transmissibility response for multi d.o.f. system. Accordingly, modal damping ratio corresponding to each peak of the response curve can be determined from the methodology devised, in the following section, for the support motion analysis of single d.o.f. system.

The transmissibility ratio (*TR*) for a single d.o.f system subjected to harmonic support motion is (Rao & Gupta, 1999):

$$|TR| = \left| \frac{\overset{..}{x}}{\overset{..}{y}} \right| = \sqrt{\frac{1+\left(2\xi r\right)^2}{\left(1-r^2\right)^2+\left(2\xi r\right)^2}} \qquad (3.20)$$

where, ξ is the damping ratio, $r = \omega/\omega_n$ is the frequency ratio and ω_n is the natural frequency of system. The frequency ratio corresponding to peak value of *TR* (Rao & Gupta, 1999) is expressed as

$$r_{pk}^{TR} = \frac{\omega_{pk}^{TR}}{\omega_n} = \frac{\sqrt{\left[\left(\sqrt{1+8\xi^2}\right)-1\right]}}{2\xi} \qquad (3.21)$$

The dynamic magnifier for forced vibration of single d.o.f system is:

$$DM = \frac{X}{X_{st}} = \frac{1}{\sqrt{\left(1-r^2\right)^2+\left(2\xi r\right)^2}} \qquad (3.22)$$

and the frequency ratio corresponding to peak value of *DM* is given by

$$r_{pk}^{DM} = \frac{\omega_{pk}^{DM}}{\omega_n} = \sqrt{1 - 2\xi^2}$$ (3.23)
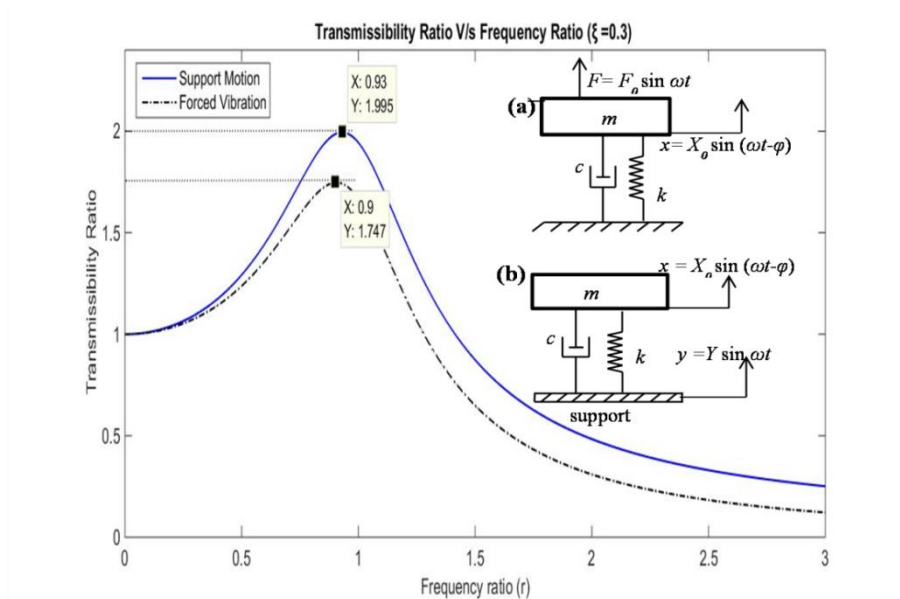
Fig. 3.6: Response of single d.o.f. system (a) for forced vibration and (b) under support excitation

Modulus of *TR* and *DM* are plotted as a function of frequency ratio (*r*) in Fig. 3.6, for ξ =0.3. It is evident from Fig. 3.6 that the frequencies corresponding to peaks for *TR* and *DM* are quite close to each other and in close proximity to the natural frequency of the system (*r* = 1.0). For example, if ξ =0.3 and $\omega_n = \sqrt{k/m}$ =10 rad/s for vibratory systems shown in Figs. 3.6(a, b); the frequency corresponding to respective peaks, calculated using Eqs. (3.21, 3.23), comes out to be: $\omega_{pk}^{TR} = 9.30$ and $\omega_{pk}^{DM} = 9.05$. The difference between ω_{pk}^{TR} and ω_{pk}^{DM} is found to be less than 3%. Hence, peaks in *TR* plots can be considered to be located nearly at the natural frequencies of system and therefore the estimated value of modal damping ratios using the iterative scheme described in the next section can be attributed to respective natural frequencies. The correspondence between estimated modal damping ratio and

natural frequency is essential for determining modal damping ratios of those natural frequencies for which peaks in the experimental plots are suppressed.

3.5.2 Iterative scheme to determine modal damping ratios: A sample plot of *TR* as a function of excitation frequency (ω) of support motion is shown in Fig. 3.7.
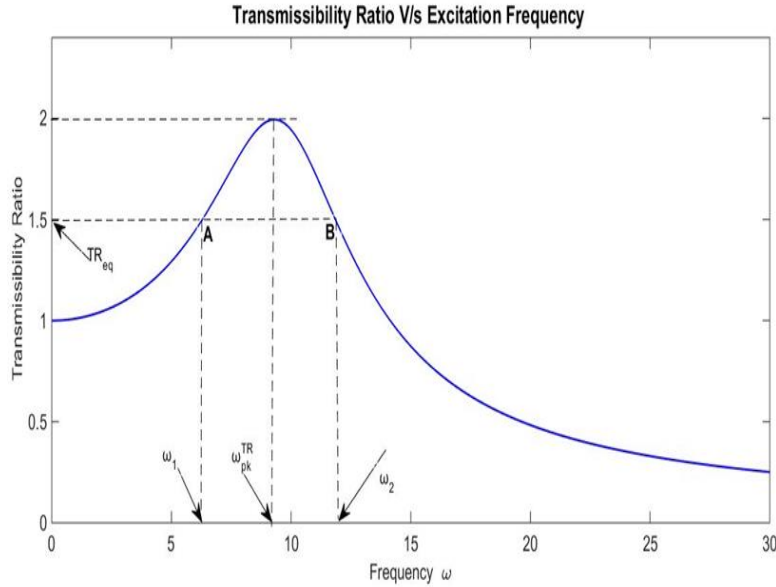
Fig. 3.7: Sample plot for response of single d.o.f. system under support excitation

In Fig. 3.7, ω_{pk}^{TR} is the excitation frequency for peak value of *TR* and ω_1 & ω_2 are excitation frequencies on either side of ω_{pk}^{TR} having the same value of *TR*, i.e. TR_{eq}. Using these data from Fig. 3.7, an iterative algorithm is developed to determine damping ratio corresponding to any specific peak of *TR*. Firstly, Eq. (3.20) is rearranged as

$$\xi = \left| \left(\frac{1}{2r} \right) * \sqrt{\frac{\left(1 - r^2\right)^2 TR^2 - 1}{\left(1 - TR^2\right)}} \right| \tag{3.24}$$

Frequency ratio corresponding to peak value of *TR* is:

$$r_{pk}^{TR} = \frac{\omega_{pk}^{TR}}{\omega_n} = \frac{\sqrt{\left[\left(\sqrt{1+8\xi^2}\right)-1\right]}}{2\xi} \tag{3.25}$$

Now an initial guess of damping ratio is made, say $\xi^{(0)}$. From Eq. (3.25):

$$\omega_n^{(0)} = \omega_{pk}^{TR} \frac{2\xi^{(0)}}{\sqrt{\left[\left(\sqrt{1+8\left(\xi^{(0)}\right)^2}\right)-1\right]}} \tag{3.26}$$

This value of natural frequency is substituted in Eq. (3.24) to estimate ξ. As Eq. (3.24) is valid for both ω_1 & ω_2, we can write

$$\xi_1 = \left(\frac{1}{2r_1^{(0)}}\right)*\sqrt{\left|\frac{\left(1-r_1^{(0)^2}\right)^2 TR_{eq}^2-1}{\left(1-TR_{eq}^2\right)}\right|} \qquad \text{where } r_1^{(0)} = \frac{\omega_1}{\omega_n^{(0)}}$$

$$\xi_2 = \left(\frac{1}{2r_2^{(0)}}\right)*\sqrt{\left|\frac{\left(1-r_2^{(0)^2}\right)^2 TR_{eq}^2-1}{\left(1-TR_{eq}^2\right)}\right|} \qquad \text{where } r_2^{(0)} = \frac{\omega_2}{\omega_n^{(0)}} \tag{3.27}$$

ξ_1 and ξ_2 are estimated values of damping ratios at excitation frequencies ω_1 and ω_2 respectively. Taking the average of these two damping ratios, $\xi^{(1)}$ is determined for the subsequent iteration as

$$\xi^{(1)} = \frac{\xi_1 + \xi_2}{2} \tag{3.28}$$

Using modified value of damping ratio i.e. $\xi^{(1)}$, above steps from Eq. (3.26) to Eq. (3.28) are repeated to determine the value of damping ratio $\xi^{(2)}$. The iterative process continues until the difference between values of damping ratios calculated from two successive iterations is less than a very small predefined value, which has been taken equal to 0.001 in the present study. To check validity of ξ thus

determined, it is substituted in Eq. (3.20) along with the corresponding value of ω_n and the computed value of TR_{pk} is compared with TR_{pk} measured from experimental TR-frequency response curve. As discussed earlier, for a multi d.o.f. system, this value of ξ estimated from the iterative scheme, will be equal to modal damping ratio for the mode whose frequency is closest to the frequency of peak in TR-frequency curve.

Assuming proportional damping for thirteen d.o.f. vibratory model, damping ratio for r^{th} mode is given by

$$\xi_r = \frac{\alpha}{2\lambda_r} + \frac{\beta\lambda_r}{2} \qquad (3.29)$$

where α, β are unknown constants and λ_r is the natural frequency corresponding to r^{th} mode. Using the iterative scheme, two modal damping ratios are estimated for any two peaks of experimental TR-frequency response curve. Thereafter, ξ_r for all the remaining modes can be determined by using Eq. (3.29).

3.5.3 Optimal Value of Elastic Moduli: Incorporating modal damping ratios and corresponding natural frequencies in Eq. (3.19), the TR are computed at different excitation frequencies through modal analysis. The optimal values of elastic moduli for ellipsoidal body segments are achieved by comparison of theoretically computed values of TR with the experimental results, for 50th percentile U.S. male. The objective function taken for optimization is

$$\text{Minimize} \quad Q = \sum_{i=1}^{N} \left[\left(TR(\omega_i)_{ex} - TR(\omega_i)_{th} \right)^2 \right] \qquad (3.30)$$

where $TR(\omega_i)_{ex}$ is the mean experimental value of the platform-to-head transmissibility ratio and $TR(\omega_i)_{th}$ is theoretically computed value for the same. 'N' is

the number of discrete values of frequencies, taken in optimization process, in the range of 0-25 Hz. Fig. 3.8 shows flow chart of the scheme used for estimation of elastic moduli for different ellipsoidal body segments using optimization.
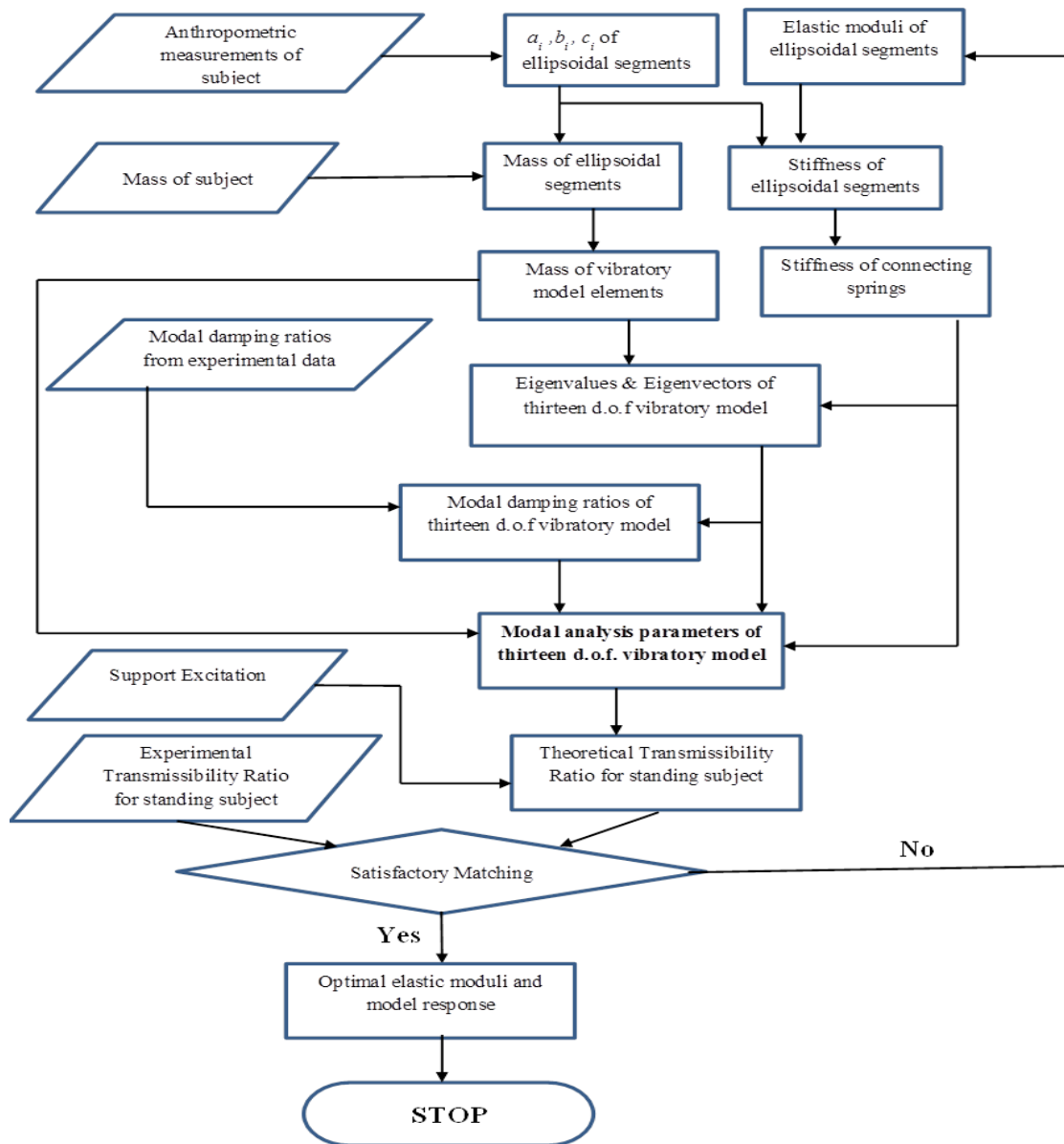
Fig. 3.8: Optimization Scheme for Elastic Moduli for Anthropometric Vibratory Model

3.5.4 Apparent Mass of standing person: As mentioned earlier, the parameters based on the driving point response, such as Apparent Mass, DPMI, have also been

used to quantify effects of vibratory stimulus on human body. Apparent Mass (AM) of a person under support excitation is defined as (Boileau & Rakheja, 2002):

$$AM = \frac{F_{interface}}{\ddot{y}}$$
(3.31)

where, $F_{interface}$ is the force at driving point interface and $\ddot{y}$ is the acceleration of supporting platform/interface. Rewriting Eq. (3.15):

$$\ddot{\eta}_r + 2\xi_r\lambda_r\dot{\eta}_r + \lambda_r^2\eta_r = P_r \qquad r = 1,2,....,13$$

$$\bar{\eta}_r = \frac{P_r}{\left(\left(\lambda_r^2 - \omega^2\right) + j\left(2\xi_r\lambda_r\omega\right)\right)} = \left(A_r + jB_r\right)y \quad \text{(suppose)}$$
(3.32)

$$\text{where } \bar{\eta}_r = \eta_r e^{-j\phi}$$

The dynamic response can be written as

$$\{x\} = \sum_{r=1}^{13}\{u\}^r \bar{\eta}_r$$

$$x_i = \sum_{r=1}^{13} u_i^r \bar{\eta}_r = (C_i + jD_i)y \quad \text{(suppose)}$$
(3.33)

For the vibratory model, shown in Fig. 3.3, under harmonic support excitation;

$$F_{interface} = \sum_{j=1}^{13} m_j \ddot{x}_j + \sum_{j=14}^{15} m_j \ddot{y}$$
(3.34)

Substituting Eq. (3.33) and Eq. (3.34) in Eq. (3.31), Apparent Mass of a standing subject under support excitation can be determined. As the dynamic response calculated from Eq. (3.33) is a complex quantity, *AM* determined from Eq. (3.34) is also a complex quantity containing both modulus and phase.

3.5.5 Modification of Segment Elastic Moduli: The transmissibility ratio of vibratory model for a standing subject is investigated for 50th percentile U.S. male, whose anthropometric measurements are listed in Table-B, Appendix I. Using Eq. (3.1) and formulae listed in Table-A (Appendix), the mass and semi-axes of different ellipsoidal segments are calculated and tabulated in Table 3.5.

Table 3.5: Mass & semi-axis of ellipsoidal segments (for 50th percentile U.S. male; M_{total} = 74.9 kg)

Segment No.	Body Segment	a_i (cm)	b_i (cm)	c_i (cm)	M_i (kg)
1	H	7.785	7.785	9.930	2.861
2	N	6.040	6.040	1.240	0.215
3	UT	16.445	11.660	18.770	17.109
4,5	RUA, LUA	5.239	5.239	18.770	2.449
6,7	RLA, LLA	4.628	4.628	24.345	2.479
8	CT	14.110	10.755	21.558	15.551
9	LT	17.715	11.595	12.173	11.885
10,11	RUL, LUL	5.927	5.927	27.825	4.646
12,13	RLL, LLL	5.303	5.303	23.115	3.090
14,15	RF, LF	4.675	12.700	3.455	0.975

The stiffness value computed using $E_i = E_G$ for all ellipsoidal segments (as done for previous model) are listed in column 3 of Table 3.6. These stiffness values are compared, with the stiffness values reported in the literature, representing connecting springs between similar segments of human body. Although the specific values of stiffness differ from the values found in literature, but their order of magnitude are same. This result justifies the assumption of taking E_G as the geometric mean of elastic moduli of bone and tissue.

The assumption of taking equal elastic moduli (i.e. $E_G = \sqrt{E_b E_t}$) for all segments is relaxed for the present model. From physiological structure of the human

body, it can be asserted that the elastic moduli for the bony parts like legs, limbs, upper and lower torso would be higher than for the fleshy parts like central torso, neck and feet.

Table 3.6: Comparison of stiffness of spring elements for vibratory models of human body

Spring Element (Fig. 3.3)	Interconnected Body Segments	Initial Stiffness ($E_i = E_G$) (kN/m)	Garg & Ross (1976)] (kN/m)	Qassem et al. (1994) (kN/m)	Amirouche et al. (1994) (kN/m)	Modified Stiffness (E_i Table 3.7) (kN/m)
k_1	Head & Neck	681.38	175.12	52.62	120	613.2
k_2	Neck & Upper Torso	846.54	175.12	52.62	120	610.5
k_3	Upper Torso & Central Torso	465.27	3.15	52.62	105	292.3
$k_4 = k_5$	Upper Torso & Upper Arm	142.82	26.25	67.54	50	142.8
$k_6 = k_7$	Upper Arm & Lower Arm	98.23	26.25	67.54	50	98.2
k_8	Central Torso & Lower Torso	554.55	37.25	53.49	105	334.8
$k_9 = k_{10}$	Lower Torso & Upper Leg	131.13	358.75	25.01	50	193.3
$k_{11} = k_{12}$	Upper Leg & Lower Leg	69.16	358.75	-	50	103.8
$k_{13} = k_{14}$	Lower Leg & Foot	1918.49	358.75	-	-	1630.7

Estimated values of k_1 and k_2, given in column 3 of Table 3.6, having contribution from neck-stiffness, are much higher than the stiffness values reported in the literature (Columns 4, 5 and 6; Table 3.6). Moreover, the neck is essentially a tissue structure with small fraction of it occupied by cervical vertebrae. The cervical extends into the head and upper torso as well. Therefore, the effective Young's modulus for neck and head should be lowered from E_G.

The central torso is largely a tissue structure which gets support from the backbone. Gupta (2007) has taken the stiffness of central torso equal to the parallel

combination of stiffness of complete torso with $E_i = \sqrt{E_b E_t}$ and stiffness of central torso with $E_i = E_t$. This modification resulted in lower values of stiffness of spring elements connecting central torso with the upper torso and the lower torso and consequently better match of theoretical response with the experimental results. Similar improvement in present vibratory model can be produced by taking smaller fraction of E_G for the determination of stiffness of central torso. Moreover, comparing the values of k_3 and k_8 in column 3 of Table 3.6, which represent stiffness of spring elements connecting the central torso with upper torso and lower torso respectively, it is observed that the values for present vibratory model are quite high with regard to the stiffness values published in the literature, as shown in columns 4 to 6. Therefore the effective value of E for the central torso should also be reduced from the value used by Nigam & Malik (1987).

Furthermore, comparing the stiffness values k_9 to k_{14} of column 3 with column 4 to 6, it seems that the elastic moduli of upper leg and lower leg must be increased whereas for the feet it should be decreased. For a person in standing posture, load in upper and lower legs is mainly supported by the bony parts, suggesting for higher elastic moduli of legs. The presence of fat pads at heel and ball of the feet also rationalizes using lower value of elastic modulus for the feet.

Based on the above discussion and considering the presence of active muscles; the elastic moduli/stiffness of different parts of human body should be taken in decreasing order as follows: Legs, Lower torso, Arms, Upper torso, head, feet, central torso and neck. Accordingly, the values of elastic moduli for different ellipsoidal segments have been modified, while keeping in view Eq. (3.2) and the scheme given in Table 3.1, and shown in Table 3.7.

Table 3.7: Modified elastic modulus of ellipsoidal body segments ($E_G = \sqrt{E_b E_t}$)

Body Segment	H	N	UT	RUA, LUA	RLA, LLA	CT	LT	RUL, LUL	RLL, LLL	RF, LF
Modified Elastic Modulus * E_G	0.9	0.4	1.0	1.0	1.0	0.5	1.2	1.5	1.5	0.85

Using the elastic moduli listed in Table 3.7, the stiffness of spring elements of vibratory model are recalculated and shown in column 7 of Table 3.6.

3.5.6 Modal damping ratio: Experimental measurements of platform-to-head transmissibility ratio for a group of standing subject under vertical excitation from platform (Garg & Ross, 1976) has been employed to estimate modal damping ratios corresponding to the first few natural frequencies of human body in upright posture.

Fig. 3.9 shows average value of transmissibility ratio measured for eight U.S. persons standing on a platform subjected to vertical harmonic motion. Experiments were conducted on a total of twelve people but the results of four subjects were excluded from the averaging process as their dynamic response differed substantially from other subjects. The average frequency response was constructed by lateral (frequency axis) shift of individual plots such that the peaks of individual plots occurred at the average frequency of corresponding peaks of all the eight subjects. Two successive peaks of transmissibility ratio are chosen in Fig. 3.9 i.e., point B (close to 6 Hz) and point C (close to 18 Hz), to identify damping ratios using iterative scheme discussed in section 3.5.2.
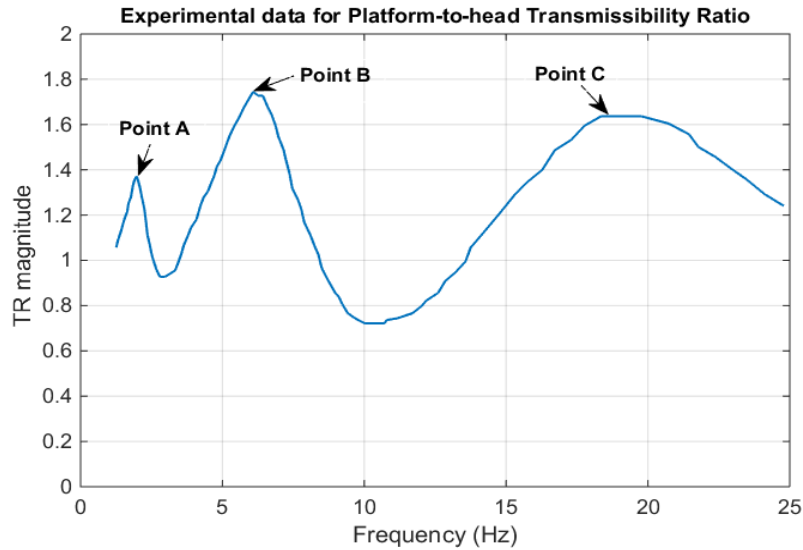
Fig. 3.9: Experimental data for average platform-to-head transmissibility ratio of U.S. male (Garg & Ross, 1976)

The first peak at point A (near 2 Hz) has been ignored for estimating modal damping ratios and further comparison of results, as different experimental studies of standing subjects (Paddan & Griffin, 1993; Harazin & Grzesik, 1998; Coermann, 1962) have not reported this peak. Also this peak near 2 Hz may be attributed to the bending motion of human body (Amirouche & Ider, 1988). Whole-body vibration analysis of a seated person using a finite element model (Kitazaki & Griffin, 1997) indicated a mode near 2.8 Hz corresponding to bending of neck-spinal column. Experimental measurements of transmissibility for standing person (Matsumoto & Griffin, 1998) also indicated a peak around 3 Hz for transmissibility to the knee only in the legs bent posture. This peak was attributed to significant bending of knee and pitching motion of upper body. In the present mathematical model, rotational motion of body segments has not been taken into account; therefore the first peak corresponding to 2 Hz has not been considered for the estimation of modal damping ratios. The data utilized for iterative scheme, corresponding to points B and C, and the modal damping ratios estimated thereof are shown in Table 3.8. Using estimated

values of damping ratios, TR_{pk} and ω_n value are determined from Eq. (3.20) and Eq. (3.26) respectively as shown in last two columns of Table 3.8. Computed values of TR_{pk} are found to be in good agreement with the measured values. Thus it validates the proposed iterative scheme, for the identification of damping ratios from experimentally measured transmissibility ratio of multi d.o.f. systems.

Table 3.8: Data used for iterative scheme and estimated modal damping ratios

Peak TR point	ω_{peak} (Hz)	TR_{pk} (Fig. 3.9)	Value for the left side of peak		Value for the right side of peak		Modal Damping ratio (ξ) using iterative scheme	TR_{pk} (Eq. 3.20)	Computed ω_n (Eq. 3.26) (Hz)
			ω_1 (Hz)	TR_1	ω_2 (Hz)	TR_2			
Point B	6.083	1.745	4.224	1.241	7.776	1.228	0.377	1.714	6.75
Point C	18.86	1.637	15.32	1.292	24.12	1.292	0.422	1.604	21.328

Estimated value of modal damping ratios, i.e. $\xi_1 = 0.377$ and $\xi_2 = 0.422$ and corresponding value of ω_n's are substituted in Eq. (3.29) to determine α and β for proportional damping model. Using natural frequencies of standing subject determined from eigenvalue analysis and calculated values of α (=3.6569) and β (=0.0316), modal damping ratios corresponding to thirteen modes of vibratory model are determined, which are listed in Table 3.9. Since the estimated values of first two natural frequencies from iterative scheme are slightly different from natural frequencies determined from Eigen-value analysis, therefore, the computed values of damping ratios for first two modes, as shown in Table 3.9, are marginally different than the values estimated from iterative scheme.

Table 3.9: Modal damping ratios and natural frequencies for thirteen d.o.f. vibratory model

Mode No.	1	2	3	4	5	6	7	8	9	10	11	12	13
Natural Frequencies (Hz)	6.22	19.4	22.21	27.72	36.47	39.76	51.16	53.7	54.79	60	119.4	119.4	383.9
Modal Damping Ratio (ξ)	0.39	0.4	0.433	0.504	0.626	0.674	0.844	0.882	0.899	0.978	1.9	1.9	6.07

Employing mass of ellipsoidal segments from Table 3.5, modified values of spring stiffness from column 7 of Table 3.6 and, corresponding modal damping ratios from Table 3.9, the transmissibility ratio of thirteen d.o.f. damped vibratory model is determined from Eq. (3.21). In the present investigation, the amplitude of harmonic support excitation (Y) is taken as unity, i.e.

$$y = 1.\cos(\omega t)$$

In Eq. (3.5), we require the values of k_{13}, k_{14} and c_{13}, c_{14} to compute 12th and 13th elements of force vector. Values of k_{13} and, k_{14} are already calculated and listed in Table 3.6 column 7. It should be noted that the effect of c_{13} and c_{14} in damping matrix **[C]** is carried forward in the dynamic response through proportional damping in modal analysis but the availability of only ξ_r's as listed in Table 3.9 does not facilitate determination of c_{13} and c_{14}.

The value of c_{13} and, c_{14}, corresponding to the dampers connecting feet and lower legs, are taken equal to the damping constants of ellipsoidal feet segments (B_{14} and B_{15}) from Eq. (3.4).Only for the determination of B_{14} and B_{15}, the ellipsoidal segments are taken as uncoupled single d.o.f systems.

Damping ratio ξ_j in Eq. 3.4 are assumed equal to the lowest value of modal damping ratios calculated. The premise for this assumption is mainly bony structure of legs and feet, indicated by higher values of k_{13} and k_{14} in Table 3.6, resulting to low energy dissipation during vibration. Using the lowest value of modal damping ratio i.e. 0.392, from Table 3.9, B_{14} and B_{15} are calculated which are equal to c_{13} and c_{14} as mentioned earlier.

Now from Eq. (3.19), the platform-to-head transmissibility ratio (*TR*) is determined as a function of excitation frequency (ω) and compared with the average experimental transmissibility ratio, as shown in Fig. 3.10. It is observed in Fig. 3.10 that with the estimated values of E_i in Table 3.7 and modal damping ratios determined from experimental response, the theoretical *TR*-frequency curve does not match with experimental curve. The frequency corresponding to the first peak of *TR* in theoretical response curve is lesser than the frequency for corresponding peak in experimental measurements and value of *TR* at first peak is much lower for theoretical plot. For the range of 10-25 Hz, the two curves diverge markedly and second peak for *TR* is not evident in the response calculated for vibratory model. So it is required to further modify the elastic moduli for various segments, which is conducted by optimization process while enforcing constrains based on the physiological structure as discussed earlier.

3.5.7 Optimal Values of E_i: To estimate optimal elastic moduli of ellipsoidal segments, Genetic Algorithm (GA) technique, and a global search method available in Matlab®; was utilized for optimization. The objective function for optimization of elastic moduli is given by Eq. (3.30).
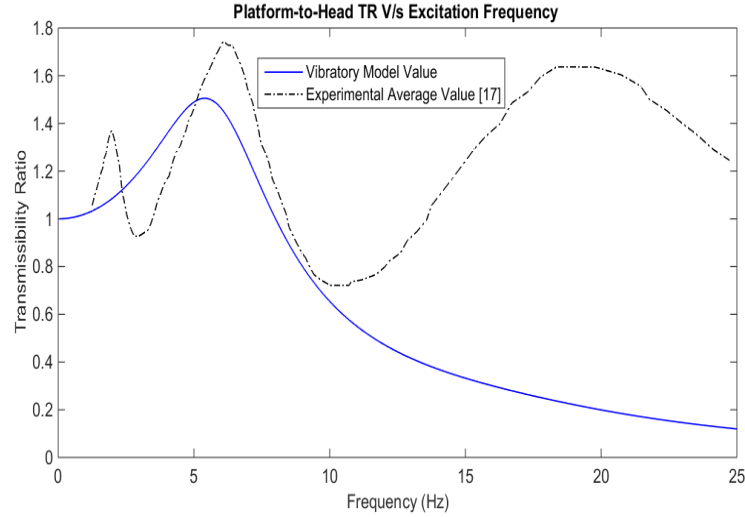
Fig. 3.10: Comparison of *TR* for vibratory model (modified *E$_i$*) and average experimental *TR*

The constraints upon E_i during optimization were:

$$0.01\,E_G \leq E_{3,}E_5, E_7, E_9, E_{10}, \mathrm{E}_{12} \; \leq \; 10\,E_G$$
$$0.01\,E_G \leq E_1, E_2, E_8, E_{14} \leq E_G$$
$$E_2 \leq E_7$$
$$E_{14} \leq E_{12}$$

$$(3.35)$$

The limits and constraints for individual E_i's have been decided keeping in view that the stiffness of spring elements determined (using Table 3.1) are of the same order as available in the literature and also taking into account the foregoing discussion about the order of elastic moduli for different body segments. It is to be noted here that although the human body has been divided into 15 ellipsoidal segments (Fig. 3.1); only ten unique values of E_i are being optimized due to the symmetry present in anthropometric vibratory model. Because output (set of E_i) from GA is not unique; therefore, 50 trials were performed for the minimization of objective function. The optimal values of E_i have been expressed as a fraction of E_G in Table 3.10.

63

Table 3.10: Optimal value of elastic modulus for ellipsoidal body segments (as fraction of E_G)

Body Segment	H	N	UT	RUA, LUA	RLA, LLA	CT	LT	RUL, LUL	RLL, LLL	RF, LF
Elastic Modulus	0.104	0.409	1.072	0.014	2.407	0.518	0.102	4.131	9.990	0.143

Using optimal values of E_i from Table 3.10, α, β determined from Table 3.8 and mass of ellipsoidal segments from Table 3.7; different parameters for the anthropometric vibratory model are calculated and given in Table 3.11. Comparing Table 3.11 with Table 3.6; it is observed that the stiffness values k_1, k_8, k_{13} calculated using optimal elastic moduli are substantially lower than those listed in column 7 Table 3.6. Also these values are closer to the ones available in literature for similar elements of human body model for a standing person.

Table 3.11: Vibratory model parameters using optimal E_i values (50th percentile U.S. male)

Element no. i	1	2	3	4	5	6	7	8	9	10	11	12	13	14	15
Mass M_i (kg)	2.86	0.21	17.11	2.45	2.45	2.48	2.48	15.55	11.88	4.65	4.65	3.09	3.09	0.98	0.98
Stiffness k_i (kN/m)	55.41	700.62	305.72	2.35	2.35	236.52	236.52	91.76	101.76	101.76	500.83	500.83	273.88	273.88	
Mode No.	1	2	3	4	5	6	7	8	9	10	11	12	13		
Natural Freq. ω_i (Hz)	3.24	3.47	6.19	19.28	22.5	33.05	33.6	37.14	69.82	69.82	92.19	92.24	300.11		
Modal Damping Ratio ξ_i	0.52	0.49	0.34	0.35	0.38	0.50	0.51	0.56	0.99	0.99	1.29	1.29	4.16		

This outcome reinforces the rationale adopted for the order of elastic moduli for individual body segments as discussed earlier and evident in Eq. (3.35).

Now, platform-to-head *TR* is computed for the model with parameters listed in Table 3.11 and compared with the experimentally measured *TR* as function of excitation frequency, as shown in Fig. 3.11.
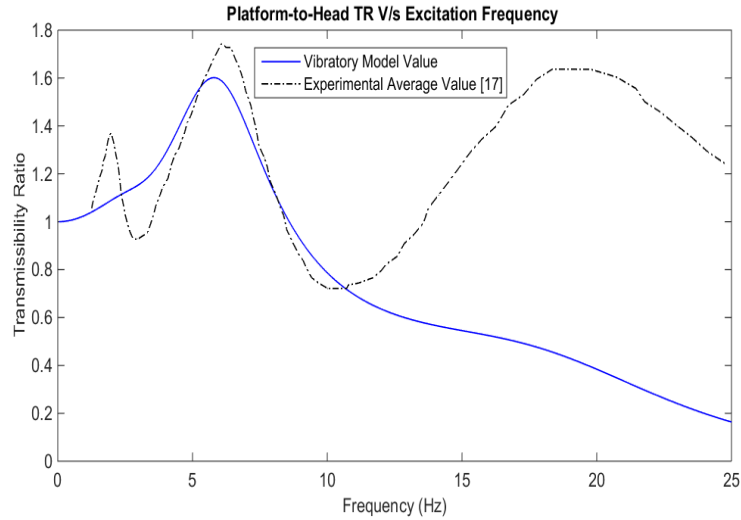
Fig. 3.11: Comparison of *TR* for vibratory model (optimal *E_i*) and average experimental *TR*

The equivalence between the two curves has improved near the first peak vis-à-vis that attained in Fig. 3.10, but the two curves still differ substantially around the second peak at nearly 18 Hz. Theoretical response curve does show a peak near 17-18 Hz in Fig. 3.11 but the peak is barely perceptible. Eigenvalue analysis of vibratory model with *E_i* values before and after the optimization process indicated a natural frequency in the range of 18-20 Hz. But, as can be observed from Fig.3.10 and Fig. 3.11, the peak corresponding to this frequency is not well-defined in the theoretical simulation results for *TR*. This suggests that contribution of the mode/modes neighboring the frequency of 18-20 Hz is being heavily damped. Therefore, numerical simulations were carried out to investigate this aspect further, by modifying the damping ratios of different modes, one at a time. It was found that upon reducing *ξ_4*, which corresponds to the mode having natural frequency around 18-20 Hz, to 50% of its original value; excellent match was obtained between theoretical and experimental

TR, as shown in Fig. 3.12. This remarkable change in *TR* due to ξ_4 modification substantiates the fact established from numerical simulation in this work, that the *TR* response around the peak is dominated by the mode corresponding to natural frequency closest to peak location.
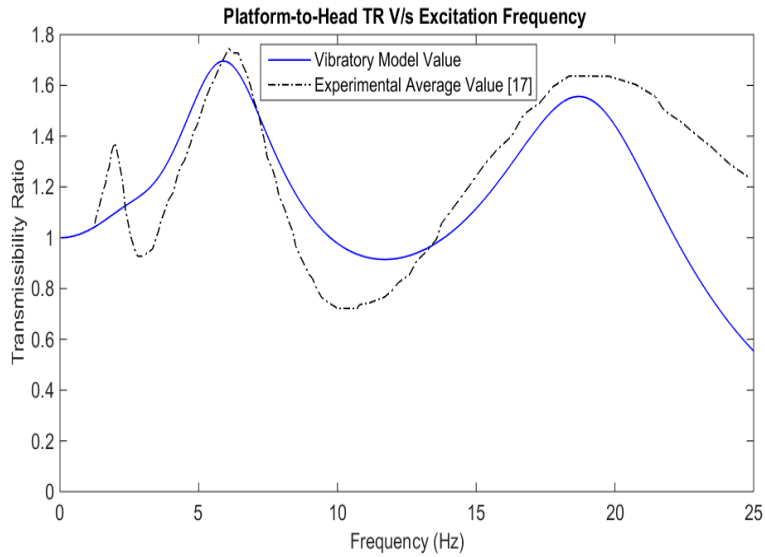
Fig. 3.12: *TR* **for vibratory model (optimal E_i & modified ξ_4) and average experimental *TR***

Thus, the anthropometric measurements along with elastic moduli, and modal damping ratios concluded in Table 3.10 and Table 3.11 (ξ_4 as 50%) respectively; completely facilitate us to construct the lumped parameter damped vibratory model for human body in standing posture under vertical excitation from feet. Reduction of modal damping ratio corresponding to dominant 4th mode, so as to improve the match for second peak, was based on detailed theoretical simulations. It was found that the estimated value of modal damping ratios from experimental measurements was sensitive to the vertical gap between response peak and line AB (refer Fig. 3.7). Accordingly the values of *α, β* and all thirteen *ξ*'s also changed and thus affect the participation of individual modes in theoretical response, particularly around the peaks of transmissibility. Also due to this, there will be a substantial effect upon estimated

66

values of modal damping ratio even if there was a minor error during experimental measurements. Since the average frequency response for 50th percentile U.S. male was obtained by lateral shifting of individual response curves, this influences modal damping ratio values estimated for U.S. male.

3.5.8 *TR* for Indian male: The anthropometric measurements of average Indian males (M_{total} =58.2 kg), used for determining parameters of ellipsoidal segments, are given in Table-B of Appendix. The optimal values of elastic moduli estimated for 50th percentile U.S. male, listed in Table 3.10, have been used to determine stiffness of spring elements for vibratory model of Indian male.

Table 3.12: Mass, stiffness of spring elements and modal damping ratios (Average Indian male)

Element no. i	1	2	3	4	5	6	7	8	9	10	11	12	13	14	15
Mass M_i (kg)	3.038	0.235	11.689	1.206	1.206	1.571	1.571	11.747	9.296	4.444	4.444	2.395	2.395	1.48	1.481
Stiffness k_i (kN/m)	84.02	431.87	264.17	1.38	1.38	165.5	165.5	113.16	129.32	129.32	405.05	405.05	221.42	221.42	
Mode No.	1	2	3	4	5	6	7	8	9	10	11	12	13		
Natural Freq. ω_i (Hz)	3.42	3.54	7.26	20.98	26.05	34.88	37.08	42.29	78.48	78.48	91.94	92.04	237.4		
Modal Damping Ratio ξ_i	0.494	0.483	0.36	0.54	0.641	0.826	0.873	0.985	1.784	1.784	2.084	2.087	5.349		

Then, following the procedure discussed above, the modal damping ratios have been estimated from the experimental measurements of *TR*.   The average *TR*-frequency response, for a group of 100 Indian male, measured by Gupta (2007) is taken from the literature. Table 3.12 lists the value of different parameters of the vibratory model for an average Indian male.   With these parameters, platform-to-head *TR* of Indian male is calculated and compared with envelop of the experimental results (Gupta, 2007) and shown in Fig. 3.13.
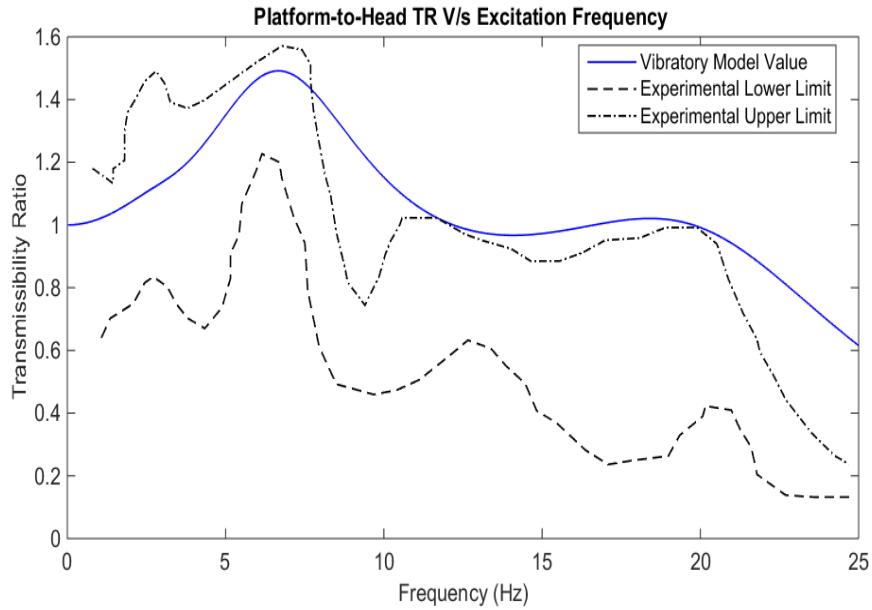
Fig. 3.13: *TR* from vibratory model (optimal *E_i*) and experimental *TR* envelop for Indian male

From Fig. 3.13, it can be discerned that the theoretical response for an Indian male is within the range of experimental results. During simulation, the value of damping ratio for fourth mode (ξ_4) was reduced by 50% to exhibit the peak related to fourth mode noticeable. This outcome substantiates the methodology used in the present study to develop human body vibratory model using anthropometric measurements and modal damping ratio based on experimental response.

3.5.9 Apparent Mass for 50th percentile US male: The estimated values of optimal elastic moduli and modal damping ratio, as described above, can further be established / validated by comparing modulus of Apparent Mass (*AM*) of a standing subject with experimental results available in the literature. Using the same parameters as in Table 3.12, the Apparent Mass of the vibratory model is calculated for 50th percentile U.S. male and compared, as shown in Fig. 3.14, with the experimental data synthesized by Rakheja et al (2010). Rakheja et al selected the dynamic response (*AM*) of 55 adult males subjected to vertical excitation in standing posture to determine upper and lower limits of experimental response envelop.
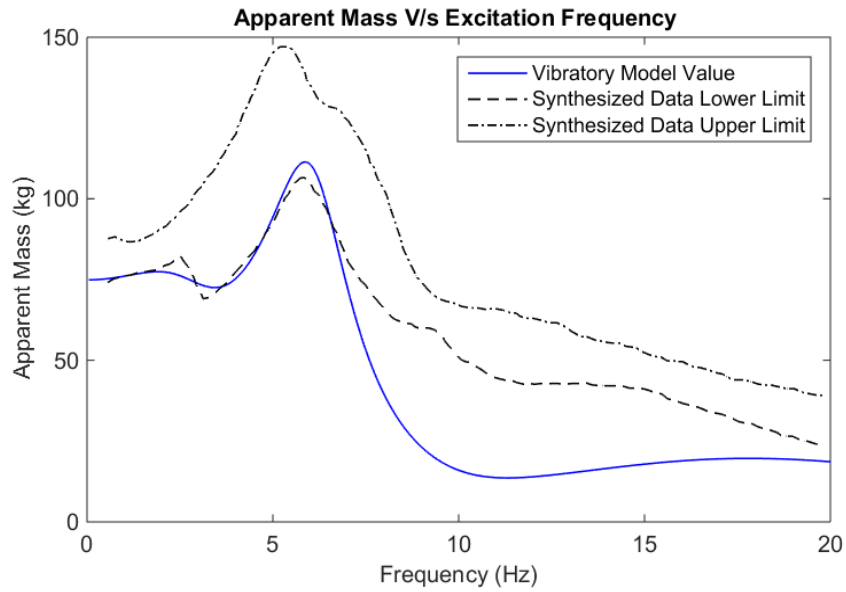
Fig. 3.14: Apparent Mass of US male from vibratory model (optimal E_i) and experimental Apparent Mass envelop (Rakheja et al. , 2010)

In the present work, similar to the case of *TR* for U.S. male; theoretical *AM* is computed by reducing ξ_3 (modal damping ratio corresponding to natural frequency of 6.19 Hz) to 55% of its original value. Figure 3.14 shows that the vibratory model response curve matches quite well with the lower limit of experimental data up to 7.5 Hz and particularly around the peak. Lower value of theoretical Apparent Mass, at excitation frequency more than 7.5 Hz, may be attributed to varied mass distribution and anthropometric measurements of the human beings involved in experimental studies. It is to noted that modal damping ratios were determined from the transmissibility plots and elastic moduli were determined through optimization based on experimental data of transmissibility. The set of parameters, i.e. damping ratio and elastic moduli, employed for determination of Apparent Mass are same as that for *TR*. Therefore, little dissatisfaction for the agreement between experimental and theoretical values of Apparent Mass is acceptable as the trend of theoretical curve is analogous to the experimental envelope.

This comparison for Apparent Mass further validates the modal damping ratios, optimized values of elastic moduli and methodology employed to determine inertial and elastic properties from anthropometric data. Also the optimal elastic moduli estimated for individual body segments, listed in Table 3.10, can serve as indicative values for the purpose of human body modelling.

3.6 Conclusions:

Lumped parameter models of human body which evolve from its physical measurements are straightforward to formulate and could deliver subject specific simulations to predict the effects of vibratory stimulus encountered in our day-to-day activities. Towards this goal, a thirteen d.o.f. damped vibratory model of standing person under vertical excitation has been formulated in this chapter and transmissibility ratio is calculated as a function of frequency of vibrating platform. Simplicity of the model lies in the fact that inertial and stiffness parameters are determined from the physical properties and anthropometric measurements of human body.

Relaxing the assumption used by earlier researchers, of constant elastic moduli to calculate stiffness of all segments; different values of elastic moduli have been proposed for individual ellipsoidal segments. Initially different elastic moduli are estimated by comparing stiffness of spring elements in the vibratory model with the values available in the literature and also taking into account the physiological structure of human body. These values are later optimized by comparing transmissibility response of vibratory model and experimentally measured response curves. Energy dissipative characteristics inherent in human body are incorporated in the model through modal damping ratios. Unlike to previous endeavors for

determination of damping constants based solely on optimization, this paper illustrates a novel scheme to determine modal damping ratios from experimentally measured transmissibility response.

For optimization of elastic moduli, the theoretical transmissibility response for 50th percentile U.S. male is compared with available experimental results. Also, numerical simulations have been performed to investigate the contribution of individual modes in theoretical response. It was found that reduction in the damping ratio for the mode neighboring second peak of experimental response resulted to close match between theoretical transmissibility ratio calculated with optimal E_i's and experimental measurements, in the frequency range of 4-22 Hz. While studying standing subjects, researchers have observed predominant peaks in this frequency range for dynamic response. Hence the anthropometric vibratory model established in this investigation emulates the behavior of human body for the range of foremost interest in vibrational studies.

Furthermore, transmissibility ratio of average Indian male in standing posture was simulated using optimal elastic moduli determined for 50th percentile U.S. male. An acceptable match between model response and envelop of experimental response was achieved. Apparent Mass of standing subject calculated using the same parametric values of vibratory model is found to be in satisfactorily agreement with the experimental response envelop; authenticating the present methodology of constructing human body vibratory model from anthropometric data, optimal values of elastic moduli of individual body segments and experimentally estimated modal damping ratios.

After further refinements, the thirteen d.o.f anthropometric vibratory model developed in this study can be used to predict interactive forces generated between adjacent parts of the human body; as a first step towards studies for vibration injuries of standing subjects. To improve the confidence interval for values estimated through optimization; present work should be extended in future to include sensitivity analysis of Transmissibility Ratio and Apparent Mass against optimal values of elastic moduli. Furthermore, similar models can be developed for persons in sitting posture thereby exploring the effect of posture on the parameters of human body model.

Chapter 4

Finite Element Vibratory Model of Standing Subject

In Chapter 3; lumped parameter vibratory models of standing subject under vertical excitation from platform-feet interface have been developed. These models, developed from physical measurements of subjects, deal primarily with overall dynamic response to WBV. For reliable estimation of the human body segments/locations prone to vibration related injuries, continuum models of human body are preferable. As discussed in chapter 2, existing human body FE models have significantly high d.o.f. In this chapter, a finite element vibratory model of standing subject is formulated based on anthropometric data with relatively low d.o.f.

4.1 Human Body Segmentation and Element Formulation

A FE model for human body consisting of fifteen truncated ellipsoidal elements, which correlate with anatomical structure, is formulated. This model, as shown in Fig. 4.1, is used to calculate the dynamic response of subjects standing in normal posture and undergoing WBV due to vertical excitation (along z axis) at feet-platform interface.
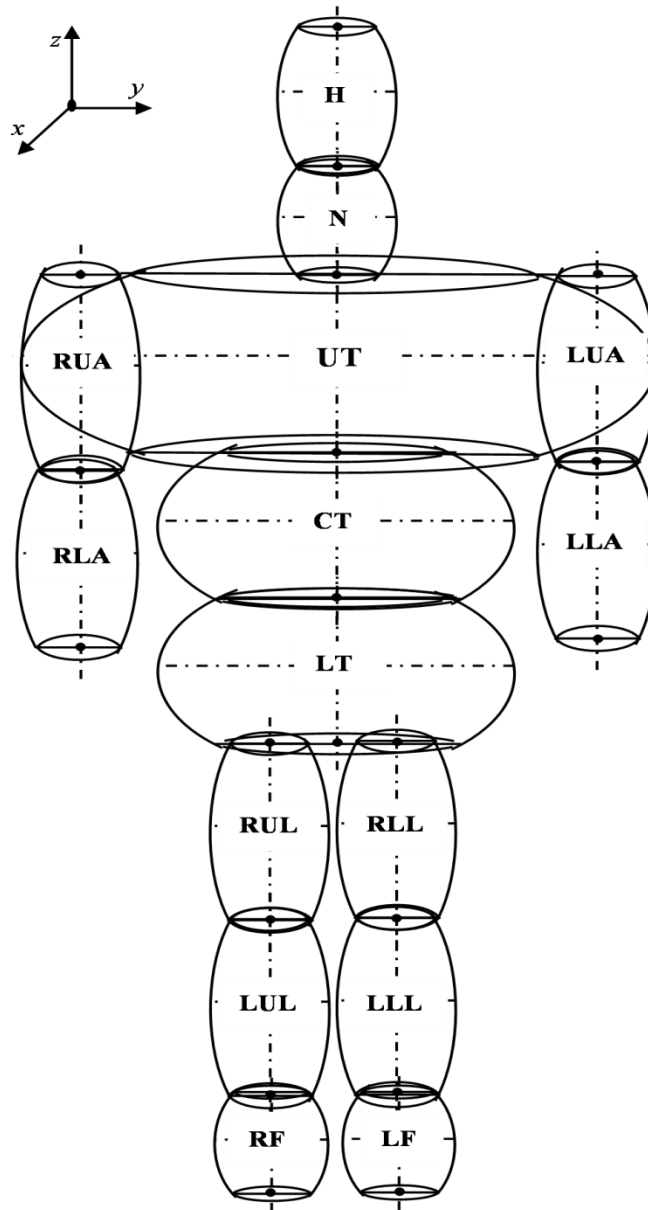
Fig. 4.1 Human body model constructed using truncated ellipsoidal elements
(**H**: Head, **N**: Neck, **UT**: Upper Torso, **CT**: Central Torso, **LT**: Lower Torso, **LUA**: Left Upper Arm, **RUA**: Right Upper Arm, **LLA**: Left Lower Arm, **RLA**: Right Lower Arm, **LUL**: Left Upper Leg, **RUL**: Right Upper Leg, **LLL**: Left Lower Leg, **RLL**: Right Lower Leg, **LF**: Left Foot, **RF**: Right Foot)

Semi-axes of un-truncated ellipsoids (*a, b, c*), as shown in Fig. 4.2 (a), are calculated from the anthropometric measurements of subjects by employing the scheme developed by Bartz and Gianotti (1975), and listed in Table A of Appendix.

Since actual body segments have overlapping area contact instead of point contact; therefore, the ellipsoids have been assumed to be truncated at both ends along

the vertical axis, as shown in Fig. 4.2 (b). For the present work, a truncation factor of 5% has been taken at both ends, i.e. the lower and upper nodes (Nodes A and B) are taken at $z = -d$ and $z = +d$ respectively; where $d = 0.95\ c$.
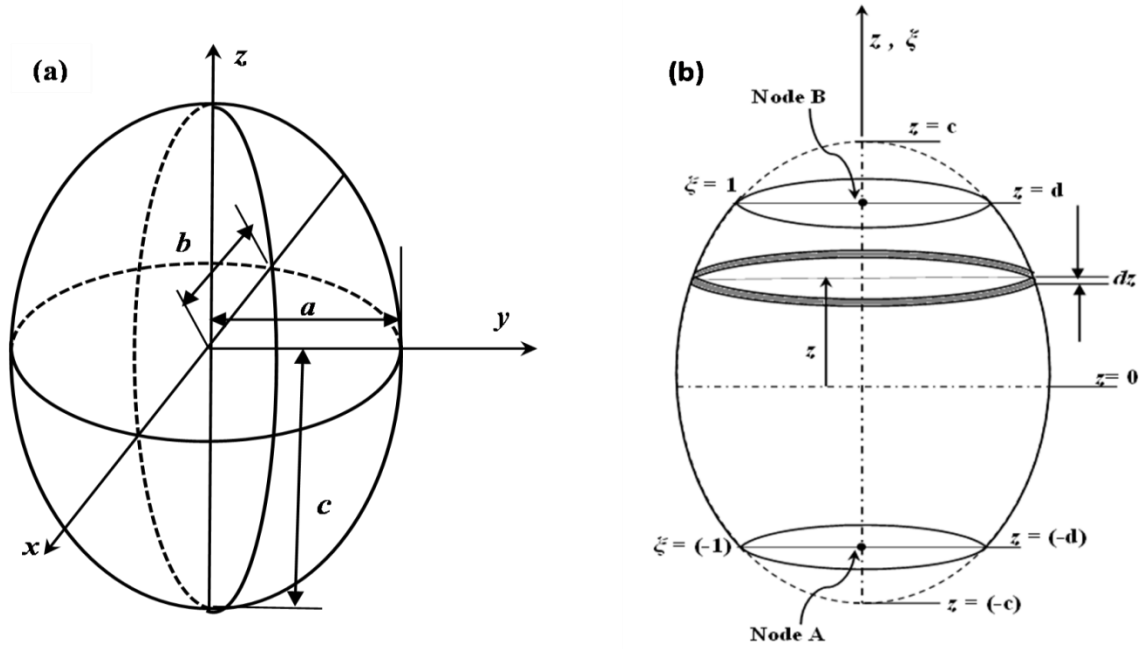
Fig. 4.2 (a) Un-truncated ellipsoid showing semi-axes (b) Truncated ellipsoidal finite element

Individual truncated ellipsoidal elements are assumed to be homogenous, isotropic and viscoelastic. Experimental studies (Shuck & Advani, 1972; Hayes & Mockros, 1971; Linde, 1994; Johnson et al., 1994; Saraf et al., 2007; Jaimson IV et al., 2013) on human body constituents such as muscles, tissues, spinal column etc., have shown a strain rate dependent response when subjected to external loading. Consequently, researchers have used these constituents as viscoelastic material in conjunction with bones to model human body segments (Terry & Roberts, 1968; Rosen & Arcan, 2003; Fard et al., 2003, Forlani et al., 2015) for studying their response under impact/dynamic loading in numerous studies. In the present study, the ellipsoidal body segments are assumed to be viscoelastic with an average elastic moduli and average dynamic viscosity. The Kelvin-Voigt model for viscoelastic

materials is adopted here to incorporate both stiffness and damping in the human body vibratory model. For uni-directional strain along z-axis (Fig. 4.2(b)), the total stress (σ) is given as (Christensen, 1982):

$$\sigma = \sigma_E + \sigma_{vis} = E\varepsilon_z + \eta \frac{\partial}{\partial t}(\varepsilon_z) \tag{4.1}$$

where, σ_E , σ_{vis} , ε_z are the elastic stress, time varying viscous stress, and axial strain respectively; along the vertical z-direction; E is the elastic modulus and η is the average dynamic viscosity of individual body segment. For standing subjects under vertical excitation at platform-feet interface, elemental deformation along the z axis is considered to be dominant (Nigam & Malik, 1987; Gupta, 2007) and therefore cross-axis deformations can be neglected. With this assumption, the resulting stress/strain fields become uni-directional.

4.1.1 Shape Functions: For FE modeling of ellipsoidal elements, shape functions are derived from the exact solution for deformation of an ellipsoid under uni-axial load. The change in length (ΔL_{dz}) of an elliptical strip of length dz at a distance z form the origin, as shown in Fig. 4.2(b), under the action of unit load at node B is given by

$$\begin{aligned} \Delta L_{dz} &= \frac{(1) \cdot dz}{E \cdot A(z)} \\ \Delta L_{dz} &= \frac{dz}{E \cdot \pi ab \left(1 - \dfrac{z^2}{c^2}\right)} \end{aligned} \tag{4.2}$$

Total deformation (ΔL_z) of a partial segment of ellipsoid up to a distance z from the lower end of truncated ellipsoid can be written as

$$\Delta L_z(z) = \int_{-d}^{z} \frac{d\tau}{E \cdot \pi a b \left(1 - \frac{\tau^2}{c^2}\right)} \tag{4.3}$$

where, τ is used as a dummy variable. Integration of Eq. (4.3) yields

$$\Delta L_z(z) = \frac{c}{2\pi E a b}\left(\ln\left(\frac{1 + \frac{z}{c}}{1 - \frac{z}{c}}\right) + \ln\left(\frac{1 + \frac{d}{c}}{1 - \frac{d}{c}}\right)\right) \tag{4.4}$$

Total deformation of truncated ellipsoidal element, as shown in Fig. 4.2(b), for

$z = z_{\max} = +d = 0.95c$:

$$\Delta L_z(z_{\max} = +d) = \frac{c}{2\pi E a b}(7.3271) \tag{4.5}$$

From Eq. (4.4) and Eq. (4.5), normalized deformation ($\Delta L(z)$) for partial

segment of ellipsoid up to a distance z can be expressed as

$$\Delta L(z) = \frac{\Delta L_z(z)}{\Delta L_z(z_{\max})} = \frac{1}{7.3271}\left(\ln\left(\frac{1 + \frac{z}{c}}{1 - \frac{z}{c}}\right) + \ln\left(\frac{1 + \frac{d}{c}}{1 - \frac{d}{c}}\right)\right) \tag{4.6}$$

As $|z| \le |d| < |c|$ for all values of z; applying Taylor series expansion to Eq. (4.6)

yields

$$\Delta L(z) = \frac{1}{7.3271}\left(2*\left(\left(\frac{z}{c}\right) + \frac{1}{3}\left(\frac{z}{c}\right)^3 + \frac{1}{5}\left(\frac{z}{c}\right)^5 + \frac{1}{7}\left(\frac{z}{c}\right)^7 + \frac{1}{9}\left(\frac{z}{c}\right)^9\right) + G_1\right) \tag{4.7}$$

where G_1 is a constant and given by

$$G_1 = \ln\left(\frac{1 + \frac{d}{c}}{1 - \frac{d}{c}}\right) = 3.66356 \quad (\text{for } d = 0.95c)$$

Using the first five terms in Taylor series, the difference between the exact solution given by Eq. (4.6) and the approximate solution given by Eq. (4.7) is very small, as shown in Fig. 4.3.
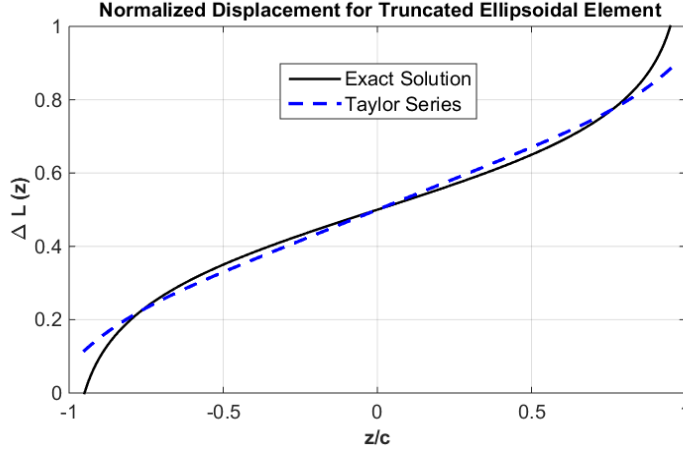
Fig. 4.3: N**ormalized displacement using exact solution (Eq. 4.6) & Taylor series expansion (Eq. 4.7)**

For $\left|\dfrac{z}{c}\right| \le 0.90$, error is less than 2.5% and maximum difference between the two curves is 7.4% for $\left|\dfrac{z}{c}\right| = 0.95$. For $d = 0.95$ c, Eq. (4.7) can be written as

$$\Delta L(\xi) = \frac{1}{7.3271}\left(2*\left(0.95\xi + \frac{(0.95)^3}{3}\xi^3 + \frac{(0.95)^5}{5}\xi^5 + \frac{(0.95)^7}{7}\xi^7 + \frac{(0.95)^9}{9}\xi^9\right) + G_1\right) \quad (4.8)$$

where $\quad \xi = \dfrac{z}{d}$ (4.9)

ξ is the non-dimensional natural co-ordinate used for FE formulation. Referring to Fig. 4.2(b), $\xi = -1$ at $z = -d$ and $\xi = +1$ at $z = +d$. From Eq. (4.8), after conforming with the basic definition of a shape function; i.e. $N_B\big|_{(\xi=-1)} = 0$ and $N_B\big|_{(\xi=+1)} = 1$, shape function N_B corresponding to the node B comes out to be

78

$$N_B(\xi) = \frac{1}{6.2412}\left(3.1207 + 2*\left(0.95\,\xi + \frac{(0.95)^3}{3}\xi^3 + \frac{(0.95)^5}{5}\xi^5 + \frac{(0.95)^7}{7}\xi^7 + \frac{(0.95)^9}{9}\xi^9\right)\right) \qquad (4.10)$$

Following the same steps, shape function corresponding to the node *A* is

$$N_A(\xi) = \frac{1}{6.2412}\left(3.1207 - 2*\left(0.95\,\xi + \frac{(0.95)^3}{3}\xi^3 + \frac{(0.95)^5}{5}\xi^5 + \frac{(0.95)^7}{7}\xi^7 + \frac{(0.95)^9}{9}\xi^9\right)\right) \qquad (4.11)$$

Fig. 4.4 shows the comparison between normalized displacement fields along the vertical axis of ellipsoid using the exact solution given by Eq. (4.6) and shape functions N_A, N_B based on Taylor series given by Eqs.(4.10) and (4.11) respectively. It is clearly observed that displacement fields predicted using N_A and N_B are in satisfactory match with the normalized deformation of truncated ellipsoid determined using exact solution. It has been confirmed that $N_A + N_B = 1$ for $-1 \le \xi \le +1$; satisfying the basic requirement for shape functions.
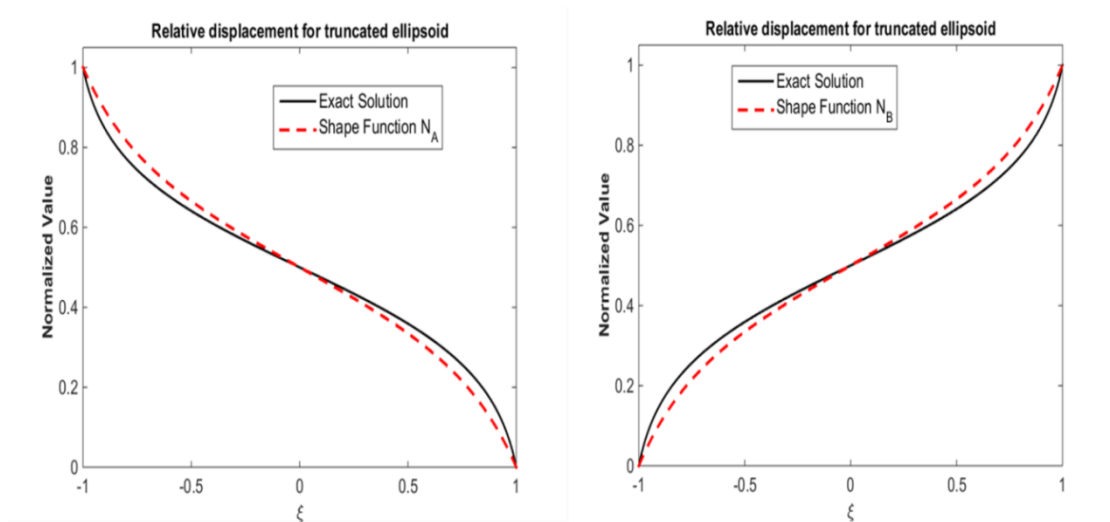
Fig. 4.4 Normalized displacement of a point along vertical axis due to axial load at respective nodes of truncated ellipsoid

Now, the internal displacement field ($u(\xi)$) of ellipsoidal finite element can be expressed, in terms of nodal displacements, as

$$u(\xi) = [\mathbf{N}]\{\boldsymbol{q}\} \qquad (4.12)$$

where, $[\mathbf{N}] = [N_A \ N_B]$ is the shape function matrix and $\{\boldsymbol{q}\} = [q_A \ q_B]^T$ is the corresponding nodal displacement vector. Axial strain due to the displacement field $u(\xi)$ is given by

$$\varepsilon_z = \frac{du}{dz} = \frac{\partial u}{\partial \xi} \cdot \frac{d\xi}{dz}$$

$$\Rightarrow \varepsilon_z = \frac{\partial}{\partial \xi}([\mathbf{N}]\{\boldsymbol{q}\}) \cdot \frac{1}{d}$$

$$\Rightarrow \varepsilon_z = [\mathbf{B}]\{\boldsymbol{q}\} \qquad (4.13)$$

where, $[\mathbf{B}]$ is the element strain-displacement matrix given as

$$[\mathbf{B}] = \frac{2}{6.2412\,d}\left[\left(0.95 + (0.95)^3 \, \xi^2 + (0.95)^5 \, \xi^4 + (0.95)^7 \, \xi^6 + (0.95)^9 \, \xi^8\right)\left[-1 \ 1\right]\right] \qquad (4.14)$$

4.2 Equations of Motion for Ellipsoidal Element: The governing equations of motion for a standing subject under vertical excitation at feet-platform interface have been derived using Hamilton's principle (Cheng et al., 2007; Petyt, 2010), which is given by

$$\int_{t_1}^{t_2} \left(\delta T - \delta U + \delta W_{vis} + \delta W_{ext}\right) dt = 0 \qquad (4.15)$$

where, δT is the first variation of the kinetic energy, δU is the first variation of elastic strain energy, δW_{vis} is the virtual work done by internal viscous forces (i.e. non-

conservative forces) and δW_{ext} is the virtual work done by external forces. In following sections, these terms are derived for a truncated ellipsoidal finite element.

4.2.1 Strain Energy (U): For viscoelastic materials that follow constitutive stress-strain relationship given by Eq. (4.1); strain energy (U) stored in the element corresponds to the elastic component of stress, i.e. σ_E. The first variation of strain energy δU is given by

$$\delta U = \int_v \sigma_E \delta \varepsilon_z dv = \int_v E \varepsilon_z \cdot \delta \varepsilon_z dv \tag{4.16}$$

Substituting Eq. (4.13) into Eq. (4.16) yields

$$\begin{aligned}
\delta U &= E \int_v \{q\}^T [\mathbf{B}]^T [\mathbf{B}] \{\delta q\} dv \\
&= E \int_z \{q\}^T [\mathbf{B}]^T [\mathbf{B}] \{\delta q\} A(z) dz \\
&= E \int_{-d}^{+d} \{q\}^T [\mathbf{B}]^T [\mathbf{B}] \{\delta q\} * \pi ab \left(1 - \frac{z^2}{c^2}\right) dz \\
&= E \int_{-1}^{+1} \{q\}^T [\mathbf{B}]^T [\mathbf{B}] \{\delta q\} * \pi abd \left(1 - \frac{\xi^2 d^2}{c^2}\right) d\xi
\end{aligned}$$

Using Eq. (4.14),

$$\delta U = \frac{\pi E ab}{3.6773 * d} \{q\}^T \begin{bmatrix} 1 & -1 \\ -1 & 1 \end{bmatrix} \{\delta q\} \tag{4.17}$$

4.2.2 Kinetic Energy (T): Assuming uniform density ρ of human body, kinetic energy (T) of ellipsoidal element is expressed as

$$T = \frac{1}{2} \int_v (dm) \dot{u}^2 = \frac{1}{2} \int_v (\rho dv) \dot{u}^2 \tag{4.18}$$

The first variation of kinetic energy is given by

$$\delta T = \delta\left(\frac{1}{2}\int_v \rho \, \dot{u}^2 \, dv\right) = \int_v \rho \dot{u} \, \delta\dot{u} \, dv \tag{4.19}$$

Substituting Eq. (4.12) into Eq. (4.19) yields

$$\delta T = \rho\int_v \left\{\dot{\boldsymbol{q}}\right\}^T [\mathbf{N}]^T[\mathbf{N}]\left\{\delta\dot{\boldsymbol{q}}\right\}dv$$

$$= \pi abd\rho\left\{\dot{\boldsymbol{q}}\right\}^T\left(\int_{-1}^{+1}\left(1-\frac{\xi^2 d^2}{c^2}\right)\begin{bmatrix} N_A^2 & N_A N_B \\ N_A N_B & N_B^2 \end{bmatrix}d\xi\right)\left\{\delta\dot{\boldsymbol{q}}\right\}$$

Simplifying and using Eqs. (4.10) and (4.11), the first variation of kinetic energy comes out to be

$$\delta T = \pi\rho abd\left\{\dot{\boldsymbol{q}}\right\}^T\begin{bmatrix} 0.3921 & 0.3071 \\ 0.3071 & 0.3921 \end{bmatrix}\left\{\delta\dot{\boldsymbol{q}}\right\} \tag{4.20}$$

4.2.3 Work done by viscous forces (W_{vis}): Using Kelvin-Voigt model of viscoelasticity as expressed by Eq. (4.1), the virtual work done by internal non-conservative viscous forces is given by

$$\delta W_{visc} = -\int_v \sigma_{vis}\delta\varepsilon_z dv = -\int_v \eta\frac{\partial\varepsilon_z}{\partial t}\bullet\delta\varepsilon_z dv \tag{4.21}$$

Substitution from Eq. (4.13) into Eq. (4.21) yields

$$\delta W_{visc} = -\int_v \eta\left\{\dot{\boldsymbol{q}}\right\}^T[\mathbf{B}]^T[\mathbf{B}]\{\delta\boldsymbol{q}\}dv$$

$$= -\eta\int_{-1}^{+1}\left\{\dot{\boldsymbol{q}}\right\}^T[\mathbf{B}]^T[\mathbf{B}]\{\delta\boldsymbol{q}\}*\pi abd\left(1-\frac{\xi^2 d^2}{c^2}\right)d\xi$$

Using Eq. (4.14),

$$\Rightarrow \delta W_{visc} = -\frac{\pi \eta ab}{3.6733*d} \left\{\dot{q}\right\}^T \begin{bmatrix} 1 & -1 \\ -1 & 1 \end{bmatrix} \left\{\delta q\right\} \tag{4.22}$$

4.2.4 Work done by external forces (W_{ext}): WBV of a standing subject due to excitation from supporting platform is essentially a case of support motion; external force is applied on the platform, not on the human body per se. The external force acting on an ellipsoidal finite element is the gravity force acting downwards (in $-z$ direction as shown in Fig.4.2 (b)). The virtual work done by the gravity is,

$$\delta W_{ext} = \delta W_G = \delta \left(\int_v (dm\, g)u \right) = \delta \left(\int_v (\rho\, dv\, g)u \right) \tag{4.23}$$

Using the value of displacement field from Eq. (4.12) and simplifying yields

$$\delta W_{ext} = \pi abd \rho\, g \begin{bmatrix} 0.6992 & 0.6992 \end{bmatrix} \left\{\delta q\right\} \tag{4.24}$$

Substituting contributions of different energies and forces in Eq. (4.15), yields;

$$\int_{t_1}^{t_2} \left(\pi \rho abd \left\{\dot{q}\right\}^T \begin{bmatrix} 0.3921 & 0.3071 \\ 0.3071 & 0.3921 \end{bmatrix} \left\{\dot{\delta q}\right\} - \frac{\pi E ab}{3.6733*d} \left\{q\right\}^T \begin{bmatrix} 1 & -1 \\ -1 & 1 \end{bmatrix} \left\{\delta q\right\} - \frac{\pi \eta ab}{3.6733*d} \left\{\dot{q}\right\}^T \begin{bmatrix} 1 & -1 \\ -1 & 1 \end{bmatrix} \left\{\delta q\right\} + \pi \rho abd\, g \begin{bmatrix} 0.6992 \\ 0.6992 \end{bmatrix} \left\{\delta q\right\} \right) dt = 0 \tag{4.25}$$

Integrating by parts the first term of Eq. (4.25) and employing $\left\{\delta q\right\}\big|_{t_1} = \left\{\delta q\right\}\big|_{t_2} = 0$,

$$\int_{t_1}^{t_2} \left(-\pi \rho abd \left\{\ddot{q}\right\}^T \begin{bmatrix} 0.3921 & 0.3071 \\ 0.3071 & 0.3921 \end{bmatrix} - \frac{\pi E ab}{3.6733*d} \left\{q\right\}^T \begin{bmatrix} 1 & -1 \\ -1 & 1 \end{bmatrix} - \frac{\pi \eta ab}{3.6733*d} \left\{\dot{q}\right\}^T \begin{bmatrix} 1 & -1 \\ -1 & 1 \end{bmatrix} + \pi \rho abd\, g \begin{bmatrix} 0.6997 \\ 0.6992 \end{bmatrix} \right) \left\{\delta q\right\} dt = 0 \tag{4.26}$$

As the virtual displacements $\left\{\delta q\right\}$ are arbitrary; therefore the bracketed part in Eq. (4.26) can be put equal to zero and it represents the equations of motion of an individual ellipsoidal element

$$[\mathbf{M}]\{\ddot{q}\}^{T} + [\mathbf{H}]\{\dot{q}\}^{T} + [\mathbf{K}]\{q\}^{T} = \left\{F_{G}\right\} \qquad (4.27)$$

where, $[\mathbf{M}], [\mathbf{H}], [\mathbf{K}]$ represent elemental mass, viscoelastic damping and stiffness matrices respectively and $\{F_{G}\}$ is the equivalent gravitation force vector acting on respective nodes. It can be observed in Eq. (4.27) that accounting for gravity force results in a non-homogeneous differential equation. Here,

$$[\mathbf{M}] = \pi \rho a b d \begin{bmatrix} 0.3921 & 0.3071 \\ 0.3071 & 0.3921 \end{bmatrix}; [\mathbf{H}] = \frac{\pi \eta a b}{3.6733*d} \begin{bmatrix} 1 & -1 \\ -1 & 1 \end{bmatrix}; [\mathbf{K}] = \frac{\pi E a b}{3.6733*d} \begin{bmatrix} 1 & -1 \\ -1 & 1 \end{bmatrix}; \left\{F_{G}\right\} = \pi \rho a b d g \begin{bmatrix} 0.6992 \\ 0.6992 \end{bmatrix} (4.28)$$

It is to be noted that in Eq. (4.28), E and η are average elastic modulus and average dynamic viscosity of an individual element, whereas ρ is the average density of whole body, i.e. constant for all the elements.

4.3 Response of standing subject under vertical excitation: Table 4.1 lists the connectivity matrix of for the FE model of standing subject, required to assemble global matrices of mass $[\underline{\mathbf{M}}]$, viscoelastic damping $[\underline{\mathbf{H}}]$, stiffness $[\underline{\mathbf{K}}]$ and gravity force $\{\underline{F_{G}}\}$ vector.

Table 4.1: Element Connectivity matrix showing local nodes and global nodes for respective elements

Element Name	H	N	UT	RUA	LUA	RLA	LLA	CT	LT	RUL	LUL	RLL	LLL	RF	LF
Node A (q_A)	1	2	3	3	3	5	6	4	9	10	10	11	12	13	14
Node B (q_B)	2	3	4	5	6	7	8	9	10	11	12	13	14	15	16

Figure 4.5 shows a schematic representation of human body FE model developed in the present paper. It is to be noted that in Fig. 4.5; nodes 3, 3*r* and 3*l* are

one and same and shown displaced only for the clarity of representation. Same caveat applies for the nodes 10, 10*l* and 10*r*.
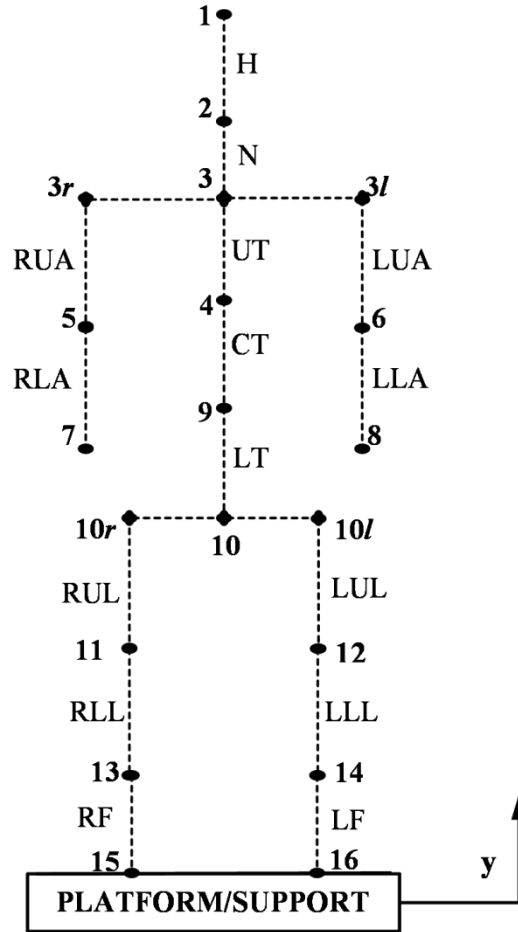
Figure 4.5: Schematic diagram for FE model of standing subject under vertical excitation

After element assembly using Table 4.1, equations of motion for a standing subject under vertical excitation at feet-platform interface are

$$[\underline{\mathbf{M}}]_{16X16}\left\{\underline{\ddot{q}}\right\}_{16X1} + [\underline{\mathbf{H}}]_{16X16}\left\{\underline{\dot{q}}\right\}_{16X1} + [\underline{\mathbf{K}}]_{16X16}\left\{\underline{q}\right\}_{16X1} = \left\{\underline{F_G}\right\}_{16X1} \qquad (4.29)$$

Excitation of human body is caused by the imposed/prescribed displacement of rigid platform and there is no relative motion between plantar aspects of subject's feet and the vibrating platform. This boundary condition is premised on the relative position of human body on the vibrating platform for experimental studies (Garg &

85

Ross, 1976; Gupta, 2007). Thus, the motion of lower nodes of subject's feet, as shown in Fig. 4.5, is equal to the motion of platform (y).

$$q_{15} = q_{16} = y \tag{4.30}$$

Accordingly column matrix of nodal displacements ($\{\underline{q}\}_{16X1}$) can be split into prescribed/specified nodal displacements ($\{\underline{q_s}\}_{2X1}$) and unknown/remainder nodal displacements ($\{\underline{q_r}\}_{14X1}$) (Petyt, 2010).

$$\{\underline{q}\}_{16X1} = \begin{Bmatrix} \{\underline{q_r}\}_{14X1} \\ \{\underline{q_s}\}_{2X1} \end{Bmatrix} = \begin{Bmatrix} \{q_1 \quad q_2 \quad ... \quad q_{13} \quad q_{14}\}^T \\ \{q_{15} \quad q_{16}\}^T \end{Bmatrix} \tag{4.31}$$

Eq. (4.29) can also be partitioned as,

$$\begin{bmatrix} \underline{M_{rr}} & \underline{M_{rs}} \\ \underline{M_{sr}} & \underline{M_{ss}} \end{bmatrix} \begin{Bmatrix} \ddot{q_r} \\ \ddot{q_s} \end{Bmatrix} + \begin{bmatrix} \underline{H_{rr}} & \underline{H_{rs}} \\ \underline{H_{sr}} & \underline{H_{ss}} \end{bmatrix} \begin{Bmatrix} \dot{q_r} \\ \dot{q_s} \end{Bmatrix} + \begin{bmatrix} \underline{K_{rr}} & \underline{K_{rs}} \\ \underline{K_{sr}} & \underline{K_{ss}} \end{bmatrix} \begin{Bmatrix} \underline{q_r} \\ \underline{q_s} \end{Bmatrix} = \begin{Bmatrix} \underline{F_{Gr}} \\ \underline{F_{Gs}} \end{Bmatrix} \tag{4.32}$$

Separating equations of motion corresponding to unknown nodes and prescribed nodes, Eq. (4.32) becomes

$$\begin{bmatrix} \underline{M_{rr}} \ \ddot{q_r} + \underline{H_{rr}} \ \dot{q_r} + \underline{K_{rr}} \ \underline{q_r} \end{bmatrix} + \begin{bmatrix} \underline{M_{rs}} \ \ddot{q_s} + \underline{H_{rs}} \ \dot{q_s} + \underline{K_{rs}} \ \underline{q_s} \end{bmatrix} = \begin{Bmatrix} \underline{F_{Gr}} \end{Bmatrix} \tag{4.33}$$

Equation (4.33) represents a set of fourteen simultaneous, linear, non-homogenous, second order differential equations. Using Eq. (4.33), unknown nodal displacements $\{\underline{q_r}\}$ are computed as function of prescribed nodal displacements $\{\underline{q_s}\}$ i.e. motion of the platform. Nodal displacements $\{\underline{q_r}\}$ and $\{\underline{q_s}\}$ combined with Eq. (4.12), which defines field variable in terms of nodal variable, completely describe the

86

dynamic response at every point of the human body in vertical direction for standing posture under vertical support excitation. Assuming harmonic excitation of rigid platform as

$$y = Y\ e^{j\omega t} \tag{4.34}$$

where, Y and ω are the amplitude and the frequency of vibrating platform respectively. From Eq. (4.30)

$$\{\underline{q}_s\} = \begin{Bmatrix} q_{15} \\ q_{16} \end{Bmatrix} = Y\ e^{j\omega t} \begin{Bmatrix} 1 \\ 1 \end{Bmatrix} \tag{4.35}$$

For harmonic excitation of the platform (i.e. feet), represented by Eq. (4.35), general solution of unknown nodal displacements can be written as,

$$\{\underline{q}_r\} = \{\underline{Q}_r\}e^{j\omega t} + \{\underline{C}_r\} \tag{4.36}$$

where, $\{\underline{Q}_r\}_{14X1}$ are the complex amplitude of unknown nodal displacements due to harmonic excitation (solution of the homogeneous part), calculated as,

$$\{\underline{Q}_r\} = -\left[\underline{\mathbf{K}}_{rr} - \omega^2\underline{\mathbf{M}}_{rr} + j\omega\underline{\mathbf{H}}_{rr}\right]^{(-1)}\left[\left[\underline{\mathbf{K}}_{rs} - \omega^2\underline{\mathbf{M}}_{rs} + j\omega\underline{\mathbf{H}}_{rs}\right]Y\ \begin{Bmatrix} 1 \\ 1 \end{Bmatrix}\right] \tag{4.37}$$

$\{\underline{C}_r\}_{14X1}$ are the particular solution related to $\{\underline{F}_{Gr}\}$. As $\{\underline{F}_{Gr}\}$ is due to constant gravity force (not function of time and frequency of applied excitation); thus resulting $\{\underline{C}_r\}$ are also constant.

4.3.1 NAMS of standing subject: Using dynamic response of standing subject, as determined in section 4.3, driving point parameters such as NAMS, transmissibility

etc. can be computed. NAMS of a standing subject (M_{NMS}) under support excitation is defined as

$$M_{NMS} = \frac{1}{M_{total}} \left(\frac{F_{fp}(\omega)}{\ddot{y}(\omega)} \right) \tag{4.38}$$

where, M_{total} is the mass of the subject, $F_{fp}(\omega)$ is the frequency dependent force at feet-platform interface and $\ddot{y}(\omega)$ is the applied acceleration at feet-platform interface. For the present FE model, shown in Fig. 4.5, F_{fp} is equal to the frequency dependent force generated due to vibration of all the ellipsoidal elements i.e.,

$$F_{fp} = \sum_{i=1}^{15} \left(\int_v \left(dm \right) \ddot{u} \right)_i \qquad i = 1, 2, ..., 15 \tag{4.39}$$

For an individual element, using Eq. (4.12)

$$\int_v \left(dm \right) \ddot{u} = \int_v (\rho \, dv) \left([N_A \ N_B] \left\{ \begin{matrix} \ddot{q}_A \\ \ddot{q}_B \end{matrix} \right\} \right)$$

$$= \rho \int_z [N_A \ N_B] \left\{ \begin{matrix} \ddot{q}_A \\ \ddot{q}_B \end{matrix} \right\} A \, dz$$

$$\Rightarrow \int_v \left(dm \right) \ddot{u} = (0.69917) \pi abd\rho [1 \quad 1] \left\{ \ddot{q}_A \quad \ddot{q}_B \right\}^T \tag{4.40}$$

For harmonic excitation of the platform, values for $\ddot{q}_A$ and $\ddot{q}_B$ of individual elements are extracted from Eqs. (4.35) and (4.36) and corresponding inertial force is calculated using Eq. (4.40). Then, the complex value M_{NMS} for the standing subject is determined using Eq. (4.38).

4.3.2 Optimal Elastic Moduli and Dynamic Viscosity: Stiffness and viscoelastic damping matrices of individual finite elements are calculated using Eq. (4.28) while assigning specific values to elastic modulus (E) and dynamic viscosity (η) of different body segments. The values of E and η for all the elements are optimized, defining the objective function as the difference between theoretically computed values of M_{NMS} for 50th percentile U.S. male and the experimental results available in the literature (Matsumoto & Griffin 1998). The objective function is

$$\text{Minimize} \quad R = \sum_{l=1}^{N}\left[\left(\left|M_{NMS}\left(\omega_l\right)_{ex}\right| - \left|M_{NMS}\left(\omega_l\right)_{th}\right|\right)^2\right] + \sum_{i=1}^{N}\left[\left(\phi_{M_{NMS}}\left(\omega_l\right)_{ex} - \phi_{M_{NMS}}\left(\omega_l\right)_{th}\right)^2\right] \quad (4.41)$$

where, $\left|M_{NMS}\left(\omega_l\right)_{ex}\right|$ and $\phi_{M_{NMS}}\left(\omega_l\right)_{ex}$ are the modulus and phase respectively, for the median experimental values of NAMS (Matsumoto & Griffin 1998) of standing subject. $\left|M_{NMS}\left(\omega_l\right)_{th}\right|$ and $\phi_{M_{NMS}}\left(\omega_l\right)_{th}$ are corresponding theoretical values of NAMS computed using Eq.(4.38) for the present anthropometric FE model. Matsumoto and Griffin (1998) recorded experimental measurements of twelve male subjects in different standing postures under vertical excitation at the feet and M$_{NMS}$ was calculated at five different r.m.s. values of random vibration. In this study, median M_{NMS} measured at 1.0 ms^{-2} r.m.s. value in normal standing posture has been selected as the experimental data required for optimization. The objective function is evaluated at N number of discrete frequencies in the range of 0-20 Hz.

4.3.3 Transmissibility: To confirm and establish the optimal elastic moduli and dynamic viscosity estimated using Eq. (4.41); transmissibility at nodes joining different FE elements has been computed and compared with the experimentally measured transmissibility at similar locations/joints of standing subject (Matsumoto &

Griffin 1998, Paddan & Griffin 1993). For harmonic support excitation, transmissibility at r^{th} node ($TR|_r$) is

$$TR|_r = \frac{\ddot{q}_r}{\ddot{y}} = \frac{\omega^2 Q_r}{\omega^2 Y} \qquad r=1,2,...14 \qquad (4.42)$$

Substituting Q_r values from Eq. (36), which is based on optimal elastic moduli and dynamic viscosity, theoretical value of $TR|_r$ is computed using Eq. (42).

4.4 Results and Discussion: Anthropometric measurements of 50th percentile U.S. male (Table-A Appendix) have been used to calculate NAMS for finite element vibratory model of a standing subject. Applying the scheme listed in Appendix Table-B and using truncation factor of 5% ($d_i= 0.95\ c_i$); dimensions of ellipsoidal finite elements have been computed and listed in Table 4.2.

Table 4.2: Dimensions of truncated ellipsoidal finite element (50th percentile U.S. male)

Element No.	Body Segment	a_i (cm)	b_i (cm)	d_i (cm)
1	H	7.785	7.785	9.434
2	N	6.040	6.040	1.178
3	UT	16.445	11.660	17.832
4,5	RUA, LUA	5.239	5.239	17.832
6,7	RLA, LLA	4.628	4.628	23.128
8	CT	14.110	10.755	20.480
9	LT	17.715	11.595	11.564
10,11	RUL, LUL	5.927	5.927	26.434
12,13	RLL, LLL	5.303	5.303	21.959
14,15	RF, LF	4.675	12.700	3.282

Mass matrices $[\mathbf{M}]$ of individual elements are calculated from Eq. (4.28) using data listed in Table 4.2 and density (ρ) of the human body. In this study, ρ has been calculated as ratio of the mass of subject (M_{total}) and the total volume of all truncated ellipsoids. For 50th percentile U.S. male, with M_{total} =74.9 kg; ρ comes out to be

1.1390*10^{-3} kg/cm^3. This value is within the range of values available in literature for density of human body segments (Bartz &Gianotti, 1975; Liu & Wickstrom, 1973).

4.4.1 Optimal Values of *E* and *η*: As discussed in section 4.2, stiffness and damping matrices of finite elements of vibratory model for 50th percentile U.S. male are constructed through Eqs. (4.17) and (4.22) respectively and then optimization process is executed using Eq. (4.41) in section 4.3.2. In the present study, Jaya algorithm (Rao, 2016; Rao & Waghmere, 2017) for constrained optimization has been employed to estimate *E* and *η* of all the body segments. Jaya algorithm is a global search method, and does not require any algorithm specific control parameters. During optimization process, upper and lower limits of design variables i.e. E_i and $η_i$ were taken as

$$0.01E_G \leq E_i \ \leq \ 10E_G \qquad i=1,2,3... \ 14,15$$
$$10^2 \leq η_i \ \leq \ 10^8 \qquad i=1,2,3... \ 14,15$$

where, E_G=13.02 MN/m^2 is the value of elastic moduli used by Nigam and Malik (1987), same for all ellipsoidal segments. The undamped vibratory model developed Nigam and Malik (1987) predicted natural frequencies of standing subject to a fair degree of accuracy. Same value of elastic moduli, i.e. E_G was further established by Gupta (2007) based on the dynamic response of standing subjects undergoing vertical vibration. Therefore limits for E_i were decided keeping E_G as a reference value. To the best of ones' knowledge, FE vibratory model of human body assuming average value of dynamic viscosity for a body segment such as arm or leg or torso etc., is being attempted for the first time. Although value of dynamic viscosity for human body constituents such as specific ligaments, muscles, tissues etc. are available in literature, there is no such data available for body segments. Therefore, the limits on $η_i$ (in N-

sec/m^2) during optimization are solely based on numerical simulations conducted by the authors, which were observed to be quite wide. Symmetry of anthropometric human body model about mid-sagittal plane was ensured by applying constraints listed below

$$E_4 = E_5; \ E_6 = E_7; \ E_{10} = E_{11}; \ E_{12} = E_{13}; \ E_{14} = E_{15}$$
$$\eta_4 = \eta_5; \ \eta_6 = \eta_7; \ \eta_{10} = \eta_{11}; \ \eta_{12} = \eta_{13}; \ \eta_{14} = \eta_{15}$$ (4.43)

Table 4.3 lists the optimal values for E_i and η_i estimated after multiple trials using Jaya algorithm. Figure 4.6 shows the comparison between experimental measurements of normalized apparent mass M_{NMS} from Matsumoto & Griffin (1998) and theoretically computed value for the same.

Table 4.3: Optimal value of E_i and η_i for truncated ellipsoidal finite element

Ellipsoidal Segment	H	N	UT	RUA, LUA	RLA, LLA	CT	LT	RUL, LUL	RLL, LLL	RF, LF
Elastic Modulus (* E_G) MN/m^2	0.101	0.143	0.748	0.038	5.683	0.250	0.102	3.988	4.294	0.026
Average Dynamic Viscosity(*10^2) KN-sec/m^2	3.588	2.258	3.644	0.062	3.028	0.456	0.254	0.717	0.368	2.976
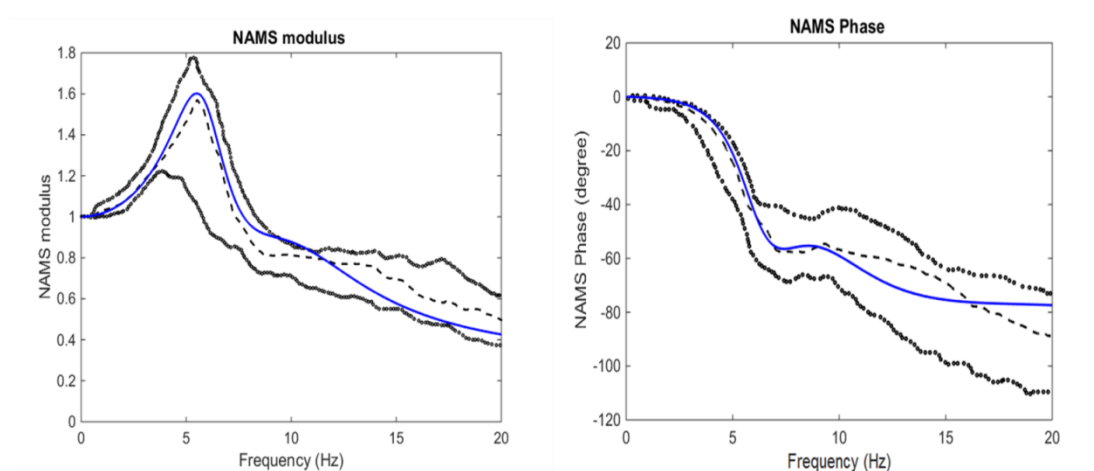
Figure 4.6: Normalized apparent mass for FE model (optimal E_i and η_i) and experimental data
(------ median experimental values; ———— FE model values; ▫▫▫▫▫▫ experimental upper and lower limit)

It is observed in Fig. 4.6 that with the optimized values of E_i and η_i listed in Table 4.3, theoretical curve for both modulus of M_{NMS} and its phase matches closely with the median experimental curves for the same. Theoretically computed values of M_{NMS} lie within the experimental envelop for the frequency range of 0-20 Hz. Moreover, the agreement between the two curves, in the proximity of the resonant frequency ($\sim$ 6-7 Hz), is quite good. These results validate the methodology used and values of E_i and η_i estimated, in the present chapter, to develop FE vibratory model of standing subjects based on their anthropometric data.

4.4.2 Transmissibility: The optimized values of E_i and η_i listed in Table 4.3 are further established through comparison of theoretical values of *TR* with the experimentally measured *TR*. Using Eq. (4.42), $TR|_r$ values for head(r=1) and shoulder(r=3) were calculated and compared, as shown in Fig.7, with experimental data available in the literature (Matsumoto & Griffin 1998, Paddan & Griffin 1993).
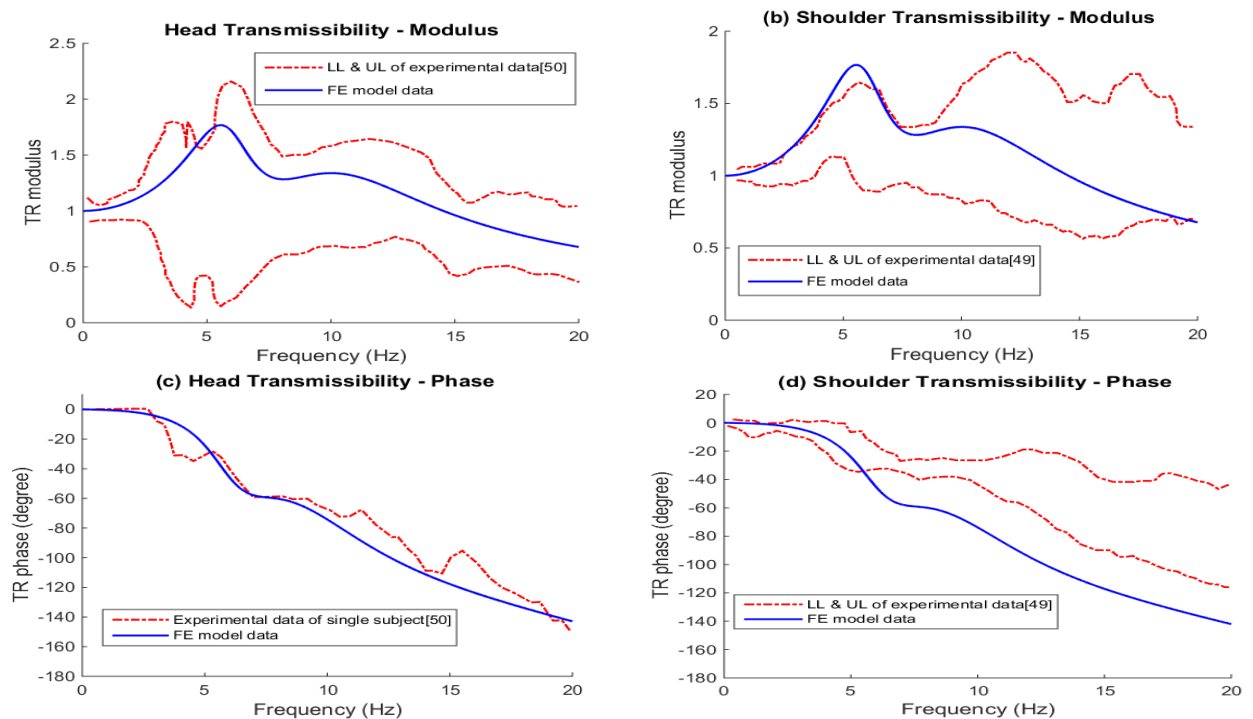
Figure 4.7: Comparison of transmissibility for FE model (optimal E_i and η_i) and experimental envelop

It is to be noted here that Paddan and Griffin (1993) showed phase data, as shown in Fig. 4.7(c), for the head transmissibility of one specific subject standing with legs in locked position and undergoing vertical vibration. As evident from Fig. 4.7, theoretical transmissibility with respect to different locations of human body lies within envelop of experimental data reported in the literature. These results further establish the scheme for the development of FE vibratory model of standing person using anthropometric data and also establish the optimal values of elastic moduli and average dynamic viscosity for different body segments.

It is important to emphasize here that the anthropometric data, used to optimize elastic moduli and dynamic viscosity, essentially belongs to the 50th percentile U.S. male. The experimental results available in the literature for NAMS and transmissibility belong to two different groups of people. Moreover, FE model has been developed assuming dominant motion in vertical direction. For some of the body segments like hip and knee, the local pitch motion of joints, which is not included in present scheme, substantially affects experimental measurements of transmissibility. Availability of anthropometric data of the group of subjects participating in experimental study and also the inclusion of rotational motion in present model should lead to better correspondence between theoretical results and experimental datasets of transmissibility.

4.4.3 Mode Shapes of standing subject: Mode shapes of a standing subject under vertical excitation have been plotted using optimal elastic moduli listed in Table 4.3 for the present FE model. Natural frequencies (ω_n) of undamped FE model are listed in Table 4.4 and corresponding mode shapes (only for ω_n<100 Hz) are plotted and shown in Fig. 4.8.

In Fig. 4.8, dotted lines represent the reference position of standing human body (refer Fig. 4.5) and solid lines represent the mode shapes corresponding to different natural frequencies. For clarity of representation, displacement of nodes along z axis (Fig. 4.1) has been shown in horizontal plane in Fig. 4.8. It is to be noted that Fig. 4.8 is not to the scale, i.e., lengths of ellipsoidal finite elements along vertical axis shown in the figure are not proportionate to the values of d_i as listed in Table 4.2.

Table 4.4: Natural frequencies of FE model using optimal E_i value for truncated ellipsoids

Mode No.	1	2	3	4	5	6	7	8	9	10	11	12	13	14
Natural Freq. ω_n (Hz)	4.55	7.16	8.1	17.7	37.5	47.14	56.24	99.88	137.60	206.52	233.48	254.23	266.09	284.03

As shown in Fig. 4.8, except the modes corresponding to 7.16 Hz and 56.24 Hz, all other modes for vertical vibration of standing subject are whole body modes. For the mode at 7.16 Hz, motion of the arms is dominant whereas the mode relating to 56.24 Hz shows only motion of the legs. Comparing the natural frequencies listed in Table 4.4 with the location of peaks in the experimental and theoretical results for NAMS in Fig. 4.6, it appears that the modes corresponding to 4.55 Hz, 7.16 Hz and 8.09 Hz must have major contribution to response near dominant peak of NAMS whereas the mode corresponding to 17.71 Hz is damped. As mentioned earlier, Fig.4.8 doesn't show different body segments proportionate to their actual length along the vertical axis, therefore, the exact locations of nodes have to be calculated for different mode shapes. The presence of node indicates completely cyclic stress within a body segment, implying critical fatigue stresses.

It is emphasized here that actual mode shapes of any human body subjected to vertical vibration will depend on many parameters like mass distribution in different body segments, age, active nature etc. of the human-being. Therefore, exact prediction

of mode shape is only possible when subject specific anthropometric data are available. Nevertheless, estimated mode shapes shown in Fig. 4.8 are important means to identify locations susceptible to vibration injuries in case of WBV.
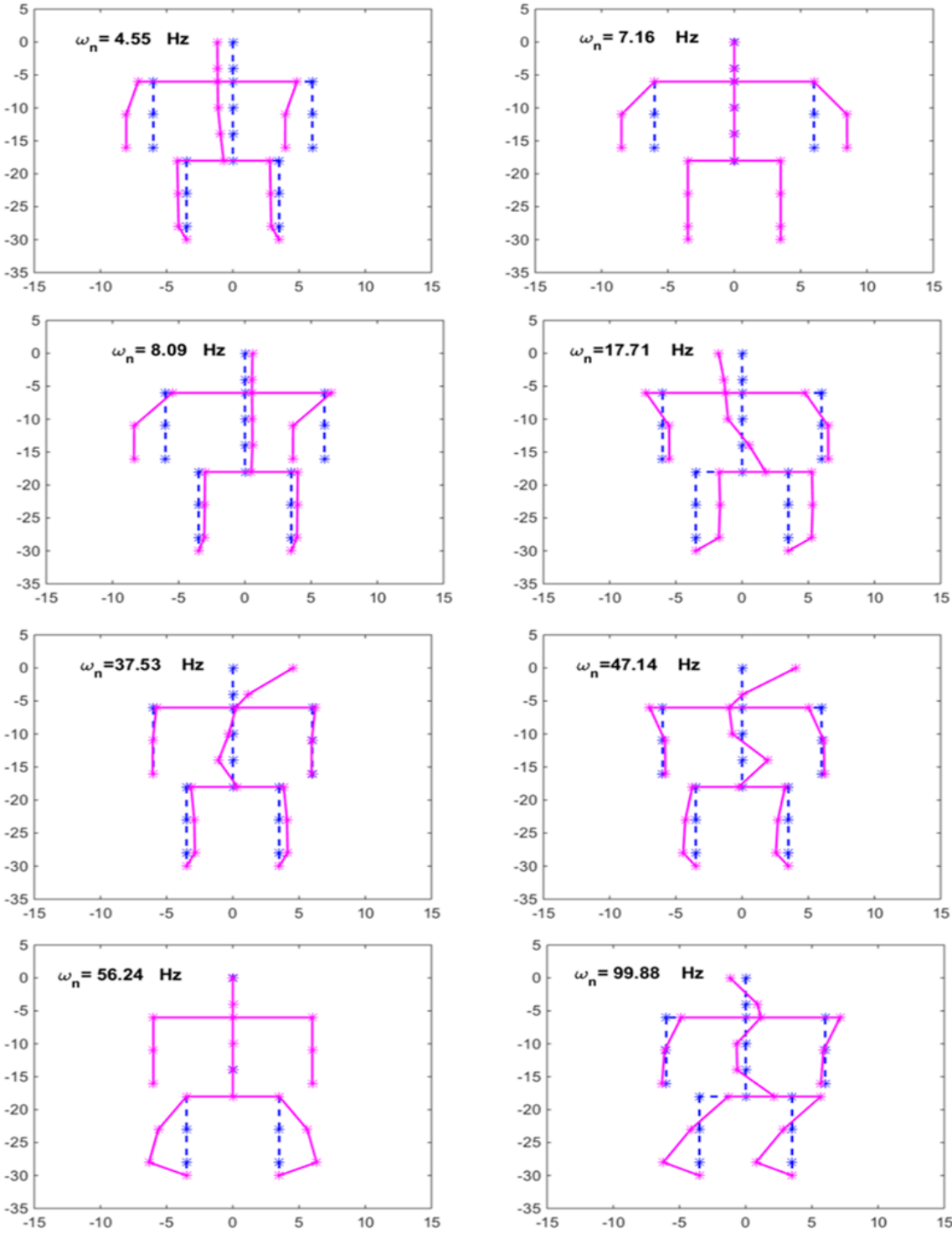
Figure 4.8: Mode Shapes of standing subject under vertical excitation using FE model
(----- undeformed; ——— mode shape)

4.5 Conclusion

The finite element modeling, proposed in this chapter, represents human body by fifteen truncated visco-elastic ellipsoidal elements and requires only anthropometric measurements and visco-elastic parameters. Following this methodology, person specific vibratory models can be developed. Shape functions for the elements are based on exact solutions for deformation of truncated ellipsoid under vertical axial load. As shown in Fig. 4.8, this model is also effective for identifying locations in standing subject corresponding to completely cyclic (fatigue) stresses. The anthropometric data of 50th percentile U.S. male is used to optimize elastic and damping properties of each ellipsoidal element through comparison of experimental data and computed values of normalized apparent mass. The elastic moduli and dynamic viscosity concluded are given in Table 4.3. Computed values for transmissibility of head and shoulder with reference to the platform also lie within envelops of experimental measurements. The correspondence between experimental measurements and theoretically predicted driving point mechanical impedance values can be made better provided the anthropometric data of group of people actually participating in experimental studies is available. The proposed model can be further improved by inclusion of rotational degrees of freedom, particularly for body segments having appreciable pitch motion.

<center>**Chapter 5**</center>

<center>**Finite Element Vibratory Model of Seated Subject**</center>

Finite Element model of a standing person based on anthropometric data was developed in the previous chapter. As one of the primary objective of present research work is to study effects of road undulation on vehicle rider (especially two-wheeler rider), it is obligatory to develop a similar model for a seated person. In the present chapter, following a step by step approach; a FE vibratory model of seated person with hands in the vertical position is formulated.

5.1 Introduction

A FE model of the human body is formulated to estimate dynamic response of a seated person in normal upright posture with hands in straight down position, under vertical excitation from the feet and the pelvis. As described in chapter 2, the human body has been divided into fifteen physically distinct segments considering its anatomical structure, whose mass and geometrical parameters are determined from anthropometric measurements and average density of the human body.

For a sitting individual, only thirteen individual segments are approximated by truncated ellipsoidal elements (Nigam & Malik, 1987; Gupta, 2007) and the remaining two body segments (upper legs) are represented by rigid rods (Liu et al., 2015). Similar to the FE model of a standing subject, whole of the truncated ellipsoid with two nodes (one at each end) is taken as a finite element and Kelvin-Voigt model for viscoelastic materials is used to incorporate stiffness and energy dissipation (damping) in ellipsoidal elements. Elastic moduli and average dynamic viscosity of individual

<center>98</center>

segments are optimized by minimizing the difference between normalized apparent mass (NAMS) calculated from the FE model and experimental data available in the literature (Fairley & Griffin, 1989). Thereafter, transmissibility at different joints of seated subjects has been investigated as a function of excitation frequency. Mode shapes are constructed to locate the critical areas of fatigue stresses.

5.2 Human Body Segmentation and Element Formulation

Figure 5.1 shows the connectivity of different truncated ellipsoids for seated human body and Fig. 5.2 represents the schematic of human body used for FE modeling in the present work. The model consists of fifteen finite elements having sixteen nodes in total. It is to be noted that in Fig. 5.2; nodes 3, 3r and 3l remain at the same level (w.r.t. to z axis) during motion. The same restriction is applicable to nodes 10, 10l and 10r. In FE model, RUL and LUL are represented by rigid rods, which are connected between 10l and 11 and 10r and 12 respectively, by torsional springs and dampers to adjacent ellipsoidal elements (Fig. 5.3(b)). Truncated ellipsoid segments, as shown in Fig. 5.3(a), are assumed (for subjects under vertical excitation) to deform dominantly along the z axis and cross-axis deformations have been neglected. For vertical excitation of sitting person, the motion of upper body (from head to lower torso) contributes significantly to experimental measurement of apparent mass (Kitazaki & Griffin, 1997). Upper leg segments, horizontal in sitting posture, contribute little to apparent mass for vertical excitation of seated human body and hip/knee joints behave as pin joints (Matsumoto & Griffin, 2001; Pankoke et al., 1998). Therefore, all body segments of a seated person which are vertical are modeled as truncated ellipsoidal elements and remaining body segments (horizontal) are modeled as rigid rods connected with rotational springs/dampers.
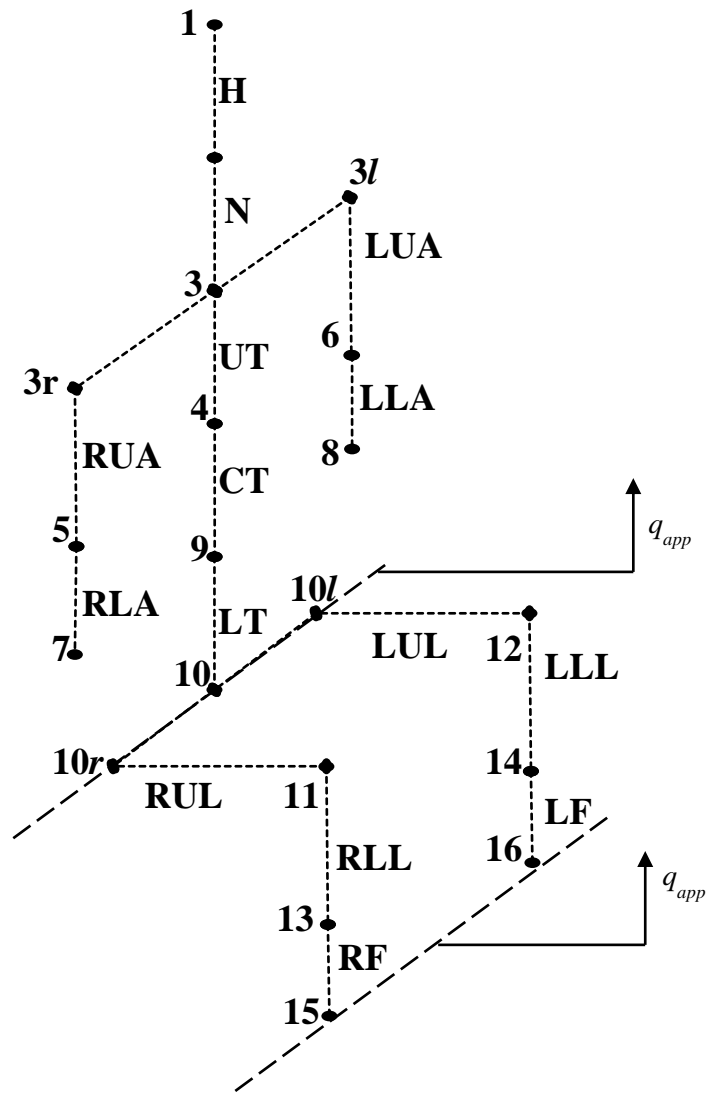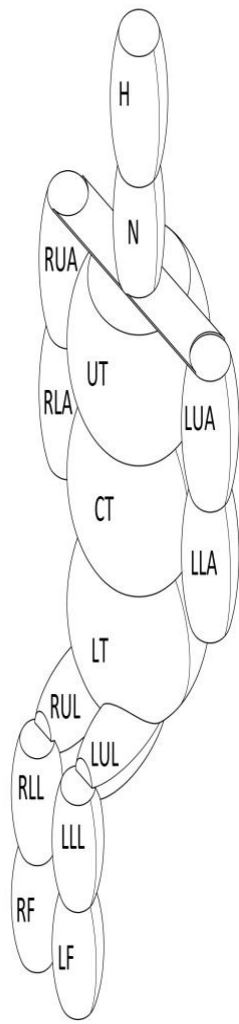
Fig. 5.1 Ellipsoidal segmentation of seated human body;   Fig. 5.2 Human body stick model
(**H**: Head, **N**: Neck, **UT**: Upper Torso, **CT**: Central Torso, **LT**: Lower Torso, **LUA**: Left Upper Arm, **RUA**: Right Upper Arm, **LLA**: Left Lower Arm, **RLA**: Right Lower Arm, **LUL**: Left Upper Leg, **RUL**: Right Upper Leg, **LLL**: Left Lower Leg, **RLL**: Right Lower Leg, **LF**: Left Foot, **RF**: Right Foot)

5.2.1 Shape Functions for Truncated Ellipsoids: For un-truncated ellipsoid, semi-axes (*a, b, c*) have been computed from anthropometric measurements of the subjects using scheme developed by Bartz & Gianotti (1975). Ellipsoids are truncated at both ends, as shown in Fig. 5.3(a), to represent area contact of actual body segments. Truncation factor of 5% has been adopted, i.e. nodes A and node B are at $z = -d$ and $z = +d$ respectively; where $d = 0.95\ c$.

100
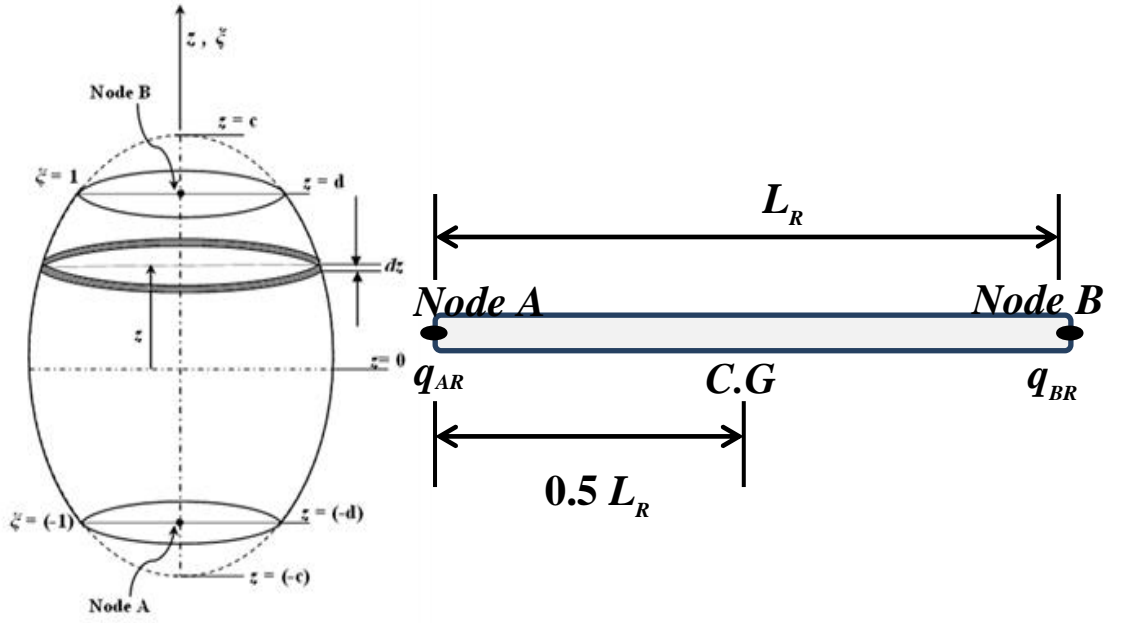
Fig. 5.3 (a) Truncated ellipsoidal finite element (b) Rigid rod element

Stress-strain behavior of truncated ellipsoids has been modelled assuming individual body segments as homogenous, isotropic and viscoelastic members having average elastic moduli (E) and average dynamic viscosity (η). In numerous experimental and theoretical studies, behavior of human body constituents has been modeled as viscoelastic member (Johnson et al, 1994; Kubo et al., 2001; Saraf et al., 2007; Marini et al., 2017). Ellipsoidal body segments are assumed to follow Kelvin-Voigt model of viscoelastic materials in present work. Total stress (σ) resulting from uni-directional strain along z-axis (Fig. 5.3(a)) is:

$$\sigma = \sigma_{ela} + \sigma_{vis} = E\varepsilon_z + \eta\frac{\partial}{\partial t}\left(\varepsilon_z\right) \tag{5.1}$$

where; σ_{ela}, σ_{vis}, ε_z are the elastic stress, time dependent viscous stress, and axial strain respectively. E and η are average elastic moduli and average dynamic viscosity

of individual body segments. For vertical excitation of body segments, neglecting cross-axis deformations, resulting stress/strain field is taken as uni-directional.

The shape functions for truncated ellipsoidal finite elements are based on the exact solution for deformation field of an ellipsoid under uni-axial load. For an elliptical strip of length dz, as shown in Fig. 3(a), deformation (ΔL_{dz}) due to unit load at node B is

$$\Delta L_{dz} = \frac{(1)dz}{E \cdot \pi ab \left(1 - \frac{z^2}{c^2}\right)} \tag{5.2}$$

For partial segment of ellipsoid, from the lower end up to a distance z, deformation (ΔL_z) is

$$\Delta L_z(z) = \int_{-d}^{z} \frac{d\alpha}{E \cdot \pi ab \left(1 - \frac{\alpha^2}{c^2}\right)} \tag{5.3}$$

Integrating Eq. (5.3) and taking $d = 0.95$ c

$$\Delta L_z(\chi) = \kappa \left(\ln\left(\frac{1+\chi}{1-\chi}\right) + \ln\left(\frac{1+0.95}{1-0.95}\right) \right) \tag{5.4}$$

where, $\kappa = \frac{c}{2\pi Eab}$ and $\chi = \frac{z}{c}$

Normalized deformation ($\Delta L(\chi)$) for the partial segment of ellipsoid mentioned above is,

$$\Delta L(\chi) = \frac{\Delta L_z(\chi)}{\Delta L_z(\chi_{max})} = \frac{1}{7.3271} \left(\ln\left(\frac{1+\chi}{1-\chi}\right) + \ln\left(\frac{1+0.95}{1-0.95}\right) \right) \tag{5.5}$$

102

As $|\chi| < 1$ for every segment of truncated ellipsoid, Eq. (5.5) can be written as

$$\Delta L(\chi) = \frac{1}{7.3271}\left(2*\left(\chi + \frac{\chi^3}{3} + \frac{\chi^5}{5} + \frac{\chi^7}{7} + \frac{\chi^9}{9}\right) + \ln\left(\frac{1+0.95}{1-0.95}\right)\right) \tag{5.6}$$

For $|\chi| \leq 0.90$, difference between $\Delta L(\chi)$ computed from Eq. (5.5) and Eq. (5.6) is less than 2.5%. Maximum difference between two values, at $|\chi| = 0.90$, is 7.4%. Eq. (5.6) can be written in terms of non-dimensional natural co-ordinate ξ ($\xi = \frac{z}{d}$) as

$$\Delta L(\xi) = \frac{1}{7.3271}\left(2*\left(0.95\xi + \frac{(0.95\ \xi)^3}{3} + \frac{(0.95\ \xi)^5}{5} + \frac{(0.95\ \xi)^7}{7} + \frac{(0.95\ \xi)^9}{9}\right) + \ln\left(\frac{1+0.95}{1-0.95}\right)\right) \tag{5.7}$$

From Eq. (5.7), for node B, shape function (N_B) is

$$N_B(\xi) = \frac{1}{6.2412}\left(3.1207 + 2*\left(0.95\xi + \frac{(0.95\ \xi)^3}{3} + \frac{(0.95\ \xi)^5}{5} + \frac{(0.95\ \xi)^7}{7} + \frac{(0.95\ \xi)^9}{9}\right)\right) \tag{5.8}$$

Similarly, shape function (N_A) for node A is

$$N_A(\xi) = \frac{1}{6.2412}\left(3.1207 - 2*\left(0.95\xi + \frac{(0.95\ \xi)^3}{3} + \frac{(0.95\ \xi)^5}{5} + \frac{(0.95\ \xi)^7}{7} + \frac{(0.95\ \xi)^9}{9}\right)\right) \tag{5.9}$$

From Eq. (5.8) and Eq. (5.9), using shape function matrix **[N]** ($[\mathbf{N}] = [N_A\ N_B]$) and nodal displacement vector displacement $\{\boldsymbol{q}\} = [q_A\ q_B]^T$; internal displacement field ($u(\xi)$) for truncated ellipsoidal finite element is written as:

$$u(\xi) = [\mathbf{N}]\{\boldsymbol{q}\} \tag{5.10}$$

Corresponding strain along vertical axis (ε_z)

$$\varepsilon_z = [\mathbf{B}]\{\boldsymbol{q}\} \tag{5.11}$$

where, $[\mathbf{B}]$ elemental strain-displacement matrix, is

$$[\mathbf{B}] = \frac{2}{6.2412\,d}\left[0.95*\left\{1+\left(0.95\,\xi\right)^2+\left(0.95\,\xi\right)^4+\left(0.95\,\xi\right)^6+\left(0.95\,\xi\right)^8\right\}\left[-1\ \ 1\right]\right] \tag{5.12}$$

5.3 Equations of Motion: For a subject sitting in upright posture on a seat with legs supported on the seat-platform interface, governing equations of motion under synchronous vertical excitation at seat and feet-platform interface have been derived using Hamilton's principle (Petyt, 2010):

$$\delta\left(\int_{t_1}^{t_2}\left(T - U + W_{vis} + W_{ext}\right)dt\right) = 0 \tag{5.13}$$

where, T, U, W_{vis} and W_{ext} are the kinetic energy, the elastic strain energy, the virtual work done by viscous forces and the virtual work done by external forces respectively. In section 5.3.1, these terms are derived for viscoelastic finite elements representing vertical body segments and in section 5.3.2, for rigid rods elements representing horizontal upper legs.

5.3.1 Truncated Ellipsoidal Element:

5.3.1.1 Strain Energy (U_e): The strain energy (U_e) of elements with viscoelastic materials, following stress-strain relationship as given by Eq. (5.1); is only due to the elastic component of stress, i.e. σ_{ela} . The first variation δU_e is

$$\delta U_e = \int_v \sigma_{ela}\,\delta\varepsilon_z dv = \int_v E\,\varepsilon_z\,\delta\varepsilon_z dv \tag{5.14}$$

Substituting Eq. (5.11) into Eq. (5.14) yields

$$\delta U_e = \frac{\pi Eab}{3.6773 * d}\{q\}^T \begin{bmatrix} 1 & -1 \\ -1 & 1 \end{bmatrix}\{\delta q\} \tag{5.15}$$

5.3.1.2 Kinetic Energy (T_e): First variation of kinetic energy (δT_e) for an ellipsoidal element assuming constant density ρ is,

$$\delta T_e = \delta\left(\frac{1}{2}\int_v \rho \,\dot{u}^2\, dv\right) = \int_v \rho \dot{u}\, \delta\dot{u}\, dv \tag{5.16}$$

Simplifying using Eq. (5.10),

$$\delta T_e = \pi\rho abd \left\{\dot{q}\right\}^T \begin{bmatrix} 0.3921 & 0.3071 \\ 0.3071 & 0.3921 \end{bmatrix}\left\{\delta\dot{q}\right\} \tag{5.17}$$

5.3.1.3 Work done by viscous forces (W_{vis_e}): For ellipsoidal elements, the virtual work by non-conservative forces arises due to time varying viscous stresses (σ_{vis}) and is given by

$$\delta W_{vis\_e} = -\int_v \eta \frac{\partial \varepsilon_z}{\partial t} \bullet \delta\varepsilon_z dv \tag{5.18}$$

After simplification,

$$\Rightarrow \delta W_{vis\_e} = -\frac{\pi\eta ab}{3.6733 * d}\left\{\dot{q}\right\}^T \begin{bmatrix} 1 & -1 \\ -1 & 1 \end{bmatrix}\{\delta q\} \tag{5.19}$$

5.3.1.4 Work done by external forces (W_{ext_e}): Gravity applies a constant downward force on all human body elements and its effect on the total response of the human body is equivalent to the addition of a constant to elemental displacement, independent of time and frequency of the applied excitation. Moreover, experimental data for dynamic response, reported in the literature, is based on the signal collected

from load cells between supporting plate and vibrating platform, which does not account the static gravity load. The signals from load cells communicate variation in force with time. Therefore, the effect of gravity on driving point impedance measurements will be zero. Nonetheless, for completeness of mathematical modeling, the work done by gravity and its first variation is as follows:

$$\delta W_{ext\_e} = \delta W_G = \delta\left(\int_v (\rho\, dv\, g)\, u\right) \tag{5.20}$$

From Eq. (5.10)

$$\delta W_{ext\_e} = \pi abd\, \rho\, g\, [0.69917 \quad 0.69917]\{\boldsymbol{\delta q}\} \tag{5.21}$$

Thus, Eq. (5.13) for a truncated ellipsoidal element becomes

$$\int_{t_1}^{t_2}\left(\pi\rho abd\,\{\dot{\boldsymbol{q}}\}^T\begin{bmatrix}0.3921 & 0.3071\\ 0.3071 & 0.3921\end{bmatrix}\{\dot{\boldsymbol{\delta q}}\} - \frac{\pi Eab}{3.6733*d}\{\boldsymbol{q}\}^T\begin{bmatrix}1 & -1\\ -1 & 1\end{bmatrix}\{\boldsymbol{\delta q}\} - \frac{\pi\eta ab}{3.6733*d}\{\dot{\boldsymbol{q}}\}^T\begin{bmatrix}1 & -1\\ -1 & 1\end{bmatrix}\{\boldsymbol{\delta q}\} + \pi\rho abd\, g\begin{bmatrix}0.69917\\ 0.69917\end{bmatrix}\{\boldsymbol{\delta q}\}\right)dt = 0 \tag{5.22}$$

Simplifying and noting $\{\boldsymbol{\delta q}\}|_{t_1} = \{\boldsymbol{\delta q}\}|_{t_2} = 0$;

$$\int_{t_1}^{t_2}\left(-\pi\rho abd\,\{\ddot{\boldsymbol{q}}\}^T\begin{bmatrix}0.3921 & 0.3071\\ 0.3071 & 0.3921\end{bmatrix} - \frac{\pi Eab}{3.6733*d}\{\boldsymbol{q}\}^T\begin{bmatrix}1 & -1\\ -1 & 1\end{bmatrix} - \frac{\pi\eta ab}{3.6733*d}\{\dot{\boldsymbol{q}}\}^T\begin{bmatrix}1 & -1\\ -1 & 1\end{bmatrix} + \pi\rho abd\, g\begin{bmatrix}0.69917\\ 0.69917\end{bmatrix}\right)\{\boldsymbol{\delta q}\}dt = 0 \tag{5.23}$$

In matrix form Eq. (5.23) can be written as,

$$[\mathbf{M}_e]\{\ddot{\boldsymbol{q}}\}^T + [\mathbf{C_e}]\{\dot{\boldsymbol{q}}\}^T + [\mathbf{K}_e]\{\boldsymbol{q}\}^T = \{\mathbf{F_G}\} \tag{5.24}$$

where; $[\mathbf{M}_e], [\mathbf{C_e}], [\mathbf{K}_e]$ and $\{F_G\}$ are given by,

106

$$[\mathbf{M}_e]=\pi\rho abd\begin{bmatrix}0.3921 & 0.3071\\0.3071 & 0.3921\end{bmatrix}\ ;\ [\mathbf{C}_e]=\frac{\pi\eta ab}{3.6733*d}\begin{bmatrix}1 & -1\\-1 & 1\end{bmatrix}\ ;[\mathbf{K}_e]=\frac{\pi Eab}{3.6733*d}\begin{bmatrix}1 & -1\\-1 & 1\end{bmatrix}\ :\ \{F_G\}=\pi\rho abd\,g\begin{bmatrix}0.69917\\0.69917\end{bmatrix}\quad(5.25)$$

and represent the mass matrix, the viscoelastic damping matrix, the stiffness matrix and the equivalent gravitation force vector acting on individual nodes respectively; for the ellipsoidal element.

5.3.2 Rigid Rod Element: Liu et al (2015) modelled femurs as rigid rods surrounded with soft tissue to represent upper legs of a seated person subjected to vertical vibration. In the present model also, both the upper leg segments of seated person have been modelled as rigid rod connected with rotational spring and dampers, as shown in Fig. 5.3(b). Dimensions and inertial parameters of these rods are scaled with reference inertial parameters given in literature Liu et al (2015), for bonny part of upper leg, and using anthropometric measurements employed in present work. As mentioned earlier, it is assumed that upper legs have only rotational motion for a seated person during vertical vibration from seat-platform interface. Figure 5.4 shows the rigid rod element with nodal displacements and location of centre of gravity (at midpoint) used for deriving equation of motion of upper leg segments.
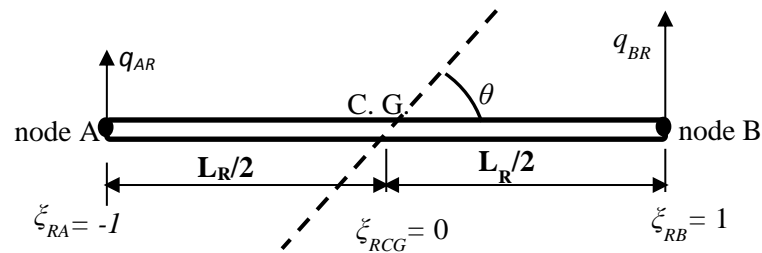
Fig. 5.4 Rigid rod finite element with location of nodes and centre of gravity

5.3.2.1 Strain Energy (U_R): The upper leg segments, modelled as rigid rods are connected to the adjacent truncated ellipsoidal elements by torsional springs and dampers. The first variation of strain energy, stored in torsional springs is given by:

$$\delta U_R = \delta\left(\frac{1}{2}K_{B\theta R}\,\theta^2 + \frac{1}{2}K_{A\theta R}\,\theta^2\right) = \left(K_{B\theta R} + K_{A\theta R}\right)\theta\,\delta\theta \qquad (5.26)$$

where, θ is the angular rotation of rigid rod about C.G. (Fig. 5.3(b)). For small rotations ($\tan\theta \approx \sin\theta \approx \theta$);

$$\theta \approx \frac{q_{BR} - q_{AR}}{L_R} \qquad (5.27)$$

where, q_{BR} and q_{AR} are the nodal displacements at each end of rigid rod as shown in Fig. 5.3(b) and L_R is the length of rigid rod. Therefore Eq. (5.26) can be written as:

$$\delta U_R = \frac{\left(K_{B\theta R} + K_{A\theta R}\right)}{L_R^2}\left[-q_{AR} \quad q_{BR}\right]\left\{\delta q_R\right\} \qquad (5.28)$$

where, $\qquad \left\{\delta q_R\right\} = \left\{\delta q_{AR} \quad \delta q_{BR}\right\}^T$

5.3.2.2 Kinetic Energy (T_R): The first variation of kinetic energy for a rigid rod is given by:

$$\delta T_R = \delta\left(\frac{1}{2}I_{CG}\,\dot{\theta}^2 + \frac{1}{2}m_R\,\dot{z}_{CG}^2\right) = \left(I_{CG}\,\dot{\theta}\right)\delta\dot{\theta} + \left(m_R\,\dot{z}_{CG}\right)\delta\dot{z}_{CG} \qquad (5.29)$$

where, I_{CG} is moment of inertia about lateral axis of the rigid rod, m_R is the mass of rigid rod and z_{CG} is the vertical displacement at center of mass of rigid rod (Fig. 5.3(b)). Substituting Eq. (5.27) and writing z_{CG} in terms of nodal displacement,

$$\delta T_R = \frac{I_{CG}}{L_R^2} \begin{bmatrix} \dot{q}_{AR} & \dot{q}_{BR} \end{bmatrix} \left\{ \delta \dot{q}_R \right\} + \frac{m_R}{2L_R} \begin{bmatrix} \dot{q}_{AR} & \dot{q}_{BR} \end{bmatrix} \left\{ \delta \dot{q}_R \right\} \tag{5.30}$$

5.3.2.3 Work done by viscous forces (W_{vis_R}): Following similar analysis as for the strain energy stored in torsional springs, work done by torsional dampers attached to the ends of rigid rod is:

$$\delta W_{visc\_R} = \frac{(K_{B\theta R} + K_{A\theta R})}{L_R^2} \begin{bmatrix} -\dot{q}_{AR} & \dot{q}_{BR} \end{bmatrix} \left\{ \delta q_R \right\} \tag{5.31}$$

5.3.2.4 Work done by external forces (W_{ext_R}): The rod representing upper leg is assumed to be rigid with a constant diameter and constant density. The variation of work done by gravity at c.g. ($\xi_R = 0$) is

$$\delta W_{ext\_R} = m_R\, g * \delta \left(\left(\frac{1 - \xi_R}{2} \right) q_{AR} + \left(\frac{1 - \xi_R}{2} \right) q_{BR} \right)_{\xi_R = 0}$$

$$\delta W_{ext\_R} = \frac{m_R\, g}{2} \begin{bmatrix} 1 & 1 \end{bmatrix} \left\{ \delta q_R \right\} \tag{5.32}$$

Using Hamilton's principle, equation of motion for the rigid rods in matrix form is

$$[\mathbf{M}_R] \left\{ \ddot{q}_R \right\}^T + [C_R] \left\{ \dot{q}_R \right\}^T + [\mathbf{K}_R] \left\{ q_R \right\}^T = \left\{ \mathbf{F_{GR}} \right\} \tag{5.33}$$

where; $[\mathbf{M}_R], [C_R], [\mathbf{K}_R]$ and $\{\mathbf{F_{GR}}\}$ are

$$[\mathbf{M}_R] = \left(\frac{2I_{CG} + m_R L_R}{2L_R^2} \right) \begin{bmatrix} 1 \\ 1 \end{bmatrix} ; [C_R] = \frac{(C_{B\theta R} + C_{A\theta R})}{L_R^2} \begin{bmatrix} -1 \\ 1 \end{bmatrix} ; [\mathbf{K}_R] = \frac{(K_{B\theta R} + K_{A\theta R})}{L_R^2} \begin{bmatrix} -1 \\ 1 \end{bmatrix} ; \{\mathbf{F_{GR}}\} = \frac{m_R\, g}{2} \begin{bmatrix} 1 \\ 1 \end{bmatrix} \tag{5.34}$$

5.4 Response of seated person under vertical excitation: Table 5.1 shows connectivity matrix of anthropometric FE model of seated subject developed in present study

Table 5.1: Connectivity matrix of anthropometric FE model for seated person

Element Name	H	N	UT	RUA	LUA	RLA	LLA	CT	LT	RUL	LUL	RLL	LLL	RF	LF
Node A (q_A)	1	2	3	3	3	5	6	4	9	10	10	11	12	13	14
Node B (q_B)	2	3	4	5	6	7	8	9	10	11	12	13	14	15	16

After assembly of global mass $[\underline{\mathbf{M}}]$, stiffness $[\underline{\mathbf{K}}]$, viscoelastic damping $[\underline{\mathbf{C}}]$ matrices and force vector $\{\underline{F_G}\}$ due to gravity using Table 5.1, equations of motion for a seated subject under synchronous vertical support excitation from seat and feet interface are

$$[\underline{\mathbf{M}}]_{16X16}\left\{\ddot{\underline{q}}\right\}_{16X1} + [\underline{\mathbf{H}}]_{16X16}\left\{\dot{\underline{q}}\right\}_{16X1} + [\underline{\mathbf{K}}]_{16X16}\left\{\underline{q}\right\}_{16X1} = \left\{\underline{F_G}\right\}_{16X1} \qquad (5.35)$$

Although, the case of WBV of a seated subject due to excitations from supporting platform is essentially a case of support motion; but while considering the human body and platform as system, the external forces from seat and footrest will be considered as applied forces. These forces (F_P) are added at appropriate locations in the force vector.

In experimental studies related to WBV effects on a seated person, a prescribed motion/displacement is imposed on seat with legs resting on vibrating platform and it is assumed that there is no loss of contact between the seat and the pelvis and also between the plantar of subject's feet and the vibrating platform. Thus,

for nodes 10, 15 and, 16 as shown in Fig. 5.2, displacement is equal to the excitation applied (q_{app}).

$$q_{10} = q_{15} = q_{16} = q_{app} \tag{5.36}$$

It is to be noted that in Eq. 5.36, displacement of nodes 10, 15 and 16 (q_{10}, q_{15} and q_{16}) has been taken equal to each other and it is applicable if the hips and legs are in contact with the vibrating platform. If the seat has spring action, displacement of node 10 might be different from nodes 15 &16 and the equation (5.36) will have to be modified accordingly. Now, $\{\underline{q}\}_{16X1}$ is split into ($\{\underline{q}_s\}_{3X1}$) and ($\{\underline{q}_r\}_{13X1}$) as shown in Petyt (2010); where, $\{\underline{q}_s\}$ is the displacement vector of nodes with imposed/applied displacement and $\{\underline{q}_r\}$ is the displacement vector for remaining nodes.

$$\{\underline{q}\}_{16X1} = \begin{Bmatrix} \{\underline{q}_r\}_{13X1} \\ \{\underline{q}_s\}_{3X1} \end{Bmatrix} = \begin{Bmatrix} \{q_1 \quad q_2 \quad \cdots \quad q_9 \quad q_{11} \quad q_{12} \quad q_{13} \quad q_{14}\}^T \\ q_{app} \{1 \quad 1 \quad 1\}^T \end{Bmatrix} \tag{5.37}$$

Separating equations of motion corresponding to un-prescribed and prescribed nodes, Eq. (5.35) becomes

$$\begin{bmatrix} \mathbf{M}_{rr} & \mathbf{M}_{rs} \\ \mathbf{M}_{sr} & \mathbf{M}_{ss} \end{bmatrix} \begin{Bmatrix} \ddot{q}_r \\ \ddot{q}_s \end{Bmatrix} + \begin{bmatrix} \mathbf{C}_{rr} & \mathbf{C}_{rs} \\ \mathbf{C}_{sr} & \mathbf{C}_{ss} \end{bmatrix} \begin{Bmatrix} \dot{q}_r \\ \dot{q}_s \end{Bmatrix} + \begin{bmatrix} \mathbf{K}_{rr} & \mathbf{K}_{rs} \\ \mathbf{K}_{sr} & \mathbf{K}_{ss} \end{bmatrix} \begin{Bmatrix} q_r \\ q_s \end{Bmatrix} = \begin{Bmatrix} F_{Gr} + 0 \\ F_{Gs} + F_P \end{Bmatrix} \tag{5.38}$$

From Eq. (5.38), extracting first equation in matrix form

$$\left[\mathbf{M}_{rr} \, \ddot{q}_r + \mathbf{C}_{rr} \, \dot{q}_r + \mathbf{K}_{rr} \, q_r \right] + \left[\mathbf{M}_{rs} \, \ddot{q}_s + \mathbf{C}_{rs} \, \dot{q}_s + \mathbf{K}_{rs} \, q_s \right] = \left\{ F_{Gr} \right\} \tag{5.39}$$

It may be noted that Eq. (5.39) is sufficient to determine 13 unknown nodal displacements and the force acting from seat and footrest (F_p) is not required. Thus, the present case becomes a vibratory system with support motion.

$\{\underline{q_r}\}$'s can be determined from Eq. (5.39) provided $\{\underline{q_s}\}$ is known as a function of time and frequency of imposed displacement. Solution of Eq. (5.39) along with Eq. (5.10) defines dynamic response of a seated human body under vertical support excitation using FE anthropometric vibratory model developed in the present study. Assuming harmonic excitation

$$q_{app} = Q_{app} \ e^{j\omega t} \tag{5.40}$$

where, Q_{app} and ω are the amplitude and the frequency of excitation respectively. From Eq. (5.36)

$$\{\underline{q_s}\} = \begin{Bmatrix} q_{10} \\ q_{15} \\ q_{16} \end{Bmatrix} = Q_{app} \ e^{j\omega t} \begin{Bmatrix} 1 \\ 1 \\ 1 \end{Bmatrix} \tag{5.41}$$

General solution of unknown $\{\underline{q_r}\}$ can be written as;

$$\{\mathbf{q_r}\} = \{\mathbf{Q_r}\} \ e^{j\omega t} + \{\underline{P_r}\} \tag{5.42}$$

where, $\{\underline{Q_r}\}_{13X1}$ is the solution of homogeneous part of Eq. (5.39) and $\{\underline{P_r}\}_{13X1}$ is the particular solution due to non-homogeneous part $\{\underline{F_{Gr}}\}$. It is important to note that $\{\underline{Q_r}\}$ is complex quantity with both magnitude and phase whereas $\{\underline{P_r}\}$ is a constant quantity because $\{\underline{F_{Gr}}\}$ is independent of time & frequency of applied excitation.

5.4.1 NAMS of subject in sitting posture: Normalised apparent mass of a seated subject can be computed from the dynamic response, computed as described in section 5.4 above, to the vertical excitation. NAMS of a subject sitting in a upright posture (M_{NMS})) under synchronous excitation from pelvis/seat interface and the feet is (Wei & Griffin, 1998)

$$M_{NMS} = \frac{1}{M_{total}} \left(\frac{F_{fp}(\omega)}{\ddot{q}_{app}(\omega)} \right) \tag{5.43}$$

where, F_{fp} is the sum of the forces at pelvis/seat interface, $\ddot{q}_{app}$ is the acceleration applied at the interface and M_{total} is mass of the subject. For anthropometric vibratory model, as shown in Fig. 5.2, F_{fp} is the sum of inertia force of all human body segments modelled as either truncated ellipsoidal finite elements or rigid rods,

$$F_{fp} = \sum_{i=1}^{15} \left(\int_v \left(dm \right) \ddot{u} \right)_i \qquad i = 1, 2, ..., 15 \tag{5.44}$$

Using nodal dynamic response computed from Eq. (5.42), sum of inertial forces can be determined. Then, using Eq. (5.43), NAMS for the seated subject is computed. As $\{Q_r\}$ is a complex quantity, therefore, NAMS is also complex quantity having both magnitude and phase.

5.4.2 Estimation of Elastic Moduli and Dynamic Viscosity: Specific values to E and η for individual ellipsoidal finite elements are required to compute elemental matrices (Eq. (5.25)). E and η values of ellipsoidal elements are estimated using Jaya algorithm of optimization, by minimizing difference between the theoretically

computed M_{NMS} of 50th percentile U.S. male and the available experimental results for group of seated person (Fairley & Griffin, 1989) . Objective function (R) is defined as

$$\text{Minimize} \quad R = \sum_{k=1}^{N}\left[\left(\left|NMS\left(\omega_k\right)_{fe}\right| - \left|NMS\left(\omega_k\right)_{\exp}\right|\right)^2\right] + \sum_{k=1}^{N}\left[\left(\varphi_{NMS}\left(\omega_k\right)_{fe} - \varphi_{NMS}\left(\omega_k\right)_{\exp}\right)^2\right] \quad (5.45)$$

where, $\left|NMS\left(\omega_k\right)_{fe}\right|$ and $\varphi_{NMS}\left(\omega_k\right)_{fe}$ are theoretically computed values of modulus and phase respectively; and $\left|NMS\left(\omega_k\right)_{\exp}\right|$ and $\varphi_{NMS}\left(\omega_k\right)_{\exp}$ are corresponding median experimental values of NAMS (Fairley & Griffin, 1989) for a seated subject. In the experimental study referred above, measurements were conducted on sixty subjects in various seated postures under vertical excitation of the seat with feet in different resting positions. To compute objective function i.e., R; median NMS measured by Fairley & Griffin (1989) at 1.0 m s^{-2} r.m.s. value in normal seated posture with feet resting on the vibration platform is selected as the required experimental data. N is the number of discrete frequencies at which the difference between two quantities is calculated.

5.4.3 Transmissibility of Seated Subject: Transmissibility at different joints of the human body indicates acceleration generated at those location in human body, relative to the applied excitation. In the present study, STHT of human body FE model has been computed using the optimal elastic moduli and dynamic viscosity estimated using Eq. (5.45). Theoretically computed STHT is compared with the experimentally measured STHT of seated subject (Paddan & Griffin, 1988). Transmissibility at r[th] node for FE model, under harmonic excitation ($TR|_r$) is

$$TR|_r = \frac{\ddot{q}_r}{\ddot{y}} = \frac{\omega^2 Q_r}{\omega^2 Y} \qquad r = 1,2,...14 \tag{5.46}$$

5.5 Results and Discussion: NAMS of a seated subject with hands in vertical position has been computed using anthropometric data of 50th percentile U. S. male (Table-A Appendix). The dimensions of ellipsoidal finite elements, as shown in Table 5.2, are calculated based on the scheme listed in Appendix Table- B while using $d_i = 0.95 c_i$.

Table 5.2: Dimensions of truncated ellipsoidal human body segments (50th percentile U.S. male)

Element No.	Body Segment	a_i (cm)	b_i (cm)	d_i (cm)
1	H	7.785	7.785	9.434
2	N	6.040	6.040	1.178
3	UT	16.445	11.660	17.832
4,5	RUA, LUA	5.239	5.239	17.832
6,7	RLA, LLA	4.628	4.628	23.128
8	CT	14.110	10.755	20.480
9	LT	17.715	11.595	11.564
10,11	RUL, LUL	5.927	5.927	26.434
12,13	RLL, LLL	5.303	5.303	21.959
14,15	RF, LF	4.675	12.700	3.282

Using Table 5.2, mass of an individual element is calculated based on the volume of element and the average density (ρ) of human body, assumed constant for all segments. Average density ($\rho = 1.1390*10^{-3}$ kg cm^{-3}), calculated by taking ratio of the mass of the subject ($M_m = 74.9$ kg) and the total volume of all truncated ellipsoids, is within the range available in literature (Bartz &Gianotti, 1975; Liu & Wickstrom, 1973). As RUL and LUL are modelled as rigid rods in the present work, length (d_i) and mass (m_i) of these segments are assigned to rigid rod elements. Dynamic properties of torsional spring and dampers, listed in Table 5.3, are scaled up from the values given in literature (Liu et al., 2015) and then minor adjustments are made for better correspondence between theoretical normalized apparent mass and experimental values.

Table 5.3: Properties of rigid rods segments to model Upper Leg

Property	L_R (m)	m_R (kg)	I_{CG} (kg m^2)	$K_{A\theta}$ (N m rad^{-1})	$K_{B\theta}$ (N m rad^{-1})	$C_{A\theta}$ (N m s rad^{-1})	$C_{B\theta}$ (N m s rad^{-1})
Value	0.264	4.64	0.323	488.5	303.2	45.2	148.7

5.5.1 Optimized E and η: Elastic moduli and dynamic viscosity for individual ellipsoidal body segments were optimized such that theoretically calculated NAMS corresponds with the experimental measurements available in literature (Liu et al., 2015). Jaya algorithm ((Rao, 2016; Rao & Waghmere, 2017), a global search method independent of algorithm specific parameters, is employed for optimizing objective function (Eq. (5.45)). Upper and lower limits of E_i and η_i during optimization were:

$$0.01E_G \leq E_i \ \leq \ 10E_G \qquad i=1,2,3... \ 14,15 \ ; i \neq 10,11$$
$$10^2 \leq \eta_i \ \leq \ 10^8 \qquad i=1,2,3... \ 14,15 \ ; i \neq 10,11$$

where, E_G=13.02 MN m^{-2} i.e. reference value of elastic moduli for ellipsoidal elements used by Nigam and Malik (1987). Dynamic viscosity for human body segments is not available in literature; therefore, limits on the same (in N s m^{-2}) became a necessity to keep quite wide as observed during numerous trials conducted by the authors. Because of the symmetry of human body about mid-sagittal plane, following equivalence constraints were applied on design variables:

$$E_4 = E_5; \ E_6 = E_7; \ E_{12} = E_{13}; \ E_{14} = E_{15}$$
$$\eta_4 = \eta_5; \ \eta_6 = \eta_7; \ \eta_{12} = \eta_{13}; \ \eta_{14} = \eta_{15}$$

$$(5.47)$$

Estimated values of E_i and η_i, after multiple runs using Jaya algorithm, are listed in Table 5.4.

Table 5.4: Optimal E_i and η_i for truncated ellipsoidal finite element

Ellipsoidal Segment	H	N	UT	RUA, LUA	RLA, LLA	CT	LT	RLL, LLL	RF, LF
Elastic Modulus ($* E_G$) MN m^{-2}	0.09	0.123	0.648	0.538	4.683	0.350	0.202	3.294	0.056
Average Dynamic Viscosity($*10^2$) KN s m^{-2}	3.088	1.258	2.644	0.162	2.018	0.556	0.454	0.268	2.176

Theoretically computed values of NAMS, using optimized E_i & η_i and experimental measurements of NAMS for group of seated persons are compared in Fig. 5.5:
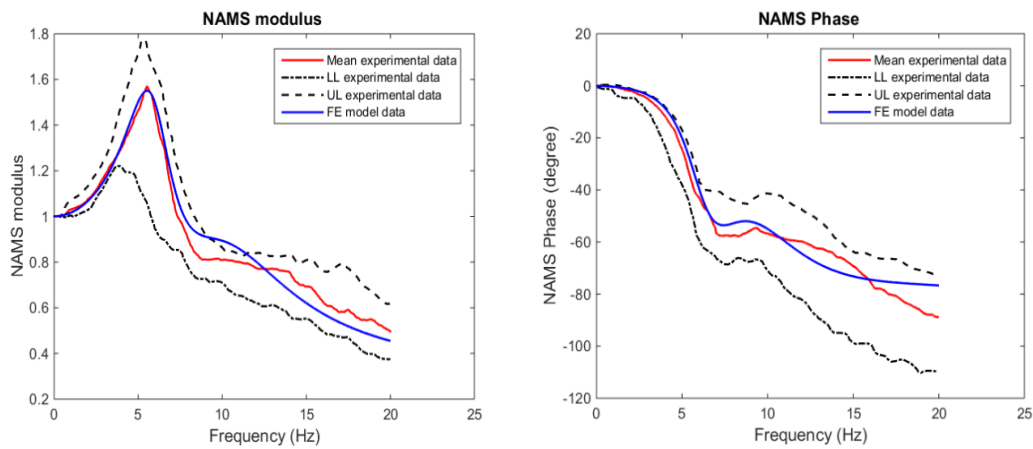
Figure 5.5: Comparison of normalized apparent mass for FE model (optimal E_i and η_i) and experimental data (a) Modulus (b) Phase

Fig. 5.5 shows conformity for modulus and phase of NAMS, between values computed from FE model and median experimental data. International standards regarding WBV effects on human body (ISO 2631-1, 1997; ISO 2631-1, 2004) have shown that vibration dose value (VDV), which determines limits of safe vibration exposure for people, is dependent heavily on driving point impedance values near the resonant frequency. A human body model that accurately predicts dynamic response near the resonant frequency is desirable for studies related to comfort and injuries. It can be observed from Fig. 5.5 that the present FE model provides an excellent match to the experimental measurements in the vicinity of the resonant frequency (~ 5-7 Hz) for NAMS. Thus the FE vibratory model of seated person developed in this chapter

and estimated values of E_i and η_i can be used in further studies for response of seated person under vertical excitation.

5.5.2 Transmissibility: Seat to head transmissibility of a seated person is computed based on the optimized values of E_i and η_i listed in Table 5.4, and compared with experimental data available in literature for the same (Paddan & Griffin, 1988). Fig. 5.6 shows the comparison for theoretical values of STHT, calculated using Eq. (5.46) for $r = 1$, and envelope of experimental measurements for twenty seated subjects under vertical excitation. It is to be noted that experimental measurements for phase of transmissibility in Paddan & Griffin (1988) were reported only for a single subject.

It is observed from Fig. 5.6 that theoretical transmissibility with respect to head lies within the bounds of experimental data reported in the literature. This result along-with the excellent match between theoretical and experimental values of NAMS near the resonant frequency, establishes anthropometric FE vibratory model of a seated person developed in present study. The average values for different body segments, established in present work, can be used as a base value for further studies regarding seated human body dynamic behavior under vertical vibration.
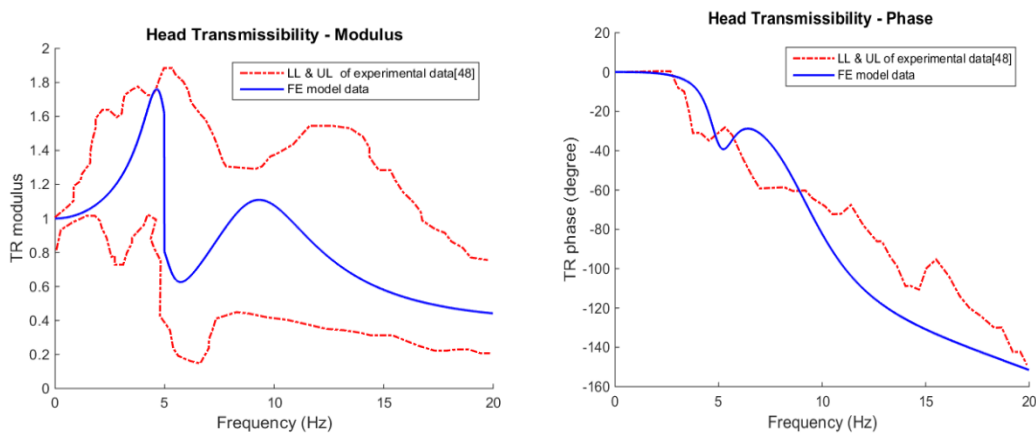
Figure 5.6: STHT of a seated person under vertical excitation (a) Modulus (b) Phase

Authors' would like to note here that the dynamic response and also mode shapes for any subject undergoing WBV depend upon various parameters like age, length, mass of different body segments, active nature etc. of that person etc. Experimental measured response (Fairley & Griffin, 1989; Paddan & Griffin (1988)) used for comparison of NAMS and STHT, does not belong to the same groups of people whose anthropometric data is used to compute dynamic response for the comparison shown in Figs. 5.5 and 5.6. Better agreement between computed value and experimental measured value for driving point mechanical impedance can be expected if subject specific anthropometric data is available.

5.5.3 Mode Shapes of seated subject: Table 5.5 lists the natural frequencies (ω_n) of a seated person computed using optimized E_i and Fig. 5.7 shows the corresponding mode shapes at different natural frequencies(only for ω_n<150 Hz).

Table 5.5: Natural frequencies of seated FE model using optimal E_i

Mode No.	1	2	3	4	5	6	7	8	9	10	11	12	13
Natural Freq. ω_n (Hz)	4.92	5.32	9.15	33. 7	43.2	53.3	53.3	121.3	195.9	195.9	218.1	252.3	271.1

Reference position of seated person under vertical excitation is shown by dotted lines and mode shapes for different natural frequencies is shown with solid lines (Fig. 5.6). For ease of visualization, vertical displacement of nodes along z axis is shown in horizontal plane (along x axis). The mode shapes shown in Fig. 5.7 are not to the scale, and only show a representative sketch of seated human body.

It is observed from Fig. 5.7, that for seated subjects under vertical excitation, motion of upper body segments (from head to lower torso) is decoupled from motion of lower

body segments (upper legs to feet). Except for the two modes corresponding to 53.3 Hz, at which only legs exhibit motion, all other modes show displacement of upper body segments only. From the analysis of theoretical results of NAMS shown in Fig. 5.5, seat to head transmissibility (STHT) shown in Fig. 5.6 and mode shapes shown in Fig. 5.7 combined with natural frequencies listed in Table 5.5; it is evident that upper body modes contribute heavily towards driving point mechanical impedance values in the frequency range of interest i.e. 0-20 Hz. This result is in agreement with other studies of seated person under vertical vibration (Kitazaki & Griffin, 1998; Liu et al., 2015) which showed the contribution of only upper body segments in the range of 0-20 Hz. As the mode shapes in Fig. 5.7 are not drawn to the scale, so, the locations of nodes in individual body segment have to be calculated based on segment dimension. Presence of node in the mode shape indicates the area within a body segment subjected to completely cyclic stress, implying fatigue stresses. Thus, Fig. 5.7 serve as important indicator of areas susceptible to vibration injuries in seated human body under vertical excitation.
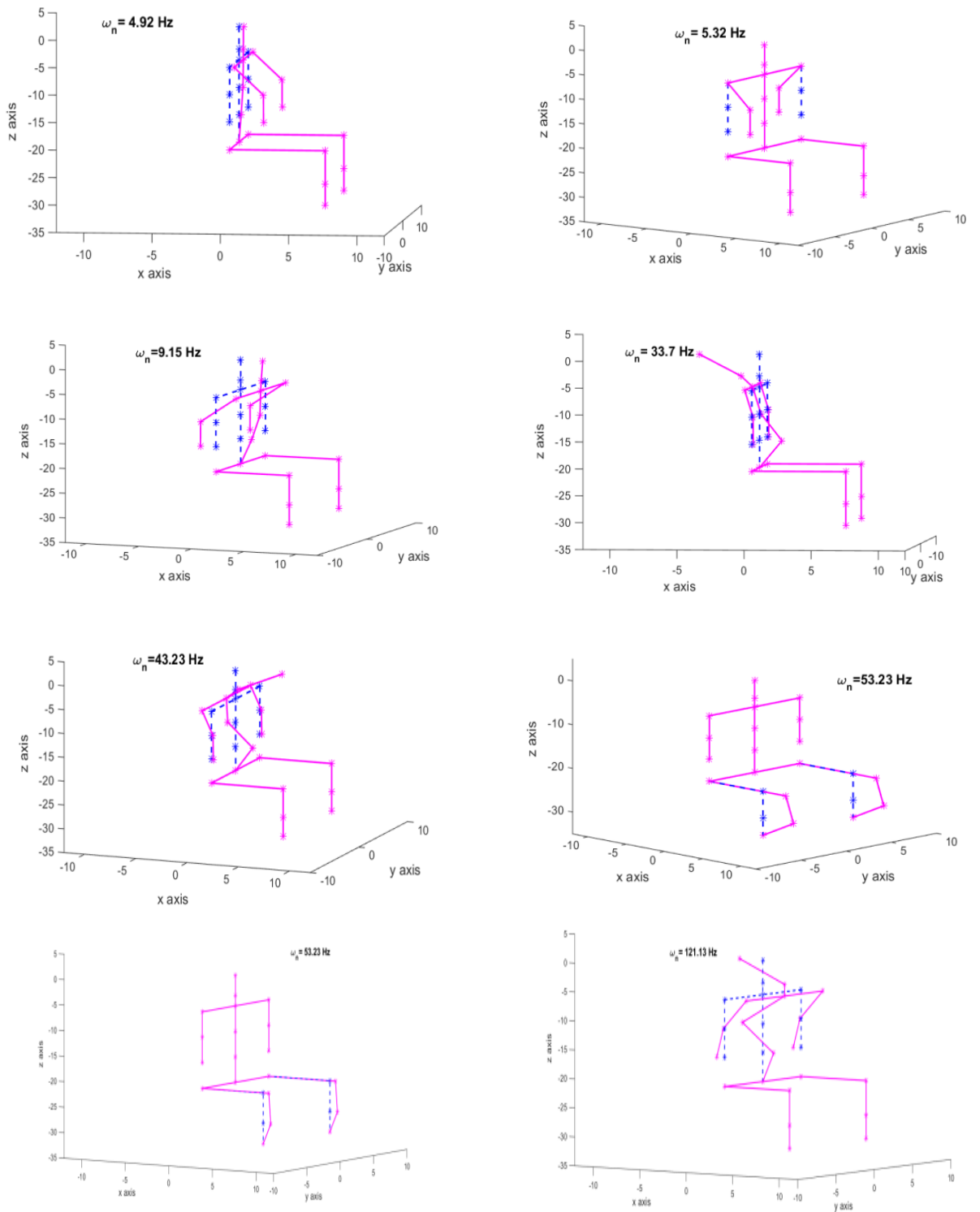
Figure 5.7: Mode Shapes of seated subject under vertical excitation using FE model

(- - - - undeformed; ———— mode shape)

121

5.6 Conclusions:

In the finite element model of seated person, proposed in this chapter, a human body is idealized by truncated visco-elastic ellipsoidal elements and rigid rods. Exact solution for deformation of a truncated ellipsoid under vertical load is used to develop shape functions of ellipsoidal elements. Lesser number of elements is required while using such shape functions. Following the proposed methodology, person-specific vibratory models can be developed from anthropometric measurements and parameters optimized in this research work, for individual body segment. Optimized values of elastic moduli and dynamic viscosity, concluded in Table 5.4, and established from the comparison between theoretical and experimental values of NAMS and seat to head transmissibility, can be used as reference values for studies related to WBV exposure of a seated person. Modal analysis indicates decoupled motion of upper and lower body segments of the seated human body in proximity to resonant frequency of NAMS. Theoretical values of driving point mechanical impedance can have a better correspondence with experimental measurements, provided the anthropometric data of people participating in experimental studies are available.

Straight Line Model of Motorcycle and Dynamic Analysis of Motorcycle-Rider Model

In the previous chapter, an anthropometric vibratory model of a person in sitting posture, which is composed of ellipsoidal finite elements, was established. In this model, the hand is in hanging state and represented by two elements for lower arm and upper arm. The present chapter is towards development of vibratory model of motorcycle-rider system. The human body is considered as multi flexible body system as discussed in previous chapter but the arm is modeled as three mass lumped parameter spring-damper system. Comparing to the rigid body rider-motorcycle system taken up by the previous researchers, the effect of considering the human body of rider as flexible vibratory system is characterized through dynamic analysis of motorcycle-rider system.

6.1 Seated Human Body Vibratory Model with Hands in Driving Posture: The arms of a seated person in the vibratory model shown in Fig. 5.1 are represented as truncated ellipsoidal finite elements in straight down posture (along z axis) with vertical displacements only. In normal driving posture of a motorcycle rider, the arms are not straight and each hand is fixed on either side of the steering column (i.e. on steering handle). Experimental studies (Rakheja, 2002, 2004) have shown that the dynamic response of human body is dependent upon the sitting posture of a person i.e., whether the arms are in vertical position or in driving posture. Also, while riding

a motorcycle, arms of a subject can undergo vertical, horizontal as well as rotational displacement.

For better correspondence with real driving posture of a motorcycle rider; the upper arm, lower arm and hand cannot be taken as connected through line springs and dampers along a straight line. Instead, the segments of human arms have to be modeled at an angle relative to each other and connected through combination of line and rotational springs and dampers. Therefore, a spring-mass-damper model of human arm developed by Fritz (Fritz 1991) has been incorporated in the rider's anthropometric vibratory model, after some modifications. As shown in Fig. 6.1, human arm consists of three lumped masses representing hand, lower arm and upper arm connected with springs and dampers in x, z and θ direction. The original spring mass damper model proposed by Fritz, 1991 has four mass segments; first two segments represented the fingers and the palm tissue separately whereas the remaining two segments modeled the forearm and the upper arm. Fingers and palm tissues were modeled separately to estimate the internal forces transmitted between them during operations that involved gripping of large handles by industrial workers. In the present analysis, the internal forces between fingers and palm are not of concern; therefore, the first two mass segments have been combined to represent hands of motorcycle rider.
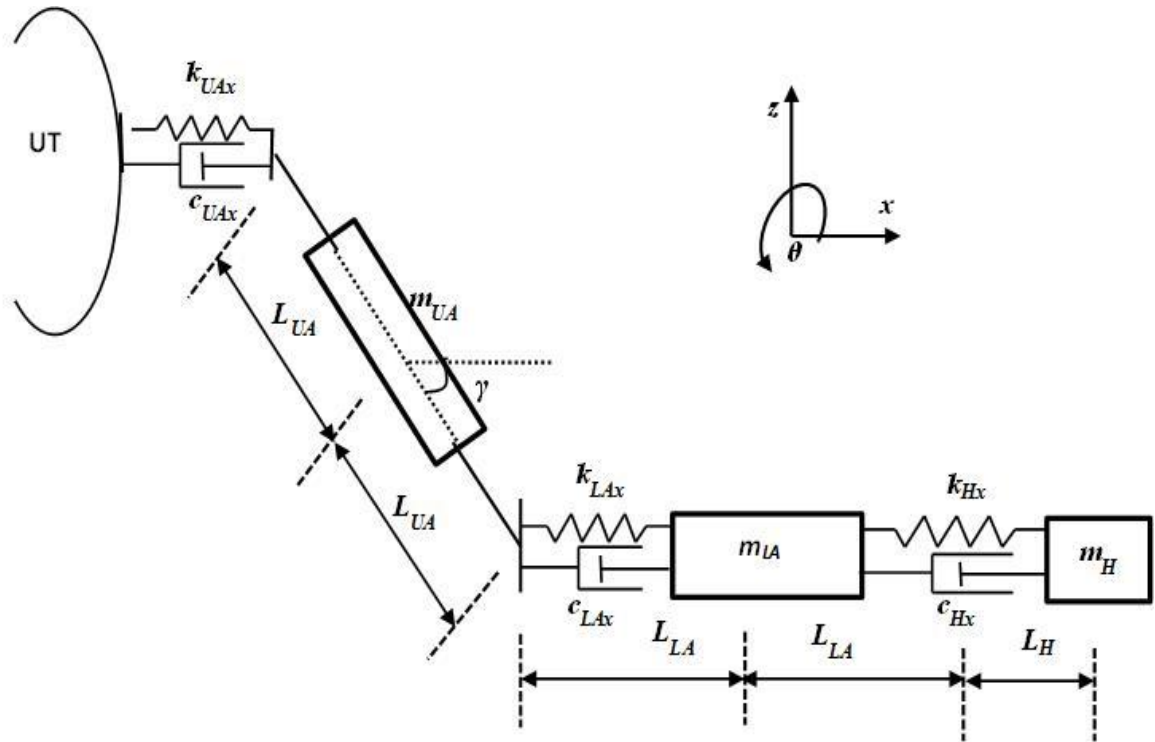
Figure 6.1: Human arm model in Bent Position for the Rider of a Motorcycle

Each arm of the person has total nine d.o.f; with each mass segment having three d.o.f. Although Fig. 6.1 shows spring and dampers in horizontal (x) direction only; all three mass segments are interconnected by springs and dampers in horizontal (x), vertical (z) and rotational (θ) direction. L_H, L_{LA}, L_{UA} are the half lengths of hand, lower arm and upper arm respectively.

6.1.1 Equations of Motion for Hand Segment:

For mass segment representing human hand (m_H); x_H, z_H and θ_H represent horizontal, vertical and rotational displacement of hand segment respectively whereas x_{LA}, z_{LA} and θ_{LA} represent horizontal, vertical and rotational displacement of lower arm segment respectively. Neglecting horizontal displacement due to small angles of rotation i.e. small θ_H and θ_{LA}, equations of motion for hand segment can be written as:

$$m_H \ddot{x}_H + c_{Hx} \dot{x}_H - c_{Hx} \dot{x}_{LA} + k_{Hx} x_H - k_{Hx} x_{LA} = 0$$

$$m_H \ddot{z}_H + c_{Hy} \dot{z}_H - c_{Hy} \dot{z}_{LA} - c_{Hy} l_H \dot{\theta}_H + c_{Hy} l_{LA} \dot{\theta}_{LA} + k_{Hy} z_H - k_{Hy} z_{LA} - k_{Hy} l_H \theta_H + k_{Hy} l_{LA} \theta_{LA} - m_H g = 0$$

$$I_H \ddot{\theta}_H + \left(c_{H\theta} + c_{Hy} l_H^2 \right) \dot{\theta}_H - \left(c_{H\theta} + c_{Hy} l_H l_{LA} \right) \dot{\theta}_{LA} - c_{Hy} l_H \dot{z}_H + c_{Hy} l_{LA} \dot{z}_{LA} - k_{Hy} l_H \dot{z}_H + k_{Hy} l_{LA} \dot{z}_{LA}$$

$$+ \left(k_{H\theta} + k_{Hy} l_H^2 \right) \theta_H - \left(k_{H\theta} + k_{Hy} l_H l_{LA} \right) \theta_{LA} = 0$$

(6.2)

6.1.2 Equations of Motion for Lower Arm Segment:

For mass segment representing lower arm of a motorcycle rider (m_{LA}); x_{UA}, z_{UA} and θ_{UA} represent horizontal, vertical and rotational displacement of upper arm segment respectively. For small angles of rotations, equations of motion for lower arm segment can be written as:

$$m_{LA} \ddot{x}_{LA} - c_{Hx} \dot{x}_H + \left(c_{Hx} + c_{LAx} \right) \dot{x}_{LA} - c_{LAx} \dot{x}_{UA} + c_{LAx} l_{UA} \dot{\theta}_{UA} - k_{Hx} x_H + \left(k_{Hx} + k_{LAx} \right) x_{LA} - k_{LAx} x_{UA} + k_{LAx} l_{UA} \theta_{UA} = 0$$

$$m_{LA} \ddot{z}_{LA} - c_{Hy} \dot{z}_H + \left(c_{Hy} + c_{LAy} \right) \dot{z}_{LA} - c_{LAy} \dot{z}_{UA} + c_{Hy} l_H \dot{\theta}_H - \left(c_{Hy} + c_{LAy} \right) l_{LA} \dot{\theta}_{LA} - k_{Hy} z_H + \left(k_{Hy} + k_{LAy} \right) z_{LA}$$

$$- k_{LAy} z_{UA} + k_{Hy} l_H \theta_H - \left(k_{Hy} + k_{LAy} \right) l_{LA} \theta_{LA} - m_{LA} g = 0$$

$$I_{LA} \ddot{\theta}_{LA} + \left(c_{H\theta} + c_{Hy} l_H^2 \right) \dot{\theta}_H - \left(c_{H\theta} + c_{Hy} l_H l_{LA} + c_{LA\theta} + c_{LAy} l_{LA}^2 \right) \dot{\theta}_{LA} - c_{LA\theta} \dot{\theta}_{UA} + c_{LAy} l_{LA} \dot{z}_{LA} - c_{LAy} l_{LA} \dot{z}_{UA}$$

$$- \left(k_{H\theta} + k_{Hy} l_H^2 \right) \theta_H - k_{LA\theta} \theta_{UA} + k_{LAy} l_{LA} z_{LA} - k_{LAy} l_{LA} z_{UA} - \left(k_{H\theta} + k_{Hy} l_H l_{LA} + k_{LA\theta} + k_{LAy} l_{LA}^2 \right) \theta_{LA} = 0$$

(6.3)

6.1.3 Equations of Motion for Upper Arm Segment:

As shown in Fig. 6.1, γ is the angle between upper arm segment and x-axis. Also, the upper arm segment is connected to lower arm at one end and the truncated ellipsoidal finite element representing upper torso on the other end. It is assumed that only vertical motion i.e. Z_{UT} is transmitted from upper arms of motorcycle rider to the upper torso through nodes *3r* and *3l*. For small angles of rotations, equations of motion for upper arm segment can be written as:

$$m_{UA}\,\ddot{x}_{UA} - c_{LAx}\,\dot{x}_{LA} + \left(c_{UAx} + c_{LAx}\right)\dot{x}_{UA} + \left(c_{UAx} - c_{LAx}\right)l_{UA}\,\dot{\theta}_{UA} - k_{LAx}\,x_{LA}$$

$$+ \left(k_{UAx} + k_{LAx}\right)x_{UA} + \left(k_{UAx} - k_{LAx}\right)l_{UA}\theta_{UA} = 0$$

$$m_{UA}\,\ddot{z}_{UA} - c_{LAy}\,\dot{z}_{LA} + \left(c_{UAy} + c_{LAy}\right)\dot{z}_{UA} - c_{LAy}\,l_{LA}\,\dot{\theta}_{LA} - c_{UAy}\,\dot{z}_{UT} - k_{LAy}\,z_{LA}$$

$$+ \left(k_{UAy} + k_{LAy}\right)z_{UA} - k_{LAy}\,l_{LA}\,\theta_{LA} - k_{UAy}\,z_{UT} - m_{UA}g = 0$$

$$I_{UA}\,\ddot{\theta}_{UA} + \left(c_{LA\theta} + c_{LAy}\,\frac{l_{UA}\,l_{LA}}{\cos\gamma}\right)\dot{\theta}_{LA} - \left(c_{LA\theta} + c_{UA\theta} + \frac{l_{UA}^2}{\sin\gamma}\left(c_{LAx} - c_{UAx}\right)\right)\dot{\theta}_{UA}$$

$$+ \frac{c_{LAx}\,l_{UA}}{\sin\gamma}\,\dot{x}_{LA} + \frac{c_{LAy}\,l_{UA}}{\cos\gamma}\,\dot{z}_{LA} - \frac{l_{UA}\left(c_{LAx} + c_{UAx}\right)}{\sin\gamma}\,\dot{x}_{UA} - \frac{l_{UA}\left(c_{LAy} + c_{UAy}\right)}{\sin\gamma}\,\dot{z}_{UA} + \frac{c_{UAy}\,l_{UA}}{\cos\gamma}\,\dot{z}_{UT}$$

$$- \left(k_{LA\theta} + k_{LAy}\,\frac{l_{UA}\,l_{LA}}{\cos\gamma}\right)\theta_{LA} - \left(k_{LA\theta} + k_{UA\theta} + \frac{l_{UA}^2}{\sin\gamma}\left(k_{LAx} - k_{UAx}\right)\right)\theta_{UA} + \frac{k_{LAx}\,l_{UA}}{\sin\gamma}\,x_{LA}$$

$$+ \frac{k_{LAy}\,l_{UA}}{\cos\gamma}\,y_{LA} - \frac{l_{UA}\left(k_{LAx} + k_{UAx}\right)}{\sin\gamma}\,x_{UA} - \frac{l_{UA}\left(k_{LAy} + k_{UAy}\right)}{\sin\gamma}\,z_{UA} + \frac{k_{UAy}\,l_{UA}}{\cos\gamma}\,z_{UT} = 0$$

(6.4)

Combining Eqs. 6.2. 6.3 and 6.4; equations of motion for bent arm of a motorcycle rider, as shown in Fig. 6.1, are written as:

$$\left[\mathbf{M_i}\right]_{9X10}\left\{\ddot{\mathbf{q}_i}\right\}_{10X1} + \left[\mathbf{C_i}\right]_{9X10}\left\{\dot{\mathbf{q}_i}\right\}_{10X1} + \left[\mathbf{K_i}\right]_{9X10}\left\{\mathbf{q_i}\right\}_{10X1} = \left\{\mathbf{F_{Gi}}\right\}_{10X1}$$

(6.5)

where,

$$\left\{\boldsymbol{q_i}\right\}_{10X1} = \left\{ x_H\ z_H\ \theta_H\ x_{LA}\ z_{LA}\ \theta_{LA}\ x_{UA}\ z_{UA}\ \theta_{UA}\ z_{UT} \right\}^{\mathrm{T}}$$

$$\left\{\boldsymbol{F_{Gi}}\right\}_{10X1} = \left\{ 0\ m_H g\ 0\ 0\ m_{LA}g\ 0\ 0\ m_{UA}g\ 0\ 0\right\}^{\mathrm{T}}$$

(6.6)

Eq. (6.5) represents nine equations with ten variables, due to the inclusion of Z_{UT} in equations for upper arm. Fritz (1991) used fixed support in place of upper torso displacement i.e., $Z_{UT} = 0$, to solve for internal forces between different segments of human arm. In this study, this arm model has been incorporated in the human body FE model shown in Fig. (5.1). In Eq. (5.35), all four segments representing two arms of a person (RUA, LUA, RLA, LLA) and their corresponding EOM'S are replaced by 9x2

= 18 equations of hand-arm model (Eq. 6.5). As previously stated, it is assumed that only vertical motion is transmitted from arms to upper torso segment through node *3r* and *3l*. The modified equations of motion for human body model with bent arms are given as:

$$[\underline{\mathbf{M}}]_{30X30} \left\{ \ddot{\underline{q}} \right\}_{30X1} + [\underline{\mathbf{H}}]_{30X30} \left\{ \dot{\underline{q}} \right\}_{30X1} + [\underline{\mathbf{K}}]_{30X30} \left\{ \underline{q} \right\}_{30X1} = \left\{ \underline{F_G} \right\}_{30X1} \qquad (6.7)$$

Following the same methodology of matrix partition into known and unknown displacement variables, as described in previous chapter; theoretical vibration response of human body model represented by Eq. (6.7) was calculated for synchronous harmonic excitations from seat-pelvis interface and feet-platform interface. Dimensions and inertial parameters of human arm model (Fig. 6.1) are scaled from the anthropometric measurements of arm given by Fritz (1991) and employed for theoretical calculations. The angle of bent upper arm from the horizontal i.e. *x*-axis (γ) is taken equal to 60^0. Table 6.1 lists the values of parameters used for bent-arm model.

Table 6.1: Parameter Values for Bent Arm Model

Arm Segment	Mass (kg)	Moment of Inertia (kg-m^2)*10^{-3}	Stiffness			Damping		
			Horizontal (kN/m)	Vertical (kN/m)	Rotational (kN/rad)	Horizontal (N-sec/m)	Vertical (N-sec/m)	Rotational (N-sec/rad)
Hands	0.45	0.4	40.64	48.1	6.4	107.27	155	66
Lower Arm	1.15	8.4	14	5	3.8	103	91	60
Upper Arm	1.96	14.9	3.5	20	5.3	90	204	100

6.2 Straight Line Motorcycle Model: The human body model of motorcycle rider developed above is coupled with a straight line model of motorcycle to analyze the effects of dynamic properties of human body on overall response of vehicle-rider

system. In the context of motorcycle dynamics, straight line model implies that the motorcycle is considered as elastically suspended rigid body (Cossalter, 2000) and lateral dynamics of the motorcycle is not analyzed. The effects of yaw angle, slip angle, steering angle on dynamics of system are not considered and also, the motorcycle is assumed to be moving along a straight line without turning or performing any maneuvers. An in-plane multi-body model of the motorcycle developed by Cossalter et al (2000) has been adopted. The model, as shown in Fig.6.2, was used (Cossalter et al, 2000) to determine optimal braking performance of a motorcycle in straight running.
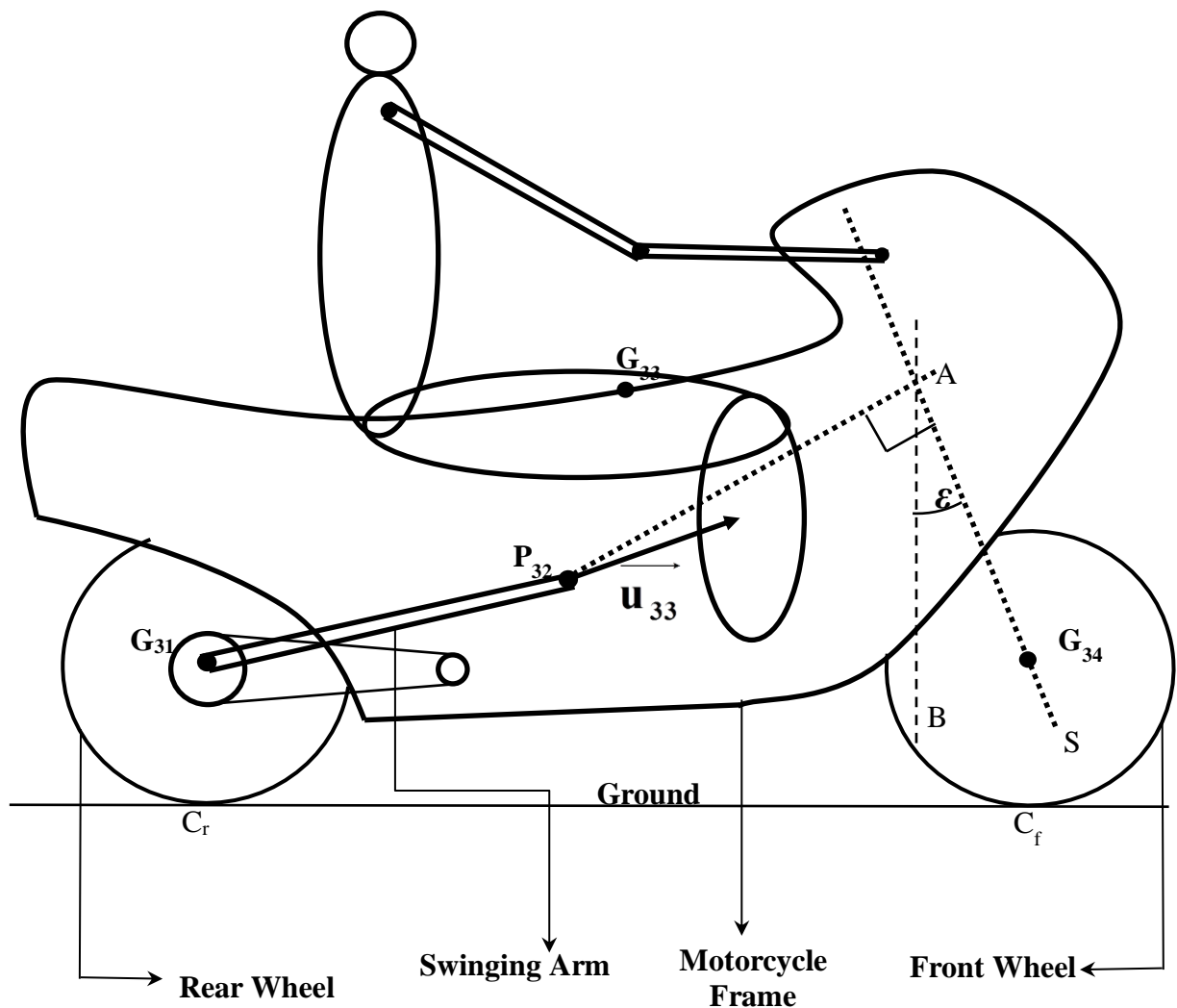
Fig. 6.2 Motorcycle multi body model with rider

6.3 Equations of Motion for Straight Line Motorcycle Model: The motorcycle was divided into four rigid bodies; the front wheel, the rear wheel, the frame of motorcycle and the swinging arm connecting rear wheel with frame; having a total of seven d.o.f. Initially, the rider was assumed to be rigidly attached to the frame and only his mass was considered while analyzing motion of the system. Ten natural coordinates (Shabana, 2005) were used to describe geometry of the system. These coordinates are

a. x_{31}, z_{31} and θ_{31}: coordinates of real wheel center G_{31} and wheel rotation respectively.

b. x_{32} and z_{32}: coordinates for point P_{32} common to frame and swinging arm.

c. s_{33} and c_{33}: direction cosines of unit vector $\vec{u}_{33}$ fixed to frame.

d. x_{34}, z_{34} and θ_{34}: coordinates of front wheel center G_{34} and wheel rotation respectively.

It is to be noted that s_{33} and c_{33} represent $\sin(\theta_{33})$ and $\cos(\theta_{33})$ respectively, where θ_{33} is the angle between $\vec{u}_{33}$ and global x axis. Objective of this work is to incorporate the model of seated human with bent arm, developed in section 6.1, into motorcycle model. Therefore, for clarity, these co-ordinates have been numbered from 31 onwards. Constraint equations for three redundant co-ordinates are:

$$\beta_1 = \left(s_{33}\right)^2 + \left(c_{33}\right)^2 - 1 = 0 \qquad \qquad \text{...6.8 (a)}$$

$$\beta_2 = \left(x_{32} - x_{31}\right)^2 + \left(z_{32} - z_{31}\right)^2 - l_{SA}^2 = 0 \qquad \qquad \text{...6.8 (b)}$$

$$\beta_3 = \left(x_{34} - x_{32}\right)\left(c_{33}\sin(\varepsilon) - s_{33}\cos(\varepsilon)\right) + \left(z_{34} - z_{32}\right)\left(s_{33}\cos(\varepsilon) + c_{33}\sin(\varepsilon)\right) - l = 0 \qquad \text{...6.8 (c)}$$

Here, Eq. 6.8(a) represents unit modulus of vector $\vec{u}_{33}$; Eq. 6.8(b) represents that the distance between point G_{31} and point P_{32}, called swinging arm length (l_{SA}), remains constant; and Eq. 6.8(c) represents the link between the frame and the front wheel by fixing point G_{34} on front suspension axis. 'l' is the distance between point

P_{32} and front suspension axis and 'ε' is the castor angle for motorcycle. First two constraint equations are straight forward and the derivation of third constraint equation is given in Appendix B.

Equations of motions for straight line motion of motorcycle were derived using Lagrange equations for constrained multibody dynamics:

$$\frac{d}{dt}\left(\frac{\partial T}{\partial \dot{q}_i}\right)-\left(\frac{\partial T}{\partial q_i}\right)+\sum_{j=1}^{3}\lambda_j\frac{\partial \beta_j}{\partial q_i}-Q_i=0 \qquad i=1,2...\,n \tag{6.9}$$

where, T is the kinetic energy of the system, β_j are the constraint equations , λ_j are the unknown Lagrange multipliers corresponding to the constraint equations, Q_i are the generalized forces, q_i are the generalized co-ordinates and n is the number of generalizes co-ordinates. For the straight line motorcycle model, $n=10$ and

$$\left\{q_i\right\}=\left\{x_{31} \quad z_{31} \quad \theta_{31} \quad x_{32} \quad z_{32} \quad s_{33} \quad c_{33} \quad x_{34} \quad z_{34} \quad \theta_{34}\right\}^T \tag{6.10}$$

Constraint equations (β_j) are already established by Eq. 6.8. Expressions for kinetic energy of different rigid bodies (T) and its required derivatives i.e., $\left(\frac{d}{dt}\left(\frac{\partial T}{\partial \dot{q}_i}\right)\right)$ & $\left(\frac{\partial T}{\partial q_i}\right)$; derivatives of constraint equations $\left(\frac{\partial \beta_j}{\partial q_i}\right)$ and generalized forces (Q_i) acting on motorcycle are derived below:

6.3.1 Kinetic Energy (T): Kinetic energy of different rigid bodies of the motorcycle has been derived using the co-ordinate transformation approach (Cossalter & Lot (2002)). In this approach, to determine the kinetic energy of a particular rigid body; a local reference frame is fixed in the body with origin at the point whose co-ordinates

have been taken as natural co-ordinates. Thereafter, kinetic energy of rigid body is calculated in terms of natural co-ordinates and known body parameters. If the origin of local reference frame is not coincident with the centre of mass of particular rigid body, transformation matrix is used to determine kinetic energy in terms of natural co-ordinates and known body parameters. After the expression for kinetic energy of a particular rigid has been derived, it is differentiated with respect to natural co-ordinates to determine first two-terms of Lagrange's equation (Eq. 6.9).

6.3.1.1 Rear Wheel (T_{31}): For the rear wheel, local reference frame is fixed having origin at the centre of wheel body (point G_{31}) which is also the center of mass of rear wheel. Therefore the kinetic energy of rear wheel is given as:

$$T_{31} = \frac{1}{2} m_{31} \left(\dot{x}_{31}^2 + \dot{z}_{31}^2 \right) + \frac{1}{2} I_{31} \left(\dot{\theta}_{31}^2 \right) \tag{6.11}$$

Differentiating Eq. (6.11) with respect to natural co-ordinates and their first derivatives, we get:

$$\frac{d}{dt}\left(\frac{\partial T_{31}}{\partial \dot{q}_1} \right) = \frac{d}{dt}\left(\frac{\partial T_{31}}{\partial \dot{x}_{31}} \right) = \frac{d}{dt}\left(m_{31} \dot{x}_{31} \right) = m_{31} \ddot{x}_{31}$$

$$\frac{d}{dt}\left(\frac{\partial T_{31}}{\partial \dot{q}_2} \right) = \frac{d}{dt}\left(\frac{\partial T_{31}}{\partial \dot{z}_{31}} \right) = \frac{d}{dt}\left(m_{31} \dot{z}_{31} \right) = m_{31} \ddot{z}_{31} \tag{6.12}$$

$$\frac{d}{dt}\left(\frac{\partial T_{31}}{\partial \dot{q}_3} \right) = \frac{d}{dt}\left(\frac{\partial T_{31}}{\partial \dot{\theta}_{31}} \right) = \frac{d}{dt}\left(I_{31} \dot{\theta}_{31} \right) = I_{31} \ddot{\theta}_{31}$$

It is to be noted that only non-zero derivatives/coefficients of kinetic energy (T_{31}) w.r.t. natural co-ordinates have been listed in Eq. 6.12. All other coefficients are zero.

6.3.1.2 Rear Swinging Arm (T_{32}): In the straight line model, swinging arm of the motorcycle has been taken as a rigid rod with only rotational inertia. Mass of the rod

has been distributed between the rear wheel and frame of the motorcycle. The angular velocity $\dot{\theta}_{32}$ of rear swinging arm is given as

$$\dot{\theta}_{32} = \frac{\left(\dot{z}_{32} - \dot{z}_{31} \right)\hat{k} + \left(\dot{x}_{32} - \dot{x}_{31} \right)\hat{i}}{l_{SA}}$$

Therefore its kinetic energy is written as:

$$T_{32} = \frac{1}{2} I_{32} \left(\dot{\theta}_{32}^2 \right) = \frac{1}{2} I_{32} \frac{\left(\dot{z}_{32} - \dot{z}_{31} \right)^2 + \left(\dot{x}_{32} - \dot{x}_{31} \right)^2}{l_{SA}^2} \tag{6.13}$$

where, I_{23} is the moment of inertia of rear swinging arm. Differentiating Eq. (6.13) with respect to natural co-ordinates and their first derivatives, we get:

$$\frac{d}{dt}\left(\frac{\partial T_{32}}{\partial \dot{q}_1} \right) = \frac{d}{dt}\left(\frac{\partial T_{32}}{\partial \dot{x}_{31}} \right) = \frac{d}{dt}\left(\frac{I_{32}}{l_{SA}^2}\left(-\dot{x}_{32} + \dot{x}_{31} \right) \right) = \left(\frac{I_{32}}{l_{SA}^2}\left(\ddot{x}_{31} - \ddot{x}_{32} \right) \right)$$

$$\frac{d}{dt}\left(\frac{\partial T_{32}}{\partial \dot{q}_2} \right) = \frac{d}{dt}\left(\frac{\partial T_{32}}{\partial \dot{z}_{31}} \right) = \frac{d}{dt}\left(\frac{I_{32}}{l_{SA}^2}\left(-\dot{z}_{32} + \dot{z}_{31} \right) \right) = \left(\frac{I_{32}}{l_{SA}^2}\left(\ddot{z}_{31} - \ddot{z}_{32} \right) \right)$$

$$\frac{d}{dt}\left(\frac{\partial T_{32}}{\partial \dot{q}_4} \right) = \frac{d}{dt}\left(\frac{\partial T_{32}}{\partial \dot{x}_{32}} \right) = \left(\frac{I_{32}}{l_{SA}^2}\left(\ddot{x}_{32} - \ddot{x}_{31} \right) \right) \tag{6.14}$$

$$\frac{d}{dt}\left(\frac{\partial T_{32}}{\partial \dot{q}_5} \right) = \frac{d}{dt}\left(\frac{\partial T_{32}}{\partial \dot{z}_{32}} \right) = \left(\frac{I_{32}}{l_{SA}^2}\left(\ddot{z}_{32} - \ddot{z}_{31} \right) \right)$$

6.3.1.3 Motorcycle Frame (T_{33}): The center of mass of motorcycle frame is not coincident with point P_{32} whose co-ordinates have been taken as natural co-ordinates. Therefore, to derive expression of kinetic energy in terms of natural co-ordinates; a local reference frame (X-Z) is attached to motorcycle frame with origin at point P_{32} and X axis parallel to $\vec{u}_{33}$ (with direction cosines c_{33} and s_{33}). The co-ordinates of motorcycle centre of mass (point G_{33}) in this local reference frame (a_{33}, b_{33}) are

constant as the frame is assumed to be rigid. Therefore the kinetic energy of motorcycle frame is

$$T_{33} = \frac{1}{2} m_{33} \left(\frac{d}{dt} G_{33} \right)^2 + \frac{1}{2} I_{33} \left(\dot{\theta}_{33}^2 \right)$$

$$= \frac{1}{2} m_{33} \left(\frac{d}{dt} \left([T]\{G_{COM}\} \right) \right)^2 + \frac{1}{2} I_{33} \left(\dot{c}_{33}\, \hat{i} + \dot{s}_{33}\, \hat{k} \right)^2$$

$$= \frac{1}{2} m_{33} \left(\frac{d}{dt} \left(\begin{bmatrix} c_{33} & -s_{33} & x_{32} \\ s_{33} & c_{33} & z_{32} \\ 0 & 0 & 1 \end{bmatrix} \begin{Bmatrix} a_{33}\, \hat{I} \\ b_{33}\, \hat{K} \\ 1 \end{Bmatrix} \right) \right)^2 + \frac{1}{2} I_{33} \left(\dot{c}_{33}\, \hat{i} + \dot{s}_{33}\, \hat{k} \right)^2$$

where, $\hat{i}$ and $\hat{k}$ are the unit vectors along global x-z frame and $\hat{I}$ and $\hat{K}$ are the unit vector along local X-Z frame with origin at point P_{32}. Simplifying,

$$T_{33} = \frac{1}{2} m_{33} \left(\left(\dot{c}_{33}\, a_{33} - \dot{s}_{33}\, b_{33} + \dot{x}_{32} \right)^2 + \left(\dot{s}_{33}\, a_{33} + \dot{c}_{33}\, b_{33} + \dot{z}_{32} \right)^2 \right) + \frac{1}{2} I_{33} \left(\dot{c}_{33}^2 + \dot{s}_{33}^2 \right) \quad (6.15)$$

Differentiating Eq. (6.15) with respect to natural co-ordinates and their first derivatives, we get:

$$\frac{d}{dt} \left(\frac{\partial T_{33}}{\partial \dot{q}_4} \right) = \frac{d}{dt} \left(\frac{\partial T_{33}}{\partial \dot{x}_{32}} \right) = \frac{d}{dt} \left(m_{33} \left(\dot{x}_{32} + \dot{c}_{33}\, a_{33} - \dot{s}_{33}\, b_{33} \right) \right) = m_{33} \left(\ddot{x}_{32} + \ddot{c}_{33}\, a_{33} - \ddot{s}_{33}\, b_{33} \right)$$

$$\frac{d}{dt} \left(\frac{\partial T_{33}}{\partial \dot{q}_5} \right) = \frac{d}{dt} \left(\frac{\partial T_{33}}{\partial \dot{z}_{32}} \right) = \frac{d}{dt} \left(m_{33} \left(\dot{z}_{32} + \dot{c}_{33}\, b_{33} + \dot{s}_{33}\, a_{33} \right) \right) = m_{33} \left(\ddot{z}_{33} + \ddot{c}_{33}\, b_{33} + \ddot{s}_{33}\, a_{33} \right)$$

$$\frac{d}{dt} \left(\frac{\partial T_{33}}{\partial \dot{q}_6} \right) = \frac{d}{dt} \left(\frac{\partial T_{33}}{\partial \dot{s}_{33}} \right) = \frac{d}{dt} \left(m_{33} a_{24} \left(\dot{z}_{32} + \dot{c}_{33}\, b_{33} + \dot{s}_{33}\, a_{33} \right) - m_{33} b_{33} \left(\dot{x}_{32} + \dot{c}_{33}\, a_{33} - \dot{s}_{33}\, b_{33} \right) + I_{33}\, \dot{s}_{33} \right)$$

$$= \left(m_{33} \left(\ddot{s}_{33}\, a_{33}^2 + \ddot{s}_{33}\, b_{33}^2 + a_{33}\, \ddot{z}_{32} - b_{33}\, \ddot{x}_{32} \right) + I_{33}\, \ddot{s}_{33} \right)$$

$$\quad (6.16)$$

$$\frac{d}{dt} \left(\frac{\partial T_{33}}{\partial \dot{q}_7} \right) = \frac{d}{dt} \left(\frac{\partial T_{33}}{\partial \dot{c}_{33}} \right) = \frac{d}{dt} \left(m_{33} a_{33} \left(\dot{x}_{32} + \dot{c}_{33}\, a_{33} - \dot{s}_{33}\, b_{33} \right) + m_{33} b_{33} \left(\dot{z}_{32} + \dot{c}_{33}\, b_{33} + \dot{s}_{33}\, a_{33} \right) + I_{33}\, \dot{c}_{33} \right)$$

$$= \left(m_{33} \left(\ddot{c}_{33}\, a_{33}^2 + \ddot{c}_{33}\, b_{33}^2 + a_{33}\, \ddot{x}_{32} + b_{33}\, \ddot{z}_{32} \right) + I_{33}\, \ddot{c}_{33} \right)$$

6.3.1.4 Front Wheel (T_{34}): Following similar steps as for rear wheel, kinetic energy for front wheel is given as:

$$T_{34} = \frac{1}{2} m_{34} \left(\dot{x}_{34}^2 + \dot{z}_{34}^2 \right) + \frac{1}{2} I_{34} \left(\dot{\theta}_{34}^2 \right) \tag{6.17}$$

Differentiating Eq. (6.17) with respect to natural co-ordinates and their first derivatives, we get:

$$\frac{d}{dt}\left(\frac{\partial T_{34}}{\partial \dot{q}_8} \right) = \frac{d}{dt}\left(\frac{\partial T_{34}}{\partial \dot{x}_{34}} \right) = \frac{d}{dt}\left(m_{34} \dot{x}_{34} \right) = m_{34} \ddot{x}_{34}$$

$$\frac{d}{dt}\left(\frac{\partial T_{34}}{\partial \dot{q}_9} \right) = \frac{d}{dt}\left(\frac{\partial T_{34}}{\partial \dot{z}_{34}} \right) = \frac{d}{dt}\left(m_{34} \dot{z}_{34} \right) = m_{34} \ddot{z}_{34} \tag{6.18}$$

$$\frac{d}{dt}\left(\frac{\partial T_{34}}{\partial \dot{q}_{10}} \right) = \frac{d}{dt}\left(\frac{\partial T_{34}}{\partial \dot{\theta}_{34}} \right) = \frac{d}{dt}\left(I_{34} \dot{\theta}_{34} \right) = I_{34} \ddot{\theta}_{34}$$

6.3.2 Derivatives of Constraint Equation $\left(\dfrac{\partial \beta_j}{\partial q_i} \right)$**:** For multibody systems having natural coordinates greater than system degree of freedom, unknown Lagrange multipliers (λ_i) are used to incorporate constraint equations into system equation. As mentioned before, derivatives w.r.t. natural coordinates not shown are zero.

6.3.2.1 For Constraint Equation β_1: From equation 6.8 (a), we can write:

$$\frac{\partial \beta_1}{\partial q_6} = \frac{\partial \beta_1}{\partial s_{33}} = 2 s_{33}$$

$$\frac{\partial \beta_1}{\partial q_7} = \frac{\partial \beta_1}{\partial c_{33}} = 2 c_{33} \tag{6.19}$$

6.3.2.2 For Constraint Equation β_2: From equation 6.8 (b), we can write:

$$\frac{\partial \beta_2}{\partial q_1} = \frac{\partial \beta_2}{\partial x_{31}} = 2(x_{31} - x_{32}) \qquad \frac{\partial \beta_2}{\partial q_2} = \frac{\partial \beta_2}{\partial z_{31}} = 2(z_{31} - z_{32})$$

$$\frac{\partial \beta_2}{\partial q_4} = \frac{\partial \beta_2}{\partial x_{32}} = 2(x_{32} - x_{31}) \qquad \frac{\partial \beta_2}{\partial q_5} = \frac{\partial \beta_2}{\partial z_{32}} = 2(z_{32} - z_{31})$$

$$(6.20)$$

6.3.2.3 For Constraint Equation β_3: From equation 6.8 (c), we can write:

$$\frac{\partial \beta_3}{\partial q_4} = \frac{\partial \beta_3}{\partial x_{32}} = 2(x_{31} - x_{32}) \qquad \frac{\partial \beta_3}{\partial q_5} = \frac{\partial \beta_3}{\partial z_{32}} = 2(z_{31} - z_{32})$$

$$\frac{\partial \beta_3}{\partial q_6} = \frac{\partial \beta_3}{\partial s_{33}} = 2(x_{32} - x_{31}) \qquad \frac{\partial \beta_3}{\partial q_7} = \frac{\partial \beta_3}{\partial c_{33}} = 2(z_{32} - z_{31}) \qquad (6.21)$$

$$\frac{\partial \beta_3}{\partial q_8} = \frac{\partial \beta_3}{\partial x_{34}} = (c_{33} \cos \varepsilon - s_{33} \sin \varepsilon) \qquad \frac{\partial \beta_3}{\partial q_9} = \frac{\partial \beta_3}{\partial z_{34}} = (s_{33} \cos \varepsilon + c_{33} \sin \varepsilon)$$

6.3.3 Generalised Forces (Q_i): Generalized forces (Q_i) required for Lagrange's equation (Eq. 6.9) are determined from the virtual work (δW) principle:

$$\delta W = \sum_{i=1}^{n} Q_i \ \delta q_i \qquad (6.22)$$

Expressions for virtual work done by the different forces acting on the motorcycle in straight running are determined (Cossalter, 2002) and the coefficients of individual δq_i are combined to evaluate respective Q_i.

6.3.3.1 For Gravity Load (G): The virtual work done by gravitational force acting on different rigid bodies of the motorcycle is:

$$\delta W_G = \sum_{i=31}^{34} m_i \ \vec{g} \cdot \delta \vec{G}_i \qquad (6.23)$$

where, m_i is the mass and $\vec{G}_i$ is the position vector for centre of mass of the ith body and $\vec{g}$ is the gravity vector for 2-D co-ordinate system given as:

$$\vec{g} = \{0 \quad -g \quad 1\} \qquad (6.24)$$

Following the same procedure as used for deriving kinetic energy expression of rear wheel, rear swinging arm, motorcycle frame and front wheel (in section 6.3.1); the virtual work due to gravity is:

$$\delta W_G = -g \begin{bmatrix} m_{31} & m_{33}\,a_{33} & m_{33}\,b_{33} & m_{34} \end{bmatrix} * \{\delta z_{31} \quad \delta s_{33} \quad \delta c_{33} \quad \delta z_{34}\}^T \qquad (6.25)$$

It is to be noted here that in the present model, the mass of rear swinging arm has been distributed between rear wheel and motorcycle frame; therefore m_{32} doesn't appear in Equation (6.25).

6.3.3.2 For Rear and Front Tyre Load (F_{Tf} , F_{Tf}): The virtual work done by rear tyre force (F_{Tr}) and front tyre force (F_{Tf}) acting on the contact point of ground and front tyre (C_{31}) & rear tyre (C_{34}) respectively, is given by:

$$\delta W_{TF} = \overrightarrow{F_{Tr}} \cdot \delta \overrightarrow{G_{31}} + \overrightarrow{F_{Tf}} \cdot \delta \overrightarrow{G_{34}} + \overrightarrow{G_{31}C_{31}} \times \overrightarrow{F_{Tr}} \cdot T_{31}\delta(T_{31}) + \overrightarrow{G_{34}C_{34}} \times \overrightarrow{F_{Tf}} \cdot T_{31}\delta(T_{31}) \qquad (6.26)$$

where;

$$\begin{aligned}
\overrightarrow{F_{Tf}} &= \{S_f \quad N_f \quad 0\} \qquad \text{and} \quad C_{34} = \{x_{34} \quad (z_{34} - r_f) \quad 0\} \\
\overrightarrow{F_{Tr}} &= \{S_r \quad N_r \quad 0\} \qquad \text{and} \quad C_{31} = \{x_{31} \quad (z_{31} - r_r) \quad 0\}
\end{aligned} \qquad (6.27)$$

Therefore the virtual work by tire forces is given by:

$$\begin{aligned}
\delta W_{TF} = \begin{bmatrix} S_r & N_r & S_f & N_f & S_r\,r_r & S_f\,r_f \end{bmatrix} \\
* \{\delta x_{31} \quad \delta z_{31} \quad \delta x_{34} \quad \delta z_{34} \quad \delta \theta_{31} \quad \delta \theta_{34}\}^T
\end{aligned} \qquad (6.28)$$

6.3.3.3 For Rear Suspension Torque (M_{Sr}): This torque acts between the motorcycle frame and the swing arm. The virtual work done is given by:

$$\delta W_{MSr} = M_{Sr} \left[\frac{-\left(z_{32}-z_{31}\right)}{l_{SA}^2} \quad \frac{\left(x_{32}-x_{31}\right)}{l_{SA}^2} \quad \frac{\left(z_{32}-z_{31}\right)}{l_{SA}^2} \quad \frac{-\left(x_{32}-x_{31}\right)}{l_{SA}^2} \quad c_{33} \quad -s_{33} \right]$$
$$* \left\{ \delta x_{31} \quad \delta z_{31} \quad \delta x_{32} \quad \delta z_{32} \quad \delta s_{33} \quad \delta c_{33} \right\}^T$$

(6.29)

6.3.3.4 For Front Wheel and Rear Wheel Breaking Torque (M_{Ff} & M_{Fr}): These forces act between the front wheel and motorcycle frame and the rear wheel and fork respectively. The virtual work done is given by:

$$\delta W_{MFr} = M_{Fr} \left[\frac{-\left(z_{32}-z_{31}\right)}{l_{SA}^2} \quad \frac{\left(x_{32}-x_{31}\right)}{l_{SA}^2} \quad 1 \quad \frac{\left(z_{32}-z_{31}\right)}{l_{SA}^2} \quad \frac{-\left(x_{32}-x_{31}\right)}{l_{SA}^2} \right]$$
$$* \left\{ \delta x_{31} \quad \delta z_{31} \quad \delta \theta_{31} \quad \delta x_{32} \quad \delta z_{32} \right\}^T$$
$$\delta W_{MFf} = M_{Ff} \left[-c_{33} \quad s_{33} \quad 1 \right] * \left\{ \delta s_{33} \quad \delta c_{33} \quad \delta \theta_{34} \right\}^T$$

(6.30)

6.3.3.5 For Front Suspension Force (F_{sf}): These forces act between the front wheel and motorcycle frame. The virtual work done is given by:

$$\delta W_{Fsf} = F_{sf} \left[\left(s_{33}\cos\varepsilon + c_{33}\sin\varepsilon\right) \quad \left(s_{33}\sin\varepsilon - c_{33}\cos\varepsilon\right) \quad -\frac{c_{33}\left(y_{32}-y_{34}\right)}{\left(s_{33}\sin\varepsilon - c_{33}\cos\varepsilon\right)} \quad -\frac{s_{33}\left(y_{32}-y_{34}\right)}{\left(s_{33}\sin\varepsilon - c_{33}\cos\varepsilon\right)} \quad -\left(s_{33}\cos\varepsilon + c_{33}\sin\varepsilon\right) \quad -\left(s_{33}\sin\varepsilon - c_{33}\cos\varepsilon\right) \right]$$
$$* \left\{ \delta x_{32} \quad \delta z_{32} \quad \delta c_{33} \quad \delta s_{33} \quad \delta x_{34} \quad \delta z_{34} \right\}^T$$

(6.31)

Substituting all the derivatives derived in section 6.3.1, 6.3.2 and 6.3.3 into Eq. (6.9); total ten differential equations are obtained for thirteen unknowns (including three Lagrange multipliers). Substituting all expressions in Eq. (6.9) by collecting terms for different natural co-ordinates; the equations of motion for rigid body model of motorcycle is given as:

$$\left(m_{31}+\frac{I_{33}}{l_{SA}^2}\right)\ddot{x}_{31}-\frac{I_{33}}{l_{SA}^2}\ddot{x}_{32}+2\lambda_2\left(x_{31}-x_{32}\right)=S_{Tr}+\frac{\left(y_{31}-y_{32}\right)}{l_{SA}^2}\left(M_{Fr}-M_{Sr}\right)$$

$$\left(m_{31}+\frac{I_{33}}{l_{SA}^2}\right)\ddot{y}_{31}-\frac{I_{33}}{l_{SA}^2}\ddot{y}_{32}+2\lambda_2\left(y_{31}-y_{32}\right)=-m_{31}\,g+N_{Tr}-\frac{\left(x_{31}-x_{32}\right)}{l_{SA}^2}\left(M_{Fr}-M_{Sr}\right)$$

$$I_{31}\ddot{\theta}_{31}=M_{Fr}+r_r\,S_{Tr}$$

$$\left(m_{31}+\frac{I_{33}}{l_{SA}^2}\right)\ddot{x}_{32}-\frac{I_{33}}{l_{SA}^2}\ddot{x}_{31}+m_{32}\left(a_{33}\,\ddot{c}_{33}-b_{33}\,\ddot{s}_{33}\right)-2\lambda_2\left(x_{31}-x_{32}\right)+\lambda_3\left(s_{33}\sin\varepsilon-c_{33}\cos\varepsilon\right)$$

$$=-\frac{\left(y_{31}-y_{32}\right)}{l_{SA}^2}\left(M_{Fr}+M_{Sr}\right)+\left(s_{33}\cos\varepsilon+c_{33}\sin\varepsilon\right)F_{sf}$$

$$\left(m_{32}+\frac{I_{33}}{l_{SA}^2}\right)\ddot{y}_{32}-\frac{I_{33}}{l_{SA}^2}\ddot{y}_{31}+m_{32}\left(b_{33}\,\ddot{c}_{33}+a_{33}\,\ddot{s}_{33}\right)-2\lambda_2\left(y_{31}-y_{32}\right)-\lambda_3\left(s_{33}\cos\varepsilon+c_{33}\sin\varepsilon\right)$$

$$=-m_{31}\,g+\frac{\left(x_{31}-x_{32}\right)}{l_{SA}^2}\left(M_{Ff}-M_{Sr}\right)+\left(s_{33}\sin\varepsilon-c_{33}\cos\varepsilon\right)F_{sf}$$

$$m_{32}\left(a_{33}\,\ddot{x}_{32}+b_{33}\,\ddot{y}_{32}\right)+\left\{m_{32}\left(a_{33}^2+b_{33}^2\right)+I_{32}\right\}\ddot{c}_{33}+2\lambda_1\,c_{33}+\lambda_3\left\{\left(x_{34}-x_{32}\right)\cos\varepsilon+\left(y_{34}-y_{32}\right)\sin\varepsilon\right\}$$

$$=-m_{32}\,g\,b+\left(M_{Ff}-M_{Sr}\right)s_{33}-F_{Sf}\frac{c_{33}\left(y_{32}-y_{34}\right)}{\left(s_{33}\sin\varepsilon-c_{33}\cos\varepsilon\right)}$$

$$m_{32}\left(a_{33}\,\ddot{y}_{32}-b_{33}\,\ddot{x}_{32}\right)+\left\{m_{32}\left(a_{33}^2+b_{33}^2\right)+I_{32}\right\}\ddot{s}_{33}+2\lambda_1\,s_{33}+\lambda_3\left\{\left(y_{34}-y_{32}\right)\cos\varepsilon-\left(x_{34}-x_{32}\right)\sin\varepsilon\right\}$$

$$=-m_{32}\,g\,a-\left(M_{Ff}-M_{Sr}\right)c_{33}-F_{Sf}\frac{s_{33}\left(y_{32}-y_{34}\right)}{\left(s_{33}\sin\varepsilon-c_{33}\cos\varepsilon\right)}$$

$$m_{34}\,\ddot{x}_{32}-\lambda_3\left(s_{33}\sin\varepsilon-c_{33}\cos\varepsilon\right)=S_{Tf}-\left(s_{33}\cos\varepsilon+c_{33}\sin\varepsilon\right)F_{sf}$$

$$m_{34}\,\ddot{y}_{32}+\lambda_3\left(s_{33}\cos\varepsilon+c_{33}\sin\varepsilon\right)=-m_{34}\,g+N_{Tf}-\left(s_{33}\sin\varepsilon-c_{33}\cos\varepsilon\right)F_{sf}$$

$$I_{34}\ddot{\theta}_{34}=M_{Ff}+r_f\,S_{Tf}$$

$$\dots (6.32)$$

More detailed form of the derivation of these equations can be found in literature (Cossalter & Lot, 2002). Together Eqs 6.8 and 6.32 form a set of 13 differential algebraic equations (D.A.E.'s) which can be solved for obtaining the response of motorcycle model. For solving D.A.E', the constrained equations (Eq.6.8) are differentiated twice resulting in thirteen governing differential equations for motorcycle system written as:

$$\begin{bmatrix} M & \beta_q^T \\ \beta_q & 0 \end{bmatrix} \begin{Bmatrix} \ddot{q} \\ \lambda \end{Bmatrix} = \begin{Bmatrix} Q \\ Q_d \end{Bmatrix} \tag{6.33}$$

Newmark-β scheme of numerical integration (Bathe, 1996) is applied to solve these equations in time domain. For motorcycle with rigid rider; longitudinal tire forces are modelled using Pacejka magic formula. Normal forces were modelled using simple spring-damper relationship. Data for different parameters of motorcycle model is given in Appendix B. Subsequently sitting FE model with arms in bent position is coupled with the multibody motorcycle code. Response to vertical road excitation using wheelbase filtering is computed for motorcycle model with rigid rider and motorcycle with anthropometric model developed in this study.
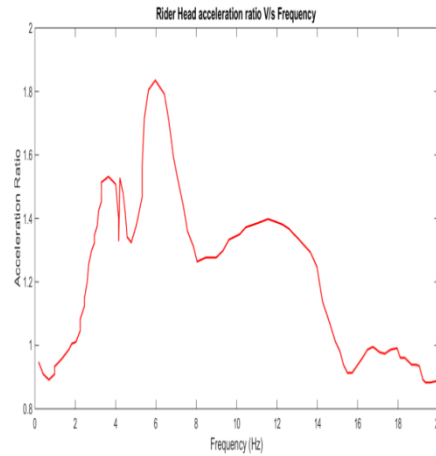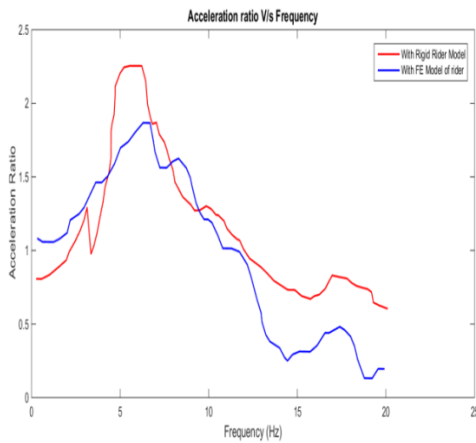
Fig. 6.3: Acceleration Ratio at Motorcycle C.G.   **Fig. 6.4: Acceleration Ratio at Head of Motorcycle Rider**

It is evident from Fig. 6.3 that the computed values of acceleration ratios at motorcycle C.G. are different when FE model of rider is incorporated compared to the values computed with rigid body model of a rider. Moreover, this anthropometric vibratory model enables us to determine dynamic response at different locations of rider body which is not possible with a rigid body model.

6.4 Conclusion: An in-plane motorcycle-rider vibratory model been adopted to study the effect of human body characteristics on the response of overall system. The motorcycle is modelled as a multi-body system comprising of front wheel, rear wheel, swinging arm and motorcycle frame. Initially, the rider has been considered as a rigid attachment to the motorcycle frame. Equations of motion for this model have been derived from principles of constrained multibody dynamics using Lagrange's multipliers. For straight running, motorcycle is assumed to be moving at constant speed and subjected to road undulations at different excitation frequencies. Newmark-β scheme of numerical integration has been employed to compute the dynamic response of the system. Thereafter, human body vibratory model of seated person in driving posture is employed to replace the rigid rider. This modified model of motorcycle-rider system is analyzed for the same speed and road undulations as the ones employed for rigid rider model. Comparison of results for the two different models, as shown in Fig 6.3, clearly establish that the acceleration of motorcycle center of gravity is affected by including human body characteristics in overall model of the system. Numerous experimental studies regarding human body vibration have established human body as a dynamic system having its own characteristics. It has also been observed in experimental studies that dynamic characteristics of human body depend on attributes of external excitation and also on the posture of human body. Therefore, effects of road undulations on response of motorcycle-rider system as well vibration exposure of motorcycle rider can be assessed accurately only if we include human body human body characteristics in overall model of the system.

Chapter 7

Conclusions

This dissertation work was undertaken to investigate effects of road undulations on human body, especially on the rider of a motorcycle. After extensive review of available literature (chapter 2), the major objectives of research study were decided as:

- Development and validation of lumped parameter anthropometric vibratory model of human body.

- Development and validation of continuum model of human body in standing and sitting posture based on anthropometric data.

- Development of a continuum model of motorcycle rider with his hands in driving posture and its integration with a multi degrees of freedom motorcycle model.

Human body segments have been represented as truncated ellipsoidal segments, with dimensions computed from anthropometric data (Chapter 3). Initially, following the methodology proposed by Nigam and Malik (1987), ellipsoidal segments are combined to develop lumped parameter vibratory model of standing subject undergoing vertical excitation from feet-platform interface. Estimation of model parameters for human body vibratory models is always a challenging task, especially as it relates to the damping present in body segments. In the present research work, a novel iterative scheme has been formulated to estimate modal damping ratios from experimental results available (Section 3.5.2). Reference value of elastic moduli for ellipsoidal body segments have been optimized from the minimization of the difference between experimental measurements of seat to head transmissibility and

theoretical values computed from anthropometric vibratory model. Optimized values of elastic moduli (Table 3.10) can be used as reference values for individual body segments for human body vibratory modeling. Theoretical predictions of STHT computed using this lumped parameter vibratory model can be made use to determine vibration dose value for passengers of public transportation.

In chapter 4, finite element vibratory model of standing subject has been formulated to parallel the continuous nature of actual human body. Two noded truncated ellipsoidal elements, with shape functions based on the exact solution of uni-axial deformation of truncated ellipsoid, have been used to model body segments. Kelvin-Voigt model of viscoelasticity is employed to model behaviour of individual body segment under vertical excitation. Concluded values of average elastic moduli and average dynamic viscosity of individual body segments (Table 4.3) can be put to use as initial estimates for human body modelling purpose. Comparison of results for normalized apparent mass (Fig. 4.6) and mode shapes (Fig. 4.8) computed using finite element model of standing subject suggest dominant contribution of different whole body modes near resonant frequency of normalized apparent mass.

FE models for seated human body (chapter 5) have been developed using similar methodology (chapter 4) with some modifications. Modal analysis of vibratory model for seated posture (Fig. 5.7) exhibit decoupling of motion of upper body segments (from head to lower torso) from the motion of lower body segments (upper legs to feet) near resonant frequency. Driving point impedance parameters computed from anthropometric vibratory model (seated human with hands in vertical posture) demonstrate satisfactory match with the envelop of experimental measurements. Therefore, these models can be used for design and comfort analysis of vehicle riders.

In chapter 6, vibratory model for a person with hands in driving posture of a motorcycle rider is developed and incorporated in a multi-body model of motorcycle. First equations of motion for motorcycle with a rigid rider are derived based on constrained multibody dynamics using Lagrange multipliers and thereafter rigid rider is replaced with vibratory model of a seated person with arms in motorcycle driving posture. Evaluation of results computed from these two models show noticeable effect of human body flexibility (Fig. 6.3) on the dynamic response of the motorcycle-rider system. Transmissibility of human head due to excitations from road undulations (Fig. 6.4) exhibit peaks at different frequencies of road excitations. Therefore, it is essential to incorporate the dynamic characteristics of different parts of human body into combined model of motorcycle-rider system for realistic simulation of the system.

7.1 Contributions of Research Work

The contributions of the present research study can be summarized as follows:

1. Computation of driving point mechanical impedance and acceleration transmissibility for anthropometric human body vibratory model.

2. Development of novel iterative scheme to estimate modal damping ratios using experimental measurements of transmissibility and its application to human body vibratory model.

3. Reference values for elastic moduli of human body segments in standing posture.

4. Development of truncated ellipsoidal finite elements for FE vibratory model of human body in standing and sitting posture using shape functions based on exact solution of uni-axial deformation of ellipsoid.

5. Estimation of elastic moduli and average dynamic viscosity of human body segments for finite element vibratory model with low d.o.f., in standing and sitting posture.

6. Development of seated human body vibratory model in driving posture of a motorcycle rider.

7. Analysis of motorcycle-rider system to study effects on dynamic response of combined system and effect of road undulations on human body.

7.2 Recommendation for Future Work

The human body vibratory models developed in this dissertation are based on body characteristics that can be measured readily, i.e. total mass and dimensions of body segments. Following this methodology, person specific or group specific vibratory models in different posture can be developed with ease and used for WBV studies of human body. Further work, however, is required for better understanding of effects of vibration on human body. Few suggestions for future work are given below:

1. Anthropometric data, used for development of vibratory models in the present work, belonged to 50th percentile U.S. male whereas experimental measurements of driving point impedance parameters used for comparison didn't belong to the same group. For better assessment of anthropometric vibratory models developed in this study, experimental studies must be carried out on a group of people whose anthropometric measurements are also available.

2. Motorcycle model used in the present study approximates it as composed of four rigid bodies. More detailed models of motorcycle that take into account the frame compliance and elastic tyre deformations can be used for better

approximations of system dynamics, both in straight line motion and motion along a curve.

3. Ellipsoidal finite elements used to model human body segments are assumed to undergo only uni-axial displacement under application of vertical excitation. Experimental studies have suggested pitching motion of some body segments under vertical excitation of human body, in addition to vertical motion. Predicted values of impedance parameters from vibratory models developed in this study can be improved by inclusion of rotational motion for ellipsoidal segments.

4. Horizontal segments of seated human body have been modeled as rigid rod elements connected with rotational springs/ dampers, undergoing only rotational motion. Elements that represent deformation of horizontal body segments more accurately can be identified and incorporated in FE vibratory model.

References

➢ Adrian M. J., Cooper J. M., Biomechanics of Human Movement, Brown & Benchmark press, 1995.

➢ Amirouche F.M.L., Ider S.K., Simulation and Analysis of a Biodynamic Human Model Subjected to Low Accelerations- a Correlation Study, J. Sound Vib., 1988, 123(2), pp. 281-292.

➢ Amirouche F.M.L., Xie M., Patwardhan A., Optimization of the Contact Damping and Stiffness Coefficients to Minimize Human Body Vibration, ASME J Biomech. Eng., 1994, 116, pp. 413-420.

➢ Anderson C. K., Chaffin D. B., Herrin G. D., Matthews L. S., A Biomechanical Model of the Lumbosacral Joint during Lifting Activities, Journal of Biomechanics, 1985, 18(8), pp. 571-584.

➢ Baker W.D.R., Mansfield N.J., Effects of Horizontal Whole-Body Vibration and Standing Posture on Activity Interference, Ergonomics, 2013, 53(3), pp. 365-374.

➢ Bakker E., Pacejka H.B., Liner L., A new tire model with an application in vehicle dynamic studies, SAE transactions -Journal of Passenger Cars, 1989, 98, pp. 101-113.

➢ Bakker E., Pacejka H.B., The magic formula tyre model, Vehicle System Dynamics, 2007, 21, pp. 1-18.

➢ Bartz J.A., Gianotti G.R., Computer Program to Generate Dimensional and Inertial Properties of the Human Body, Journal of Engineering for Industry, 1975, 97, pp.49-57.

➢ Behr M., Arnoux P.J., Serre T., Bidal S., Kang H.S., Thollon L., Cavallero C., Kayvantash K., Brunet C., A Human Model for Road Safety: From Geometric Acquisition to Model Validation with Radioss," Computer Methods in Biomechanics and Biomedical Engineering, 2003, 6(4), pp.263-273.

➢ Bevilacqua M., Doria A., Tognazzo M., Interaction forces between the rider and the 2-wheeled vehicle and biomechanical models, Proceedings of ASME 2013 IDETC, Portland, August 4-7, 2013, pp. 1-10.

➢ Boileau P. E., Rakheja S., Whole body vertical biodynamic response characteristics of the seated vehicle driver: Measurement and model development, Industrial Ergonomics, 1998, 22 , pp. 449-472.

➢ Boileau P E, Rakheja S., Wu X, A body mass dependent mechanical impedance model for applications in vibration seat testing, Journal of Sound and Vibration, 2002, 253(1) pp. 243-264.

➢ Boshuizen, H.C., Bongers, P.M., Hulshof, C.T.J., Self-Reported Back Pain in Fork-Lift Truck and Freight-Container Tractor Driver Exposed to Whole-Body Vibration, Spine, 1992, 17, pp. 59-65.

➢ Chen H.C., Chen W.C., Liu Y.P., Chen C.Y., Pan Y.T, Whole-body vibration exposure experienced by motorcycle riders −An evaluation according to ISO 2631-1 and ISO 2631-5 standards, Int. J. Industrial Ergonomics, 2009, 39, pp. 708-718.

➢ Chen, L.H, Zhang, W, Liu, Y.Q., Modeling of Nonlinear Oscillations for Viscoelastic Moving Belt using Generalized Hamilton's Principle, ASME J Vibration and Acoustics, 2007, 129, pp. 128-132.

➢ Cho Y., Yoon Y. S., Biomechanical model of human on seat with backrest for evaluating ride quality, Industrial Ergonomics, 2001, 27, pp. 331-345.

➢ Christensen, R.M., 1982, *Theory of Viscoelasticity*: *An Introduction*, Academic Press, Cambridge, Massachusetts

➢ Cleon, L.M., Lauriks, G., Evaluation of Passenger Comfort in Railway Vehicles, Journal of Low Frequency Noise and Vibration, 1996, 15(2), pp. 53-69.

➢ Coermann, R.R., The Mechanical Impedance of the Human Body in Sitting and Standing Position at Low Frequencies, Human Factors, 1962, 4(5), pp.227-253.

➢ Cossalter V., Motorcycle Dynamics, Lulu.com, 2006, ISBN 978-1430308614.

➢ Cossalter V., Dalla Torre G., Lot R., Massaro M., An advanced multibody model for the analysis of motorcycle dynamics, 3rd International Conference on Mechanical Engineering and Mechanics, Beijing, October 21-23, 2009, pp. 1-6.

➢ Cossalter V., Doria A., Lot R., Optimum Suspension design for motorcycle braking, Vehicle system Dynamics, 2000, 34, pp. 175-198.

➢ Cossalter V., Doria A., Garbin S., Lot R., Frequency-Domain Method for Evaluating the Ride Comfort of a Motorcycle, Vehicle system Dynamics, 2006, 44(4), pp. 339-355.

➢ Cossalter V., Lio M.D., Lot R., Mathematical modelling of two-wheeled vehicle, 9th World Congress on the theory of machines and mechanisms, Milano, August 29-September 2, 1995, pp. 2842-2846.

➢ Cossalter V., Lot R., A motorcycle multi-body model for real time simulations based on the natural coordinates approach, Vehicle System Dynamics, 2002, 37, pp. 423-447.

➢ Dempster W.T., Gaughran R.L., Properties of body segments based on size and weight, American Journal of Anatomy, 1967, 120, pp. 33-54.

➢ Dempster W.T., Space Requirements of the Seated Operator," WADC-TR-55-159, 1955, Wright Air Development Center, Ohio, USA.

➢ Doria A., Tognazzo M., Cossalter V., The Response of the Rider's Body to Roll Oscillations of Two Wheeled Vehicles; experimental tests and Biomechanical Models, Proceedings of Institution of Mechanical Engineers, Part D: Journal of Automobile Engineering, 2013, 227(4), pp. 561-576.

➢ Eger, T., Salmoni, A., Cann, A., Robert, J., Whole-Body Vibration Exposure Experienced by Mining Equipment Operators, Occupational Ergonomics, 2006, 6, pp. 121-127.

➢ Fairley T E, M J Griffin, The apparent mass of the seated human body: vertical vibration, Journal of Biomechanics, 1989, 22(2), pp.81-94.

➢ Fard, M.A., Ishihara, T., Inooka, H., Dynamics of the Head-Neck Complex in Response to the Trunk Horizontal Vibration: Modeling and Identification, ASME J Biomech. Eng., 2003, 125, pp. 533-539.

➢ Forlani, M., Sancisi, N., Castelli, V.P., A Three-Dimensional Ankle Kinetostatic Model to Simulate Loaded and Unloaded Joint Motion, ASME J Biomech. Eng., 2015, 137, pp. 061005-1-061005-12.

➢ Fritz M, Simulating the response of a standing operator to vibration stress by means of a biomechanical model, Journal of Biomechanics, 2000, 33 795-802.

➢ Fritz M., An Improved Biomechanical Model for Simulating the Strain of the Hand-Arm System under Vibration Stress, J. of Biomechanics, 1991, 24(12), pp.1165-1171.

➢ Garg, D.P., Ross, M.A., Vertical Mode Human Body Vibration Transmissibility, IEEE Transactions on Systems, Mass and Cybernetics SMC-6(2), 1976, pp.102-112.

➢ Goldman, D.E., Von Gierke, H.E., The Effects of Shock and Vibration on Man," *Shock and Vibration Handbook*: *vol.3 Chapter 44*, C.M. Harris, and C.E. Crede, eds., 1961, Mcgraw Hill,.

➢ Griffin, M.J., *Handbook of Human Vibration*, Academic Press Limited, 1990, NY.

➢ Gupta T.C., Identification and experimental validation of damping ratios of different human body segments through anthropometric vibratory model in standing posture, Journal of Biomechanical Engineering, 2007, 129, pp. 566-574

➢ Harazin, B., Grzesik, J., The Transmission of Vertical Whole Body Vibration to the Body Segments of Standing Subjects, J. Sound Vib., 1998, 215(4), pp.775-787.

➢ Hayes, W.C., Mockros, L.F., Viscoelastic Properties of Human Articular Cartilage, Journal of Applied Physiology, 1971, 31(4), pp. 562-568.

➢ Hertzberg H.T.E., Clauser C., Size and motion, in: Bioastronautic Data Book, National Aeronautics & Space Administration, Washington NASA SP-3006 1964, pp. 241-271

➢ Hirsch, J., Nachemson, A., New Observations of the Mechanical Behavior of Lumbar Discs, Acta Orthorpaedica Scandinavica, 1954, 23(4), pp 254-283.

➢ International Organization for Standards ISO/CD 5982, Mechanical vibration and shock-Range of idealized values to characterize seated body biodynamic response under vertical vibration, 1999.

➢ Ishihara, H., Tsuji, H., Hirano. N., Ohshima, H., Terahata, N., Effects of Continuous Quantitative Vibration on Rheologic and Biological behaviors of the intervertebral disc, Spine, 1992, 17, pp. S7-S12.

➢ ISO 2631-1 Mechanical vibration and shock–evaluation of human exposure to whole-body vibration–Part 1: General Requirements, International Organization for Standardization, Geneva (1997).

➢ ISO 2631-5 Mechanical vibration and shock–evaluation of human exposure to whole-body vibration–Part 5: Method for Vibration Containing Multiple Shocks, International Organization for Standardization, Geneva (2004).

➢ Jamison IV, D., Cannella, M., Pierce, E.C., Marcolongo, M.S., A Comparison of the Human Lumbar Intervertebral Disc Mechanical Responses to Normal and Impact Loading Conditions, ASME J Biomech. Eng., 2013, 135, pp. 091009-1-091009-1.

➢ Johanning, E., Whole-Body Vibration _Related Health Disorders in Occupational Medicine –An International Comparison, Ergonomics, 2015, 58(7), pp.1239-1252.

➢ Johnson G.A., Tramaglini D.M., Levine R.E., Ohno L., Choi N.Y., Woo S.L.Y, Tensile and viscoelastic properties of human Patellar tendon, J Orthopaedic Research, 1994, 12(6), pp.796-803.

➢ Kim Ki-Sun, Jongwan Kim, Kwang-joon Kim, Dynamic modeling of seated human body based on measurements of apparent inertia matrix for fore-and-aft/vertical/pitch motion, Journal of Sound and Vibration, 2011, 330, pp. 5716-5735.

➢ Kim T.H., Kim Y.T., Yoon Y.S., Development of a biomechanical model of human body in a sitting posture with vibration transmissibility in the vertical direction, Industrial Ergonomics, 2005, 35, pp. 817-829.

➢ Kitazaki S, Griffin M.J., A modal analysis of whole-body vertical vibration, using a finite element model of the human body, Journal of Sound and Vibration, 1997, 200(1), pp. 83-103.

➢ Kitazaki S, Griffin M.J., Resonance behavior of the seated human body and effects of posture, Journal of Biomechanics, 1997, 31(2), pp.143-149.

➢ Koenen C., The dynamic behaviour of motorcycles when running straight ahead and when cornering, Ph.D. Thesis, Delft University, Netherlands, 1983

➢ Kong W.Z, Goel V.K., Ability of the Finit Element Models to Predict Response of the Human Spine to Sinusoidal Vertical Vibration, Spine, 2003, 28(17), pp. 1961-1967.

➢ Kubo M., Terauchi F., Aoki H., Matsuoka Y., An investigation into a synthetic vibration model for humans: An investigation into a mechanical vibration human model constructed according to the relations between the physical, psychological and physiological reactions of humans exposed to vibrations, Int J Ind Ergonomic, 2001, 27, pp. 219-232.

➢ Lai H.C., Liu J.S., Lee D.T., Wang L.S., Design Parameters Study on the Stability and Perception of Riding Comfort of the Electrical Motorcycles under Rider Leaning, Mechatronics, 2003, 13, pp. 49-76.

➢ Linde, F., Elastic and Viscoelastic Properties of Trabecular Bone by Compression Testing Approach, Danish Medical Bulletin, 41(2), 1994, pp. 119-138.

➢ Liu X X, Shi J., Li G.H. et al, Biodynamic response and injury estimation of ship personnel to ship shock motion induced by underwater explosion, Proceedings of 69th Shock and Vibration Symposium, St. Paul, 18 (1998), pp. 1-18.

➤ Liu Y.K., Wickstrom J.K., Estimation of inertial property distribution of the human torso from segmented cadaveric data, in: Kenedi RM (Ed.) Perspectives in Biomedical Engineering, a Symposium, Glasgow, University Park Press (1973) pp. 203-213.

➤ Liu, C., Qiu, Y., Griffin, M.J., Finite Element Modelling of Human-Seat Interactions: Vertical In-line and Fore-and-aft Cross-Axis Apparent Mass when Sitting on a Rigid Seat Without Backrest and Exposed to Vertical Vibration, 2015, 58, pp.1207-1219.

➤ Luo Z, Goldsmith W., Reaction of human head/neck/torso system to shock, Journal of Biomechanics, 1997, 24(7), pp. 449-510.

➤ Marini G., Huber G., Püschel K., Ferguson S.J., A 1-D model of the nonlinear dynamics of the human lumbar intervertebral disc, J Sound Vibration, 2017, 387, pp. 194-206.

➤ Markolf K. L., Stiffness and damping characteristics of the thoracolumbar spine, In: Proceedings of workshop on Bioengineering approaches to problems of the spine, 1970, pp. 87-143.

➤ Matsumoto Y., Griffin M.J., Dynamic response of the standing human body exposed to vertical vibration: influence of posture and vibration magnitude, Journal of Sound and Vibration, 1998, 212(1), pp. 85-107.

➤ Matsumoto Y, Griffin M. J., Mathematical models for the apparent masses of the standing subjects exposed to vertical whole-body vibration, Journal of Sound and Vibration, 2003, 260, pp. 431-451.

➤ Matsumoto Y, Griffin M.J., Movement of the upper body of the seated subjects exposed to vertical whole-body vibration at the principal resonance frequency, Journal of Sound and Vibration, 1998, 215(4), pp. 743-762.

➤ Matsumoto Y., Griffin M.J., Modelling the dynamic mechanisms associated with the principal resonance of the seated human body, Clin. Biomech, 2001, 16 (Supplement No.1), pp. S31-S44.

➤ Matthews, J.D., Effects of Moving Environments on the Physical Demands of Heavy Materials Handling Operators, Int J Ind. Ergonomics, 2007, 37, pp. 43-50.

➤ Moreno R., Cardona J., Pintado P., Chicharro J, Predictors of whole body vibration exposure in motorcycle riders, Rev. Fac. Ing. Univ. Antioauia, 2011, vol.61, pp. 93-103.

➢ Muksian R., Nash Jr. C.D., On frequency dependent damping coefficients in lumped-parameter models of human beings, Journal of Biomechanics, 1976, pp. 339-342.

➢ NASA Reference publication 1024, Anthropometric source book, volume 1: anthropometry for designers, NASA 1978.

➢ Nigam S.P., Malik M., A Study on a vibratory model of a human body, ASME J Biomech Eng, 1987, 109, pp.148-153

➢ Paddan G.S., Griffin M.J., The Transmission of translational seat vibration to the head-I. Vertical seat vibration, J. Biomech, 1998, 21(3), pp. 191-197.

➢ Paddan, G.S., Griffin, M.J., The Transmission of Translational Floor Vibration to the Heads of Standing Subjects, J. Sound Vib., 1993, 160(3), pp.503-521.

➢ Panjabi M.M., Brand Jr. R.A., White III A.A., Three dimensional flexibility and stiffness properties of human thoracic spine, Journal of Biomechanics, 1976, 9, pp. 185-192

➢ Pankoke S., Buck B., Woelfel H.P., Dynamic FE model of sitting man adjustable to body height, body mass and posture used for calculating internal forces in the lumbar vertebral disks, J Sound Vibration ,1998, 215(4), pp. 827-839.

➢ Park S J, Park S.C., Kim J.H., Kim C.B., Biomechanical parameters on body segments of Korean adults, International Journal of Industrial Ergonomics,1999, 23, pp. 23-31.

➢ Petyt M., Introduction to Finite Element Vibration Analysis, Cambridge University Press, Cambridge, UK, 2010.

➢ Privitzer E, Belytschko T., Impedance of a Three-dimensional Head-Spine model, Mathematical Modelling, 1980, 1(2), pp. 189-209.

➢ Qassem W, Othman M.O., Majeed S. A., The effects of vertical and horizontal vibrations on human body, Medical Engineering & Physics, 1994, 16, pp. 151-161.

➢ Qiu Y, Griffin M.J., Biodynamic responses of the seated human body to single-axis and dual-axis vibration, Industrial Health, 2009, 48, pp. 615-627.

➢ Rakheja S, Stiharu I., Zhang H., Boileau P.E., Seated occupant interactions with seat backrest and pan, and biodynamic responses under vertical vibration, Journal of Sound and Vibration, 2006, 298, pp. 651-671.

➢ Rakheja, S., Dong, R.G., Patra, S., Boileau, P.-E., Marcotte, P., Warrem, C., Biodynamics of the Human Body under Whole-Body Vibration: Synthesis of the Reported Data,Int. J. Industrial Ergonomics,2010 40, pp. 710-732.

➢ Rao, J.S., Gupta K., Introductory Course on Theory and Practice of Mechanical Vibrations, New Age International (P) Ltd., New Delhi, India, 1999.

➢ Rao, R.V., Jaya: A Simple and New Optimization Algorithm for solving constrained and Unconstrained Optimization Problems, International Journal of Industrial Engineering Computations, 2016, 7, pp. 19-34.

➢ Rao, R.V., Waghmare, G.G., A New Optimization Algorithm for Solving Complex Constrained Design Optimization Problems, Engineering Optimization, 2017, 49(1), pp. 60-83.

➢ Rosen. J., Arcan, M., Modeling the Human Body/Seat System in a Vibration Environment, ASME J Biomech. Eng., 2003, 125, pp. 223-231.

➢ Saraf H., Ramesh K.T., Lennon A.M., Merkle A.C., Roberts J.C., Mechanical properties of soft human tissues under dynamic loading, J Biomech, 2007, 40 pp.1960-1967.

➢ Sequenzia G., Oliveri S.M., Fatuzzo G., Cali M., An advanced multibody model for evaluating rider's influence on motorcycle dynamics, Proceedings of Institution of Mechanical Engineers, Part K: Journal of Multi-body dynamics, 2015, 229, pp. 193-207.

➢ Sharp R.S., Limebeer D.J.N, A Motorcycle model for stability and control analysis, Vehicle System Dynamics, 2001, 6, pp. 123-142.

➢ Sharp R.S., Limebeer D.J.N, Advances in the modelling of motorcycle dynamics, Vehicle System Dynamics, 2004, 12, pp. 251-283.

➢ Shuck, L.Z., Advani, S.H., Rheological Response of Human Brain Tissue in Shear, ASME J Basic Engineering, 1972, 94, pp.905-911.

➢ Singh, I., Nigam, S.P., Saran, V.H., Modal Analysis of Human Body Vibration Model for Indian Subjects under Sitting Posture, Ergonomics, 2015, 58, pp. 1117-1132.

➢ Subashi G.H.M.J., Matsumoto Y., Griffin M.J., Apparent mass and cross axis apparent mass of standing subjects during exposure to vertical whole boy vibration, Journal of Sound and Vibration,2006, 293, pp. 78-95.

➢ Subashi G.H.M.J., Matsumoto Y., Griffin M.J., Modelling resonances of the standing body exposed to vertical whole-body vibration: Effects of posture, Journal of Sound and Vibration, 2008, 317, pp. 400-418.

➢ Suggs, C.W., Abrams Jr., C.F., Simulation of Whole Body Dynamics, Proceedings of the Fifth Annual Southeastern Symposium on Systems Theory, March 1973, pp. 176-180.

➢ Suzuki, H., Momentary discomfort caused by vibration of railway vehicle, Industrial health, 1998, 36(2), pp. 98-106.

➢ Terry, C.T., Roberts, V.L., A Viscoelastic Model of the Human Spine Subjected to $+gz$ Accelerations, J of Biomech, 1968, 1, pp. 161-168.

➢ Thoung, O., Griffin, M.J., The Vibration Discomfort of Standing Persons: Relative importance of Fore-and-Aft, Lateral, and Vertical Vibration, Applied Ergonomics, 2012, 43, pp. 902-908.

➢ Tiemessen, I.J., Hulshof, C.T.J., Frings-Dresen, M.H.W., An Overview of Strategies to Reduce Whole-Body Vibration Exposure on Drivers: A Systematic Review, Int J Ind. Ergonomics, 2007, 37(3), pp. 245-246.

➢ Verma M. K., Scott R. A., Segels L., Effect of Frame Compliance on the lateral Dynamics of Motorcycles, Vehicle System Dynamics, 1980, 9, pp. 181-206.

➢ Wei L, Griffin M.J., Mathematical models for the apparent mass of the seated human body exposed to vertical vibration, Journal of Sound and Vibration, 1998, 212(5), pp. 855-874.

➢ Williams J.L., Belytschko T.L., A dynamic model of cervical spine and head, Air Force Aerospace Medical Research Laboratory, Wright-Patterson Air Force Base, Ohio, Report No. AFAMRL-TR-81-5, 1981

➢ Zheng G., Qiu Y., Griffin M.J., An analytic model of the in-line and cross-axis apparent mass of the seated human body exposed to vertical vibration with and without a backrest, Journal of Sound and Vibration, 2011, 330, pp. 6509-6525.

➢ Zhu S., Murakami S., Nishimura H., Motion Analysis of a Motorcycle taking into Account the Rider's Effects, Vehicle System Dynamics, 2012, 50(8), pp. 1225-1245.

➢ Zong Z, Lam K.Y., Biodynamic response of shipboard sitting subject to ship shock motion, Journal of Biomechanics, 2002, 35, pp. 35-43.

Appendix A

Table A: Formulas used for determining semi-axes of ellipsoidal body segments

Segment No.	Body Segment	Formulae		
		a_i	b_i	c_i
1	Head (H)	$L_7/2$	$L_7/2$	$L_6/2$
2	Neck (N)	$L_9/2\pi$	$L_9/2\pi$	$(L_1-L_2-L_6)/2$
3	Upper Torso (UT)	$L_{12}/2$	$L_{11}/2$	$L_{17}/2$
4,5	Right Upper Arm (RUA), Left Upper Arm (LUA)	$L_{19}/2\pi$	$L_{19}/2\pi$	$L_{17}/2$
6,7	Right Lower Arm (RLA), Left Lower Arm (LLA)	$L_{21}/2\pi$	$L_{21}/2\pi$	$L_{18}/2$
8	Central Torso (CT)	$L_{14}/2$	$L_{13}/2$	$(L_{17}+L_{18})/4$
9	Lower Torso (LT)	$L_{16}/2$	$L_{15}/2$	$L_{18}/4$
10,11	Right Upper Leg (RUL), Left Upper Leg (LUL)	$L_{25}/2\pi$	$L_{25}/2\pi$	$(L_2-L_{17}-L_{23})/2$
12,13	Right Lower Leg (RLL), Left Lower Leg (LLL)	$L_{27}/2\pi$	$L_{27}/2\pi$	$(L_{23}-L_{29})/2$
14.15	Right Foot (RF), Left Foot (LF)	$L_{30}/2$	$L_{31}/2$	$L_{29}/2$

Table B: Anthropometric measurements, symbols thereof & their values

Anthropometric Measurement	Symbol	Value (cm) 50th percentile U.S. male[34]	Value (cm) Average Indian male [39]
Standing Height	L_1	168.67	170.28
Shoulder Height	L_2	146.33	146.75
Armpit Height	L_3	136.02	133.75
Waist Height	L_4	108.38	103.75
Seated Height	L_5	92.96	89.18
Head Length	L_6	19.86	19.85
Head Breadth	L_7	15.57	16.95
Head to Chin Height	L_8	23.24	24.41
Neck Circumference	L_9	37.95	34.43
Shoulder Breadth	L_{10}	46.20	42.6
Chest Depth	L_{11}	23.32	20.03
Chest Breadth	L_{12}	32.89	30.64
Waist Depth	L_{13}	21.51	18.0
Waist Breadth	L_{14}	28.22	28.93
Buttock Depth	L_{15}	23.19	20.92
Hip Breadth	L_{16}	35.43	34.09
Shoulder to Elbow Length	L_{17}	37.54	35.75
Forearm Hand Length	L_{18}	48.69	48.93
Biceps Circumference	L_{19}	32.92	25.0
Elbow Circumference	L_{20}	31.42	24.27
Forearm Circumference	L_{21}	29.08	24.39
Wrist Circumference	L_{22}	17.86	16.65
Knee Height	L_{23}	53.14	53.69
Thigh Circumference	L_{24}	50.52	47.4
Upper Leg Circumference	L_{25}	37.24	37.9
Knee Circumference	L_{26}	36.20	35.92
Calf Circumference	L_{27}	33.32	31.87
Ankle Circumference	L_{28}	21.06	22.09
Ankle Height	L_{29}	6.91	10.01
Foot Breadth	L_{30}	9.35	10.7
Foot Length	L_{31}	25.40	25.95

Appendix B

This section shows the derivation of third constraint equation β_3 (i.e. Eq. 6.8(c)) and the data used for straight line motorcycle model. The third constraint equation is:

$$\beta_3 = (x_{34} - x_{32})(c_{33}\sin(\varepsilon) - s_{33}\cos(\varepsilon)) + (y_{34} - y_{32})(s_{33}\cos(\varepsilon) + c_{33}\sin(\varepsilon)) - l = 0 \qquad \text{(B.1)}$$

As stated in chapter 6, this equation represents the link between the motorcycle frame and the front wheel of motorcycle by fixing point G_{34} on the front suspension axis. Figure B.1 shows the portion of motorcycle frame and front wheel used for deriving constraint equation β_3. In Fig. B.1; x-z represents the global co-ordinate axis and X-Z represents the local co-ordinate system with origin at point P_{32} and X axis parallel to vector $\vec{u}_{33}$. The line $P_{32}A$ is perpendicular to the steering axis $G_{34}A$, and the line AB is parallel to the local Y axis. Castor angle (ε) of the motorcycle is the angle between the steering axis (S-A) and the line AB.
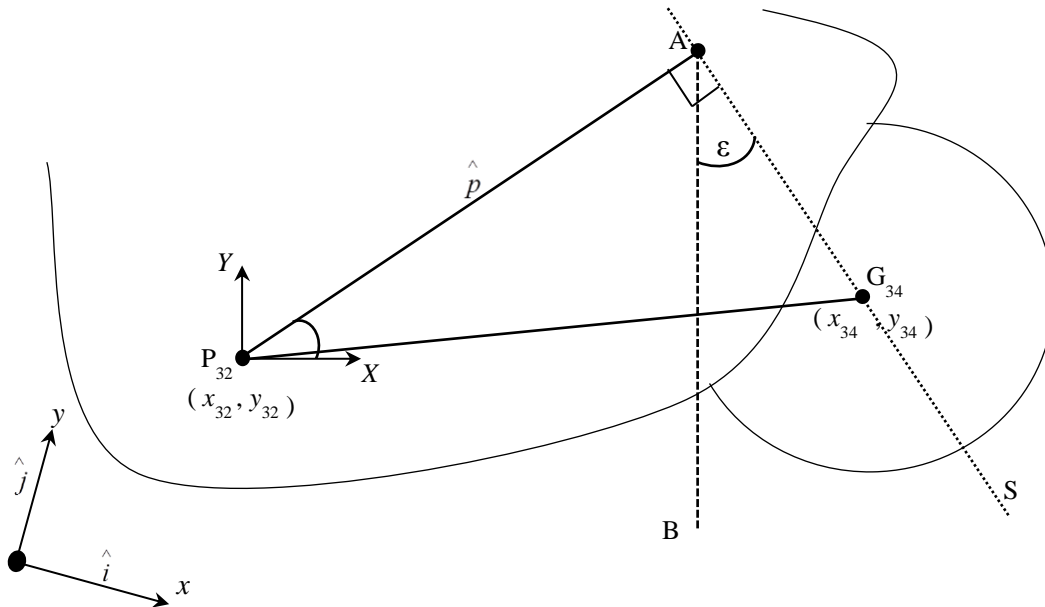
Fig. B.1   Portion of motorcycle frame and front wheel

Since the X axis has been taken parallel to vector $\vec{u}_{33}$; unit vectors $\hat{I}$ and $\hat{K}$ for local co-ordinate system, in terms of global unit vectors ($\hat{i}$ and $\hat{k}$), are defined as:

$$\hat{I} = c_{33} \ \hat{i} + s_{33} \ \hat{k}$$
$$\& \ \hat{K} = -s_{33} \ \hat{i} + c_{33} \ \hat{k} \qquad \text{(B.2)}$$

The points P_{32} and G_{34} have co-ordinates (x_{32}, z_{32}) and (x_{34}, z_{34}) respectively in global co-ordinate system. Therefore, the vector along line segment $P_{32}G_{34}$ is:

$$\overrightarrow{P_{32}G_{34}} = \left(x_{34} - x_{32}\right)\hat{i} + \left(z_{34} - z_{32}\right)\hat{k} \qquad \text{(B.3)}$$

A unit vector ($\hat{p}$) along line segment $P_{32}A$ can be written as:

$$\hat{p} = \cos\varepsilon \ \hat{I} + \sin\varepsilon \ \hat{K}$$
$$= \cos\varepsilon \left(c_{33} \ \hat{i} + s_{33} \ \hat{k} \right) + \sin\varepsilon \left(-s_{33} \ \hat{i} + c_{33} \ \hat{k} \right)$$
$$\Rightarrow \hat{p} = \left(c_{33}\cos\varepsilon - s_{33}\sin\varepsilon \right)\hat{i} + \left(s_{33}\cos\varepsilon + c_{33}\sin\varepsilon \right)\hat{k} \qquad \text{(B.4)}$$

For the condition that point G_{34} lies on the steering axis SA always, the projection of $\overrightarrow{P_{32}G_{34}}$ on the segment $P_{32}A$ should be constant. If 'l' is taken as the vertical distance between the point P_{32} and the front suspension axis, i.e. the length of line segment $P_{32}A$, then:

$$\overrightarrow{P_{32}\,G_{34}} \bullet \hat{p} = l$$

$$\Rightarrow \left[\left(x_{34} - x_{32} \right) \hat{i} + \left(z_{34} - z_{32} \right) \hat{k} \right] \bullet \left[\left(c_{33} \cos \varepsilon - s_{33} \sin \varepsilon \right) \hat{i} + \left(s_{33} \cos \varepsilon + c_{33} \sin \varepsilon \right) \hat{k} \right] = l$$

$$\Rightarrow \left(x_{34} - x_{32} \right) \left(c_{33} \cos \varepsilon - s_{33} \sin \varepsilon \right) + \left(z_{34} - z_{32} \right) \left(s_{33} \cos \varepsilon + c_{33} \sin \varepsilon \right) - l = 0 \qquad \text{(B.5)}$$

Equation (B.5) is the constraint equation 6.8(c), which fixes point G_{34} to remain on the steering axis (S-A) of the motorcycle during straight line motion.

Table C: Data for Straight Line Motorcycle Model

Motorcycle total mass	186 kg	Front wheel moment of inertia	0.54 kg m^2
Horizontal distance from rear axle to c.o.m.	0.637 m	Rear wheel moment of inertia	0.85 kg m^2
Height of c.o.m.	0.633 m	Rear arm moment of inertia	0.28 kg m^2
Wheel-Base	1.35 m	Front suspension stiffness	14000 N/m
Castor angle	0.4 rad	Front suspension damping in extension	1100 N-sec/m
Front wheel radius	0.299 m	Front suspension damping in compression	550 N-sec/m
Rear wheel radius	0.318 m	Rear suspension stiffness	70000 N/m
Rear arm length	0.560 m	Rear suspension damping in extension	6000 N-sec/m
Co-ordinated (a_{33}, b_{33}) of frame/driver c.o.m	(0.09, 0.26) m	Rear suspension damping in compression	3000 N-sec/m
Mass of frame and rider	156 kg	Radial stiffness of front tyre	100000 N/m
Front wheel mass	14 kg	Radial damping of front tyre	70 N-sec/m
Rear wheel mass	16 kg	Radial stiffness of rear tyre	130000 N/m
Frame and rider moment of inertia	23.00 kg m^2	Radial damping of front tyre	100 N-sec/m

List of publications out of this work:

1. Manoj Gupta, T C Gupta, 2017, "*Modal Damping Ratio and Optimal Elastic Moduli of Human Body Segments for Anthropometric Vibratory Model of Standing Subjects*", ASME J of Biomechanics, vol. 139, pp 101006-1 to 101006-13

2. Manoj Gupta, T C Gupta. "Anthropometric Finite Element Vibratory Model of Standing Subject Based on Exact Shape Functions and Dynamic Viscosity", Journal of Sound & Vibration, (under Review)

3. Manoj Gupta, T C Gupta. "Finite Element Vibratory Model of Seated Subject Based on Exact Shape Functions and Dynamic Viscosity", Journal of Sound & Vibration , (Uploaded)

Brief Bio-Data of the Author:

Manoj Gupta

32/25 Swarn Path, Mansarovar, Jaipur-302020

M: +91-9887931979   E-mail: mngupt@gmail.com

Education:

Ph.D. Mechanical Engineering Malaviya National Institute of Technology (M.N.I.T.), Jaipur, India *Thesis Title.* "Development of Human Body Vibratory Models and Dynamic Analysis of Motorcycle-Rider System" *Supervisor:* Dr. T. C. Gupta	(Thesis Submitted)
M.E. Aerospace Engineering Iowa State University, Ames, IA, USA; *CGPA*: 3.9/4.0	May 2010
B. Tech. (Hons.) Aerospace Engineering Indian Institute of Technology (I.I.T.), Kharagpur, India; *CGPA*: 7.42/10	June 2000
Senior Secondary School Examination Rajasthan Board of Secondary Education, Ajmer; *Percentage*: 65.5%	May 1995
Secondary School Examination Rajasthan Board of Secondary Education, Ajmer; *Percentage*: 81.2%	June 1993

Professional Experience:

Visiting Faculty, Dept. of Mechanical-Mechatronics Engineering The LNM Institute of Information Technology, Jaipur, India.	01/07/2018 to Current
Doctoral Researcher, Dept. of Mechanical Engineering Malaviya National Institute of Technology (M.N.I.T.), Jaipur, India.	04/01/2013 to 31/06/2018
Assistant Professor, Dept. of Mechanical Engineering Jaipur Engineering College & Research Center, Jaipur, India.	01/09/2009 to 31/12/2012
Teaching Assistant, Dept. of Aerospace Engineering and Engineering Mechanics; Iowa State University, Ames, IA, USA.	16/08/2001 to 15/05/2004
Graduate Trainee Engineer, TATA Autocomp Systems Ltd., Pune, India.	25/07/2000 to 29/05/2001

Publications:

- **Gupta M., Gupta T.C.;** Modal Damping Ratios and Optimal Elastic Moduli of Human Body Segments for Anthropometric Vibratory Model of Standing Subjects, 2017, **ASME Journal of Biomechanical Engineering**, vol. 139, pp. 101006-1 to 101006-13. — Published; SCI; Impact Factor 1.916

- **Gupta M., Gupta T.C.;** Anthropometric Finite Element Vibratory Model of Standing Subjects Based on Exact Shape Functions and Dynamic Viscosity, **Journal of Sound & Vibration.** — Under Review

- **Gupta M., Gupta T.C.;** Finite Element Vibratory Model of Human Body in Seated Posture using Anthropometric Measurements and Kelvin-Voigt Model, **Journal of Sound & Vibration**. — Uploaded

Participation in Continuing Education Program:

- Workshop on **High Impact Teaching Skills;** Wipro Mission 10X at Jaipur Engineering College & Research Centre, Jaipur — $9^{th} - 10^{th}$ November 2010

- Workshop on **Teaching Engineering using MATLAB & Simulink;** Jaipur Engineering College & Research Centre, Jaipur — $5^{th} - 7^{th}$ July 2011

- International Workshop on **Computational Methods in Vibration & Acoustics;** Indian School of Mines, Dhanbad — $16^{th} - 21^{st}$ March 2015

- Short Term Training Program on **Finite Element Method and its Applications;** Malaviya National Institute of Technology, Jaipur — $4^{th} - 8^{th}$ June 2018

Professional Membership:

- Life Member of Indian Society of Theoretical and Applied Mechanics (ISTAM).

- Life Member of Indian Society of Technical Education (ISTE).

Awards, Honors and Recognitions:

- Secured Third Rank at Rajasthan Pre-Engineering Test, 1996.

- Received MHRD, GOI certificate of Merit for National scholarship Scheme, 1993.